POLITECNICO DI TORINO

Faculty of Engineering

Master of Science
in Automotive Engineering

Master Thesis

Calibration and assessment of the "DIPulse" heat release predictive model for a 2.3L diesel engine for light-duty applications simulated in GT-power

Supervisors:

Prof. Roberto Finesso
Ing. Omar Marello
Prof. Stefano D'Ambrosio

Candidate:

Meir Vainer Lechtman

July 2019

Table of Contents

List of Figures

List of Tables

Representations/Symbols

SYMBOL	MEANING
C_{df}	Diffusion Combustion Rate Multiplier
C_{ent}	Entrainment Rate Multiplier
C_{ing}	Ignition Delay Multiplier
C_p	Specific Heat at Constant Pressure
C_{pm}	Premixed Combustion Rate Multiplier
C_v	Specific Heat at Constant Volume
i	Total Number of Cylinders
k	Turbulent Kinetic Energy
$\dot{m}_a$	Air Mass Flow Rate
$\dot{m}_f$	Fuel Mass Flow Rate
m_a	Mass of Air
m_f	Mass of Fuel
m_{inj}	Injected Fuel Mass
m_{pm}	Premixed Mass
n	Engine Speed
n_r	Number of Crank Revolutions for Each Power Stoke per Cycle
p	Pressure
P_b	Power Brake
P_f	Friction Power
P_{ig}	Gross Indicated Power
R	Gas constant for Dry Air = 287 $\frac{J}{K \cdot kg}$
r_c	Compression Ratio
S	Spray Tip Penetration
T	Torque
t	Time
T_2	Temperature at end the compression stroke
T_3	Temperature at end of combustion
t_{ign}	Time at Ignition
u_{inj}	Injection Velocity at the Nozzle Tip

V	Volume
V_{cyl}	Cylinder Volume
V_d	Engine Displacement
V_{max}	Maximum Cylinder Volume
V_{min}	Minimum Cylinder Volume
W	Work
β	Ratio T_3/T_2
γ	Specific Heat Ratio c_p/c_v
η_f	Fuel Conversion Efficiency
η_m	Mechanical Efficiency
η_v	Volumetric Efficiency
λ	Air/fuel ratio
ρ	Gas Density
ρ_a	Air Density
τ_{ign}	Ignition Delay
ϕ	Equivalence Ratio

Abbreviations/Nomenclature

Abbreviation	**MEANING**
A/F	Air-Fuel Ratio
ASI	After the Start of Injection
BDC	Bottom Dead Center
bmep	Brake Mean Effective Pressure
bsfc	Brake Specific Fuel Consumption
CA	Crank Angle
CFD	Computational Fluids Dynamics
CI	Compression Ignition
CPOA	Cylinder Pressure Analysis Only
DI	Direct Injection
DT	Dwell Time
EGR	Exhaust Gas Recirculation
EOC	End of Combustion
EOI	End of Injection
ET	Energizing Time

fmep	Friction Mean Effective Pressure
ICE	Internal Combustion Engine
IDI	Indirect Injection
imep	Indicated Mean Effective Pressure
IVC	Intake Valve Closure
LHV	Low Heat Value
mep	Mean Effective Pressure
MFB50	Crank Angle for 50% of Mass Fuel Burn
MUZ	Main Unburned Zone
NOD	Nozzle Opening Delay
NOx	Nitrogen Oxides
PAH	Poly-Aromatic Hydrocarbons
PM	Particulate Matter
Q_{LHV}	Lower Heating value
RLT	Results
RMSE	Root Mean Square Error
SBZ	Spray Burned Zone
SI	Spark Ignition
SOC	Start of Combustion
SOI	Start of Injection
SOI_e	Start of injection electric
SOI_h	Start of Injection hydraulic
SUZ	Spray Unburned Zone
TDC	Top Dead Center
TPA	Three Analysis Pressure

1 Introduction

Internal combustion engines (ICEs) are still dominant in the modern world. They have become the primary method of transportation – thanks to their continual improvements over the last 125 years – and will remain so for years to come [1]. Despite the efficiency and emission improvements, the basic operational principle of the ICE has not changed significantly [2]. The automotive industry is continuously researching and developing new technologies in order to improve the performance and fuel consumption while decreasing the pollutant emissions in order to comply with the strict pollutant emissions regulations and the rising fuel prices.

Compression ignition direct injection diesel engines have being widely used in marine propulsion and high-duty vehicles, because of their higher efficiency in comparison with spark-ignition engines. The main reason for this, is the use of lean air/fuel mixture under higher compression ratios, and without throttling losses during part load. On the other hand, the main drawbacks of diesel engines are their robustness (which is translated into a small power/weight ratio), their high levels of noise and their high levels of NOx and particulate matter (PM) in comparison with spark-ignition engines. Recently, however, thanks to significant improvements in injection technologies, exhaust aftertreatment systems and turbochargers, diesel engines are increasingly being used in light-duty vehicles too [3] [4] [5].

The optimization and evaluation of the combustion process by changing the combustion chamber design, trying different injection strategies, varying the pressure of the injection system, among others, leads to improvements in pollutant emissions and efficiencies. However, there are a significant amount of combinations to obtain optimum results. This is reflected in more time-consuming tasks for the experimental test [4]. Therefore, the challenge for combustion science is the development of predictive combustion models capable of optimizing the operation of advanced engines. Although the simulated results are less precise than the experimental ones, it is possible to isolate one variable at a time and analyze its effect on the system, which will not only help to improve engine performance, but also will reduce testing costs and time [4] [6]. Numerical simulations have been an important tool for the prediction and analysis of the combustion process. For example, three dimensional computational fluid dynamics (CFD) have been proved to reproduce satisfactorily the combustion process, however, it requires high computational time. Therefore, zero-dimensional (O-D) and one-dimensional (1-D) analyses have been studied for modelling the combustion processes [7]. Gamma Technologies is a software company which developed GT-Power. GT-Power – which is based on 1-D fluid dynamics – is a powerful tool capable of performing advanced engine simulations suitable for analyzing the outputs related to the engine performance. Among a wide variety of applications, GT-Power can be used to build predictive combustion models.

The aim of this thesis is to calibrate and assess a predictive combustion model for a 2.3L diesel engine for light-duty applications simulated in GT-Power. The engine is a common rail turbocharged 4 cylinder compression ignition (CI) direct injection (DI) diesel engine with a high pressure exhaust gas recirculation (EGR) system.

The calibrated model is capable of predicting the indicated mean effective pressure (*imep*), maximum pressure, crank angle at which 50% of the fuel mass fraction has burned (MFB50) and NOx emissions. The analysis has been carried out under steady state operating conditions, and the simulation results have been compared with the provided data from FPT (measured from a test rig) in different operating conditions covering a wide area of the engine performance map. As not all the results were found within the recommended thresholds, the discovered causes of the error were of significant importance.

The first part of this work reports a brief description of diesel engine basics and modelling in GT-Power. The next part explains the followed methodology –from checking the provided data and the modelling of a single cylinder, to checking the quality of the input data of the system, to the calibration of the predictive combustion model and the validation of the mentioned model. Finally, the last part is focused on the discussion of the results obtained through the performed simulations and the conclusions obtained from them.

2 Theory

The first part of this section briefly introduces the internal combustion engines (ICE). Following this, diesel engine basics will be explored, as well as the combustion in diesel engines and some injection strategies in diesel engines. The last part provides information about the combustion models used by GT-power.

In this project, a compression ignition diesel engine is studied. It is a turbocharged four stoke engine, which is fed through a direct injection system.

2.1 Internal Combustion Engines

When a mixture of fuel and air is burned or oxidized, energy is released. This chemical reaction is known as combustion. The purpose of an internal combustion engine is to convert this chemical energy into mechanical power. The working fluids in the internal combustion engines are the fuel-air mixture before combustion and the burned products after it. The interaction between these working fluids and the mechanical components of the engine provides the desired power output [8].

The reciprocating ICEs are the most common engines in the market. They are characterized by the conversion of linear motion into rotational motion through the reciprocating motion of a piston into a cylinder. The piston, which is connected to a crankshaft with a connecting rod, moves from the top dead center (TDC), closest to the cylinder head, which corresponds to the minimum cylinder volume V_{min}, to the bottom dead center (BDC), the farther distance to the cylinder head which corresponds to the maximum cylinder volume V_{max} (see Figure 1) [9].

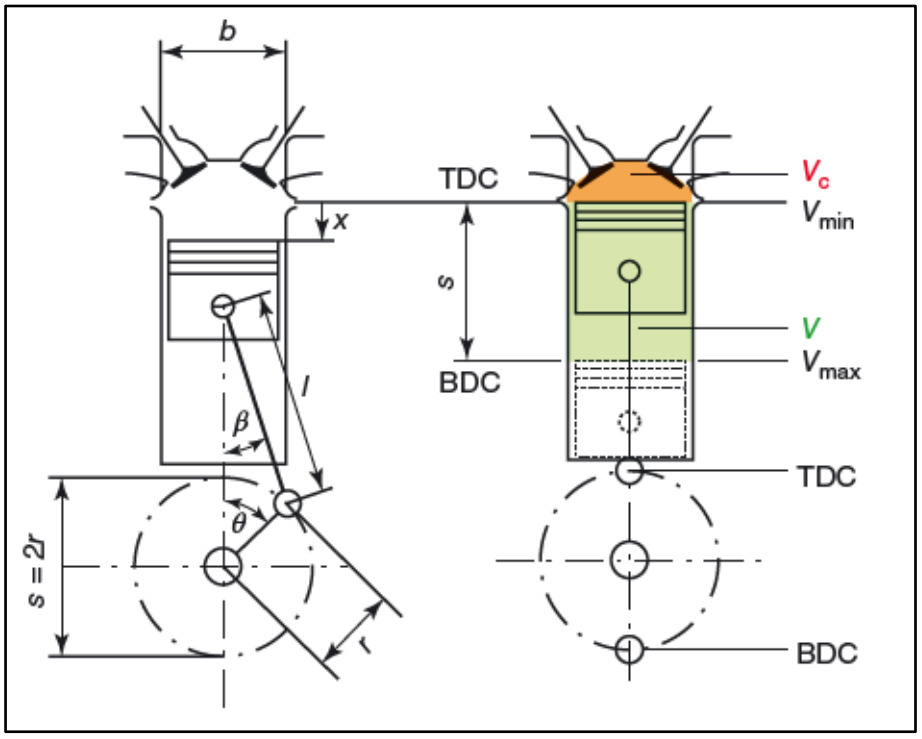

Figure 1. Main geometrical characteristics of a reciprocating ICE [9]

According to the method of ignition criteria, there are two kinds of ICEs currently in production: spark ignition (SI) engines, which are mainly operated with fuel like gasoline and compression ignition (CI) engines, which mainly use diesel fuel. According to the cycle duration criteria, they can be classified as four strokes or two strokes, depending on how many strokes they need to complete a cycle. A cycle is defined by four main processes: intake, compression, combustion and power stroke, and exhaust [10].

While the chemical reactions during combustion are very similar in CI and SI engines, both the supply and ignition of the fuel are quite different. During the intake stage of the spark ignition engine, the fuel – mainly in gaseous state – is mixed with air and induced into the cylinder, where a uniform mixture of fuel, air and residual gases are formed and ready for ignition. During compression, the cylinder can reach temperatures of about 700 K and pressures of about 20 bar. In this condition, the homogeneous fuel-air mixture cannot ignite without an external energy input, usually supplied by a spark provided by a suitable plug [9]. A defined flame front is formed and spreads through the mixture, and the combustion is initiated by means of a transfer of energy from the burned gases zone to the adjacent unburned mixture layers. This phenomenon will generate an increase in pressure in the combustion chamber that will push the piston during the power stroke [11].

Higher propagation speeds of the flame front are achieved when the air/fuel mixture is close to stoichiometric ratio[1]. Therefore, in order to maintain a high flame propagation speed at part load, not only the amount of fuel inducted has to be reduced, but also the inducted air has to be reduced too. Thus, a throttling device is required in order to control the intake load, causing additional efficiency penalties at part load [9].

On the other hand, in a compression engine, air is inducted into the combustion chamber where it is diluted with a small fraction of residual gas. This mixture can reach compression ratios (r_c)[2] between 12 and 20 (higher than the ones typically used in SI engines). Liquid fuel is injected at high velocity, and atomized into small droplets inside the cylinder near the TDC, where it gets vaporized and forms a non-uniform mixture with the hot compressed air. The combustion process starts a few crank angle degrees after the fuel injection, when the local conditions of pressure, temperature and mixing of fuel and air make it possible [11]. Due to the autoignition phenomenon, there are multiple ignition points in CI engines, so the combustion process is spread out in the combustion chamber. Thus, it is not necessary to maintain the air/fuel ratio close to the stoichiometric one to assure a proper flame propagation speed. Therefore, at part load operation conditions, load reduction is achieved reducing the quantity of fuel injected per cycle, without the need of throttling the induced air at a given engine speed [9]. Consequently, the pumping losses are lower than in SI engines.

Performance Parameters:

[1] Stoichiometric ratio: exact ratio between air and flammable gas or vapor at which complete combustion takes place.
[2] Compression ratio (r_c): ratio between the maximum or total cylinder volume and the minimum cylinder volume [8].

- Engine Torque (T): is the ability of the engine to do work. It is normally measured by a dynamometer.
- Brake power (P_b): is the rate at which work is done. The dynamometer absorbed the power (P) delivered by the engine:

$$P = Tn \tag{1}$$

- Gross indicated power (P_{ig}): is the rate of work transfer from the in-cylinder gas to the piston. Besides the brake power, it considers the friction power (P_f), which is the power needed to overcome the engine friction and pumping power, and to drive the engine accessories:

$$P_{ig} = P_b + P_f \tag{2}$$

- Mean effective pressure (mep): parameter useful to compare engines of different sizes. It is the ratio between the work per cycle (W) and the cylinder volume displaced per cycle (V_d):

$$W = \frac{P \cdot n_r}{n} \tag{3}$$

$$mep = \frac{W}{V_d} \tag{4}$$

Similar as the indicated power in equation (2), the indicated mean effective pressure ($imep$) is defined as follows:

$$imep = bmep - fmep \tag{5}$$

- Brake specific fuel consumption ($bsfc$): indicates how efficiently an engine is supplying the fuel to produce work:

$$bsfc = \frac{\dot{m}_f}{P_b} \tag{6}$$

- Air/fuel ratio (A/F): ratio between air flow rate and fuel flow rate inducted during the intake process:

$$\frac{A}{F} = \frac{\dot{m}_a}{\dot{m}_f} \tag{7}$$

- Mechanical efficiency (η_m): ratio between brake or useful power and indicated power:

$$\eta_m = \frac{P_b}{P_{ig}} = 1 - \frac{P_f}{P_{ig}} \tag{8}$$

- Fuel conversion efficiency (η_f): is the work produced per cycle divided by the amount of fuel energy supplied. Where the fuel energy supplied is defined as the mass of fuel supplied per cycle times the lower heating value of the fuel (Q_{LHV}), which is the amount of heat released during combustion:

$$\eta_f = \frac{W}{m_f \cdot Q_{LHV}} \tag{9}$$

- Volumetric efficiency (η_v): defines the effectiveness of the engine intake process. For turbocharge engines, this value can be higher than 1:

$$\eta_v = \frac{\dot{m}_a \cdot n_r}{\rho_a \cdot i \cdot V_d \cdot n} = \frac{m_a}{\rho_a \cdot i \cdot V_d} \tag{10}$$

From the ideal gas law, the density of dry air (ρ_a) can be estimated as a function of pressure and temperature:

$$\rho_a = \frac{p}{R \cdot T} \tag{11}$$

R represents the specific gas constant for dry air $287\ \frac{J}{K \cdot kg}$.

2.2 Diesel Engine Basics

As mentioned previously, unlike SI engines, compression ignition engines spray – at high injection pressures[3] – low volatile liquid fuel directly into the cylinder, few crank angles before combustion occurs. The liquid fuel is atomized into small droplets which after interacting with the compressed hot in-cylinder air and eventually with the hot walls of the combustion chamber, will evaporate. Then, the vaporized fuel will form a heterogeneous mixture with air and a small quantity of residual gas. The combustion method used in these engines depends on an appropriate local air/fuel ratio, that it is not related with the global air/fuel ratio of the cylinder. Therefore, it is possible to regulate the load of the engine just by changing the amount of fuel injected into the chamber without adjusting the inducting air at a specific engine speed [12], therefore without adding additional losses.

An operating cycle of an engine can be represented by plotting the evolution of the in-cylinder pressure (p) against its volume (V) during the cycle. In Figure 2, a typical p-V diagram of a four-stroke CI engine is shown. The processes in a cycle can be divided into compression, combustion, expansion, exhaust and intake [8].

[3] An increase of injection pressure usually reduces the size of fuel droplets, which means better vaporization. This will lead to a better mixing of fuel and air during the ignition period [30].

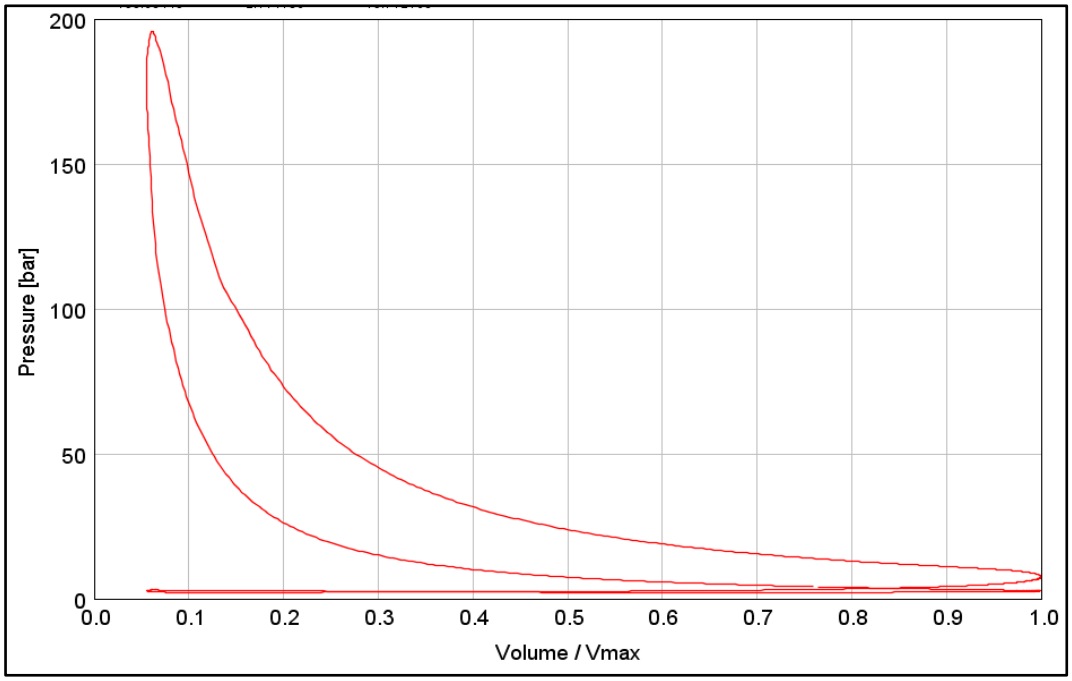

Figure 2. Pressure-Volume diagram of Diesel engine modelled in GT-Power

The ideal cycle has a set of assumptions, but the ones that differentiate the ideal cycles of both CI and SI engines are the following:

- The ideal cycle for a CI engine is called constant-pressure cycle (Otto ideal cycle), where the combustion is assumed to be slow and late.
- The ideal cycle for a SI engine is called constant-volume cycle (Diesel ideal cycle), where the combustion is assumed to be infinitely fast.

The pressure-volume diagram as well as the temperature-entropy diagram for both Otto and Diesel combustion cycles are illustrated in Figure 3.

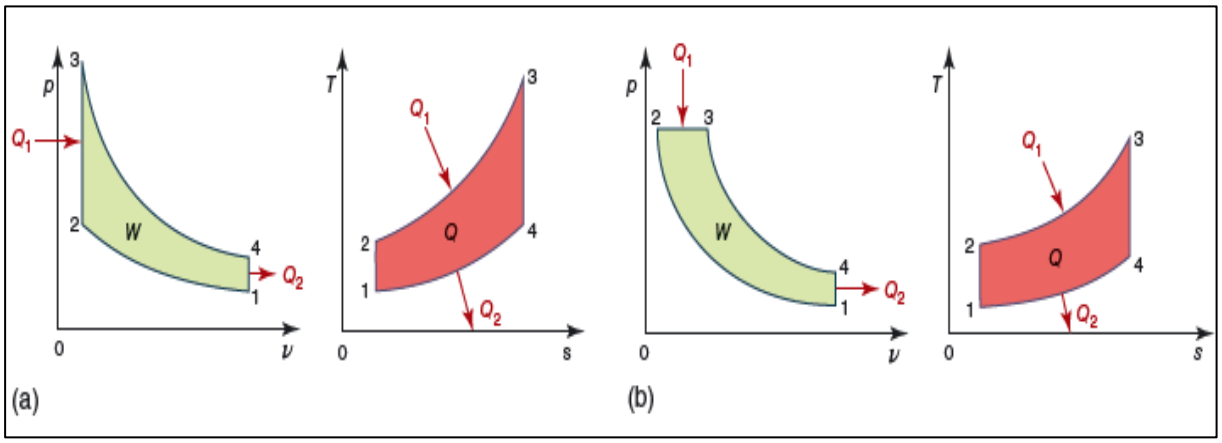

Figure 3. p-V diagram of (a) Constant-Volume cycle and (b) Constant-Pressure cycle [9]

In these ideal cycles, the working fluid is assumed to be an ideal gas, with the specific heats (c_p and c_v) constant during the whole operating cycle. The ideal fuel efficiency for both cycles are defined as follows:

- Otto ideal cycle:

$$\eta_{id,otto} = 1 - \frac{1}{r_c^{\gamma-1}} \tag{12}$$

- Diesel ideal cycle:

$$\eta_{id,diesel} = 1 - \frac{1}{r_c^{\gamma-1}} \cdot \frac{\beta^{\gamma} - 1}{\gamma(\beta - 1)} \tag{13}$$

Where γ is the specific heating ratio c_p/c_v, and $\beta = T_3/T_2$.

For a given r_c, the spark ignition cycle has a higher fuel conversion efficiency than the Diesel cycle as shown in equation (12) and (13). In addition to this, as illustrated in Figure 4 by increasing the compression ratio, the efficiency in both cycles improves [13]. Although, in order to avoid the phenomenon of knock[4], the r_c in SI engines has to be limited. On the other hand, for CI engines, because the fuel is injected just before the desired start of combustion, there is no risk of knock. Therefore, they can operate at a higher r_c which results in higher efficiency.

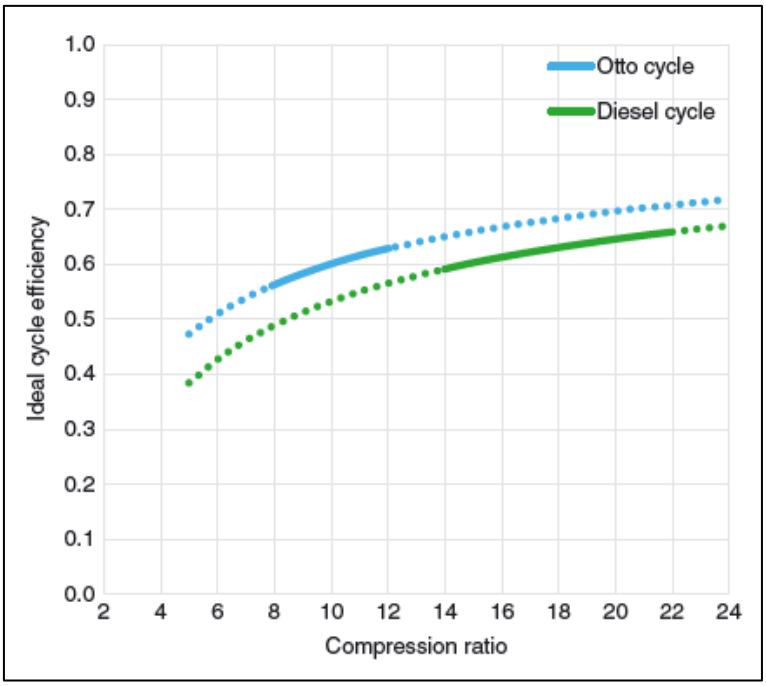

Figure 4. Fuel conversion efficiency as a function of compression ratio [9]

However, the higher the compression ratio, the higher the leakage, as well as mechanical losses such as friction in the crankshaft mechanism or between the piston and liner, and torque needed for starting. CI engines undergo higher temperatures and pressures than SI engines, therefore more robust designs are used which encompass heavier engines.

[4] Knock is an abnormal combustion phenomenon. It happens when a fraction of the air-fuel mixture autoignites before the flame front arrives.

2.2.1 Combustion in Diesel Engines

Compression engines can be classified into two basic categories according to their injection systems:

- Indirect Injection (IDI): The combustion chamber is separated in two volumes. The two regions are connected by a small aperture. The fuel passes to the main-combustion chamber after it is injected into the pre-chamber.
- Direct Injection (DI): the fuel is injected directly into the combustion chamber. The fuel is injected at high pressures to assure proper atomization and spread in the chamber to reach suitable local conditions for the combustion process.

The development of electronic control, strict emission regulations and increased demand to reduce fuel consumption without compromising output power, has led the automotive industry to focus its research and development in the electronically controlled, turbocharged, direct injection systems [5].

The typical CI diesel combustion process is characterized by the appearance of two types of flames: in the first stage of combustion, premix flames are present, followed by diffusion flames in the next phase. Figure 5 describes the evolution of diesel combustion according to the progression of both fuel injection and fuel burn rates. Four main stages can be defined in the compression ignition combustion process:

1. Ignition delay
2. Premixed or rapid combustion phase
3. Mixing-controlled or fast diffusion-controlled combustion phase
4. Late or late diffusion-controlled combustion phase

For simplification, key concepts are briefly defined as follows:

- Injection time: the time between the start of fuel injection into the combustion chamber and the end of its flow from the injector nozzle.
- Injection angle: the crank angle range between the start of injection and the end of injection.
- Delay period: the time between the start of injection and the first appearance of flame, pressure rise or heat release rise.
- Delay angle: the crank angle corresponding to the delay period.

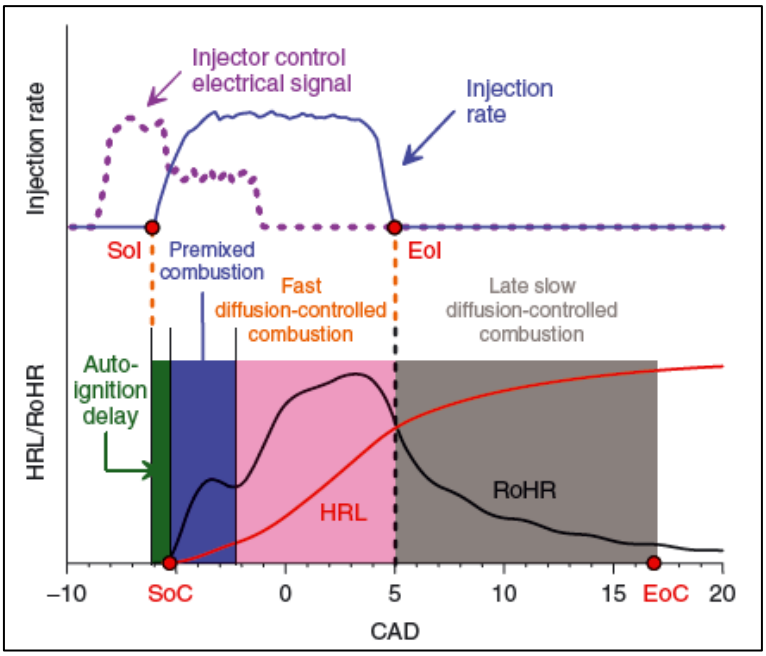

Figure 5. Injection-controlled DI engine injection event and heat release rate diagram [5]

1. Ignition delay: this first stage corresponds to the period between the start of fuel injection (SOI) into the combustion chamber and the start of combustion (SOC). It is not only the time the fuel needs to be atomized, evaporated and mixed with air to form an ignitable gaseous air-fuel mixture inside the piston, but also the chemical delay associated with the precombustion process of this mixture at the given thermodynamic conditions. The delay period is practically independent of engine speed, as the kinetics of the autoignition is much slower than the physical processes, hence the chemical process has a bigger weight controlling the duration of this delay period [13] [5]. Thus, the engine speed for CI engines are limited to operate at speed no higher than 5000 rpm.
2. Premixed combustion phase: this is the first stage of the combustion reaction. The air-fuel mixture that reaches the limit for autoignition burns rapidly in few crank angles. When combustion starts, the physical and chemical processes speed up due to both the temperature increment and the multiplicities of ignition points, causing an almost immediate burning of the air-fuel mixture - which during this period becomes ready to ignite. These high heat release rates result in a sharp pressure rise, causing vibrations in the structure and the typical engine noise. Figure 6 shows the effect of the ignition delay on both the pressure rate and pressure magnitude during this second phase. When the injection angle is larger than the delay angle, just a small portion of fuel has ignited. On the other hand, when the injection period is shorter than the autoignition delay, a bigger portion of the mixture has burnt. The amount of energy released, and therefore the amount of fuel burnt, depends on the length of the ignition delay and the quantity of injected fuel during this period [8] [13] [14].

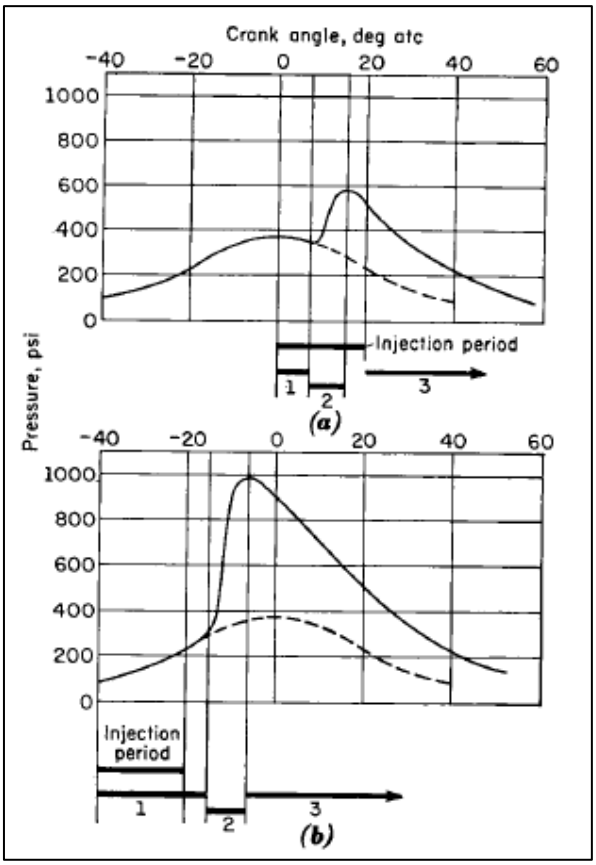

Figure 6. . Combustion stages (a) injection period longer than ignition delay, (b) ignition delay longer than injection period. 1=ignition delay, 2=rapid combustion phase, 3=mixing and late combustion phases [13]

3. Fast diffusion-controlled combustion phase: This stage occurs mainly when the fuel is still being injected after the rapid combustion phase (when the delay time is longer than the injection time, this combustion phase will involve only the fraction of fuel which has not found the necessary amount of oxygen during the previous stage). Once all the air-fuel mixture cumulated during the ignition delay has been burned in the premix phase, the heat release rate is now controlled by the rate at which mixture becomes available for burning. In this stage the chemical reactions are much faster than the physical processes which involves the fuel atomization, evaporation and mixing, thus the combustion process is controlled by the mixing process. There is not a sudden peak of pressure, but rather the heat release rate may reach a lower second peak and then decreases [8] [13].
4. Late diffusion-controlled combustion phase: This period starts after the end of injection, during the expansion stoke when the spray momentum flux dissipates, the mixing rate of fuel and air decreases, the chemical kinetics becomes slower as the in-cylinder temperature decreases. Subsequently, both the heat release rate and burn rate fall. There are several reasons for the appearance of this heat release during this period - a small fraction of the fuel may have not burned yet or a fraction of soot and fuel-rich combustion products energy can still be released, among others [8] [5] [13].

2.2.2 DEC's model

By means of advanced optical techniques, a conceptual model describing the evolution of the combustion in direct injection diesel engines was developed at Sandia National Laboratories by John E. Dec. In his research, for the liquid-phase fuel, he observed that the liquid fuel length of the jet did not depend on the heat release, as it remained constant prior to the start of combustion. Therefore, the liquid-phase penetration is not limited by the combustion heating, but by the evaporation of the fuel due to the compressed hot air that is entrained to the fuel jet. This can be observed in Figure 7, where the liquid penetration reaches its maximum at 3.0° after the start of injection (ASI), while the heat release for the same experiment occurs at 4.0° after the SOI, as shown in Figure 8 (SOI occurs at 11.5° before top dead center (BTDC), while the heat release starts at 7.5° BTDC) (this quantitative information applies only for the operating conditions used during his tests). Associated with this observation, is that it is possible to infer that increasing the inlet temperature will decrease the maximum penetration (fuel vaporization occurs faster). Also, increasing the inlet pressure results in a decrement of the maximum liquid penetration, as the density increases, mass of air increases, the enthalpy increases, so the vaporization is promoted. In addition, the liquid fuel penetration depends on the size of injector holes, as when it increases, the liquid length increases too. It is important to know the liquid penetration in order to avoid the impregnation of the in-cylinder wall by the fuel jet [15] [16].

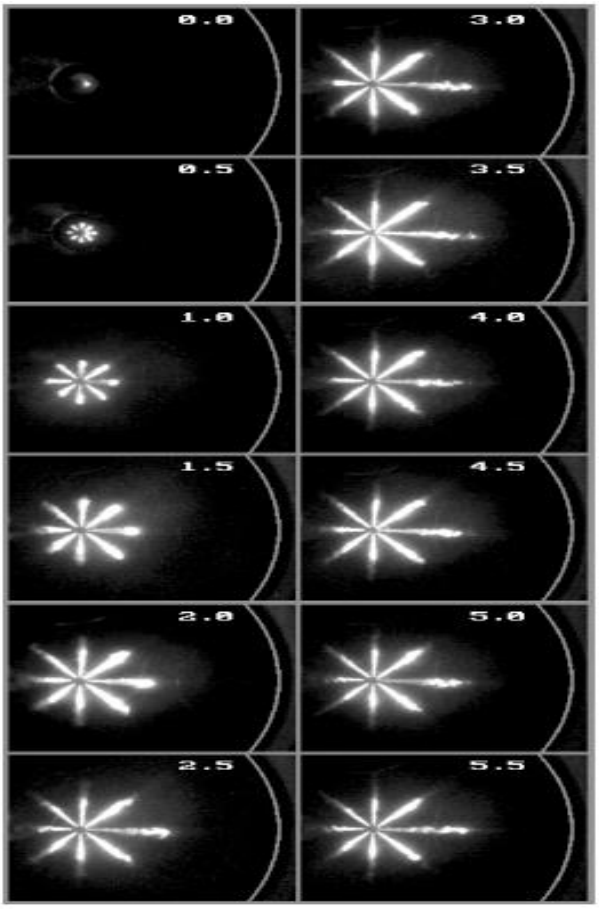

Figure 7. Elastic-scatter liquid-fuel imaging [15]

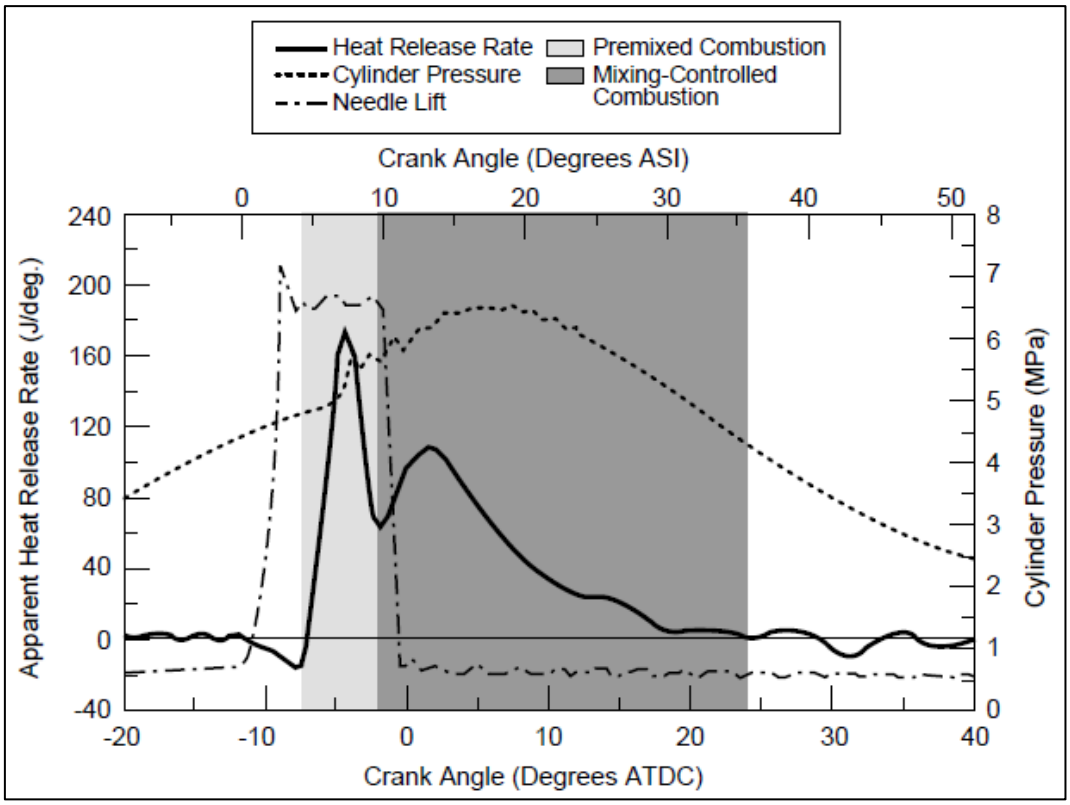

Figure 8. Apparent heat release, cylinder pressure and injector needle lift [15]

On the other hand, the vapor-phase fuel continues to penetrate after the maximum liquid penetration. Downstream of the liquid jet, the vaporized fuel and air is well mixed to an equivalence ratio[5] between 2 and 4. In other words, the initial premix combustion occurs under a rich mixture environment, even if the overall mixture inside the chamber is extremely lean. A conceptual model of the direct injection diesel combustion is illustrated in Figure 9 which represents the idealized cross section on the mid-line of the jet. Figure 9 schematizes the temporal evolution of the diesel fuel jet from the start of injection until the first part of the mixing controlled burn (this temporal sequence applies only for typical operating conditions). Varying the operating conditions (i.e. turbocharge boost, EGR, injector characteristics, among others) can change the spatial and temporal scaling [15]. The evolution of the combustion is synthetized as follows:

- Initial jet development (0.0° to 4.5° ASI):
  At 1.0° ASI, the fuel emerges from the injection tip. At this moment there is only a liquid fuel. The surrounded air is entrained and starts to mix with the liquid fuel. Then at 2.0° ASI the liquid region increases its penetration in the cylinder, while the vapor-fuel region starts to appear along the sides of it. At 3.0° ASI the liquid jet reaches maximum penetration (the entrained hot air starts to vaporize all the fuel at this point). At this point, the first appearance of chemiluminescence is present, which means that the combustion starts with its prereactions. At 4.5° ASI the gas region keeps penetrating beyond the liquid phase with ϕ between 2 and 4 [15].

[5] The equivalence ratio (ϕ) is defined as the ratio between the stoichiometric ratio (λ_{st}) and the air/fuel ratio (λ). If $\phi > 1$ there is a rich air-fuel mixture, if $\phi < 1$ there is a lean air-ful mixture.

- Autoignition and first part of premixed burn spike (4.0° to 6.5° ASI):
  The precise moment in which the ignition occurs is not well defined temporally or spatially. At 4.0° the heat release starts to increase slightly, however, between 4.5° and 5.0 °ASI the rapid heat release rise develops (see Figure 8). The autoignition is very likely to occur in this angular range. At 5.0° ASI the fuel breakdown and poly-aromatic hydrocarbons (PAH) are formed around the leading part of the jet (PAHs are the precursors of soot). This moment coincides with the rapid rise in pressure from the premixed burn. At 6.0° ASI small particles of soot begin to form and spread (with the PAH) downstream the fuel jet. Soot formation is an outcome of the fuel-rich premixed burn. At 6.5° the PAH evolves to soot and a vast fraction of the vapor-fuel region is formed by soot [15].

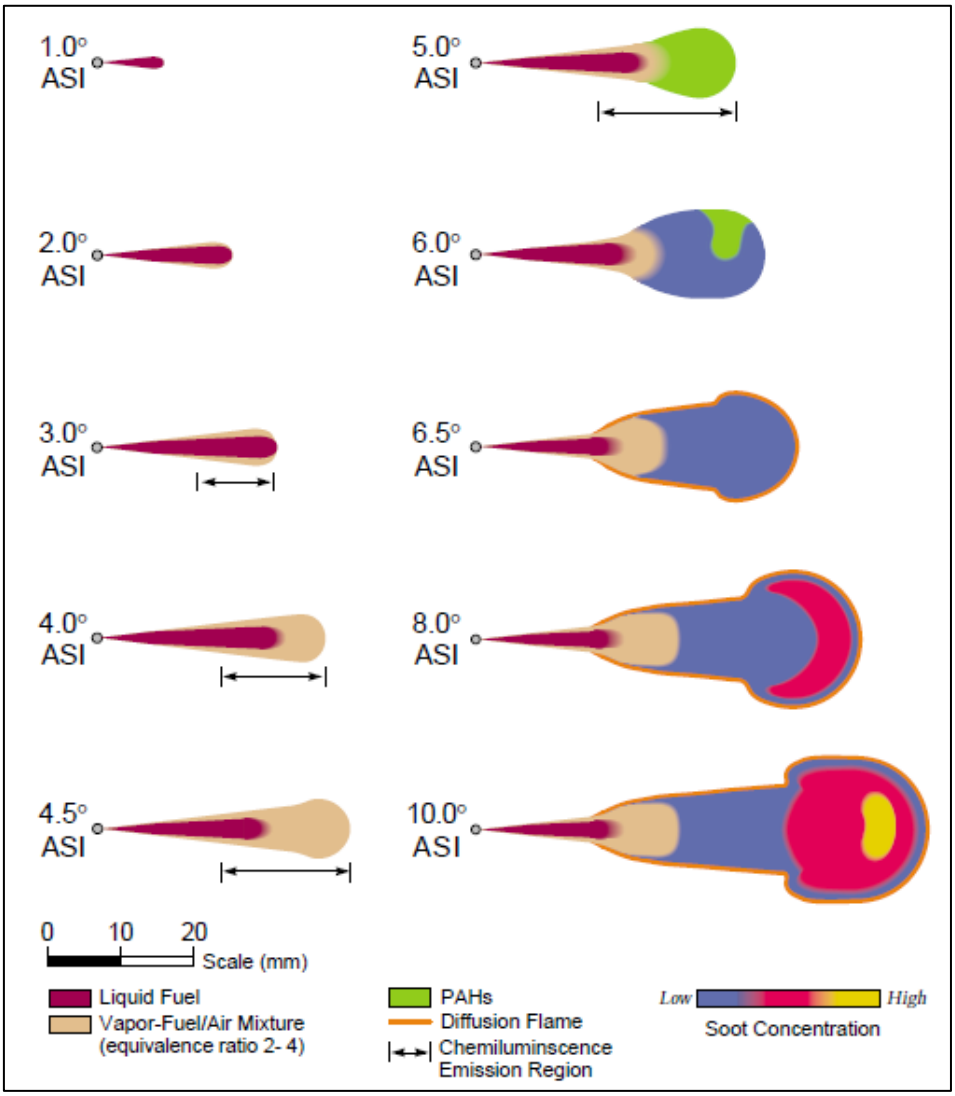

Figure 9. DEC's conceptual model for DI diesel combustion [15]

- Onset of the diffusion flame (5.5° to 6.5° ASI):
  Between 5.5° to 6.5° ASI, the diffusion flame appears at the periphery of the jet, between the products of the premixed combustion and the surrounding air. As the diffusion flame forms, local heating makes the liquid jet becomes shorter [15].

- Last part of premixed burn spike (7.0° to 9.0° ASI):
  The jet keeps growing and penetrates throughout the chamber, while the soot concentration keeps incrementing in the soot region. Upstream of the jet, in the vapor-phase, a head vortex is formed, where a high soot concentration region can be found (this can be observed at 8.0° ASI). While the larger soot particles are located at the tip of the jet, the medium particles are found in the periphery, while the smallest ones are in the central region [15].
- First part of the mixing-controlled burn (9.0° ASI to end of injection):
  The overall appearance of the jet and soot distribution pattern remains almost constant until the end of the fuel injection. The jet penetrates further and the vortex is well formed. At the vortex, the soot concentration increases even more and the size of the particles in this region have grown (see 10.0° ASI). The medium size soot particles, caused by the diffusion flame, are still present at the periphery, while the smaller soot particles remain in the central area [15].

The diffusion flame is characterized by the presence of high concentrations of OH radicals. After the end of injection, some of the soot particles that formed during the combustion process reach the diffusion flame on the periphery of the jet where they are oxidized by OH radical attack. The soot oxidation zone (prior to the end of injection) is illustrated in Figure 10. In addition, when the injector is closing, the velocity of the last fuel droplets exiting the nozzle holes can decrease, negatively affecting the atomization, therefore the mixing too. This will lead to a significant amount of soot formation and soot particle growth, which will contribute to the soot that will not oxidize at the end of the combustion. It is thought that this soot is a main contributor of tailpipe soot emissions [16]. On the other hand, NO formation is expected on the lean side of the diffusion flame, because of the high temperatures and the large amount of oxygen available. However, as the thermal NO production is a relatively slow process, NOx formation will be formed at the end of the mixing controlled burn and in the hot air region that remains after the end of combustion [15].

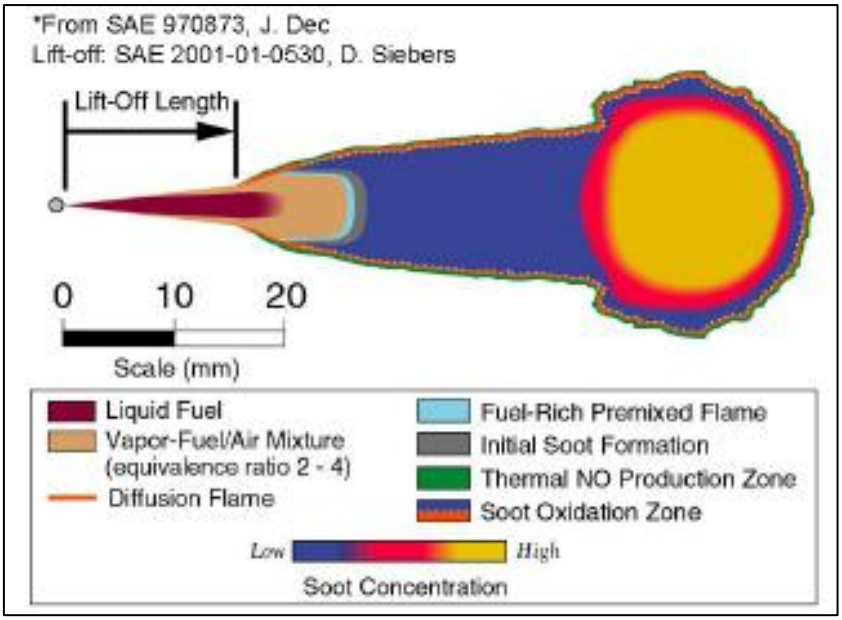

Figure 10. Schematic of the mixing controlled burn [16]

2.2.3 Injection Strategies in Diesel Engines

Recent improvements in the common rail fuel injection system have enabled higher injection pressures and more flexible control of injection strategies. The rise in injection pressure improves the atomization quality and air entrainment, and as consequence, there is an improvement in fuel consumption and a decrease in soot formation. However, this also increases the injection rate which in turn increases the fast burning premixed combustion phase. This leads to an increment of NOx emissions and higher peak pressure which is translated into higher combustion noise [14].

Splitting the head release into multiple events in order to reduce the peak heat release has been an approach used to reduce engine noise and emissions. As a result, multiple injections have become a common control strategy used in modern DI diesel engines. Multiple injections can be divided in pre-injections (or pilot injections), main injection and post-injections, as shown in Figure 11. The pilot injections are added to reduce the combustion noise, while the post-injections are used to reduce soot emissions [17].

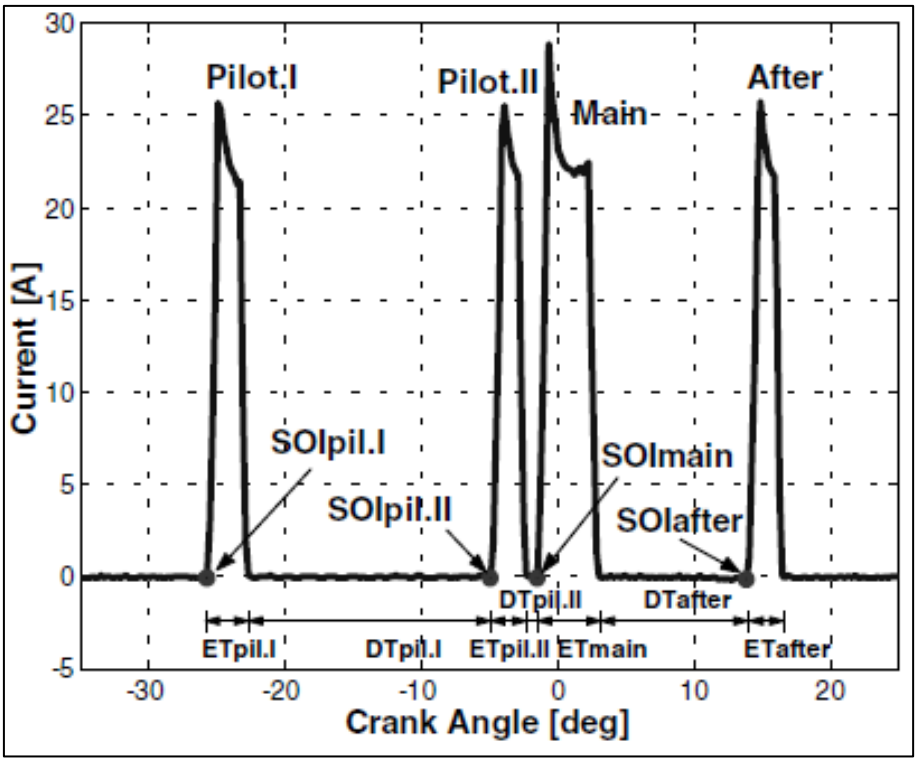

Figure 11. Multiple injection strategy [17]

Usually, early injections, also called pilot injections, consist of small quantities of fuel injected prior to the main injection. The combustion of the pilot injection increases the bulk temperature and the pressure inside the combustion chamber, resulting in a reduction in the ignition delay of the following injection. Shortening the ignition delay of the main injection results in a decline in the burn fuel fraction during the premix combustion, and a reduction in the rate of pressure rise. As a consequence, the combustion noise is improved [18]. Although the NOx formation during the premix combustion is not significant, the high pressure and the temperature the

cylinder reaches during this phase encourages the oxidation of nitrogen during the diffusion burning phase. Thus, the effect of the pilot injection on the initial rate of heat release is of great importance for NOx formation [14]. Depending on the quantity of fuel injected and the timing of the pilot injection, NOx formation may vary too, as well as particulate emissions [18] [19]. Figure 12 shows the effect of the pilot-injection on the heat release and the combustion noise.

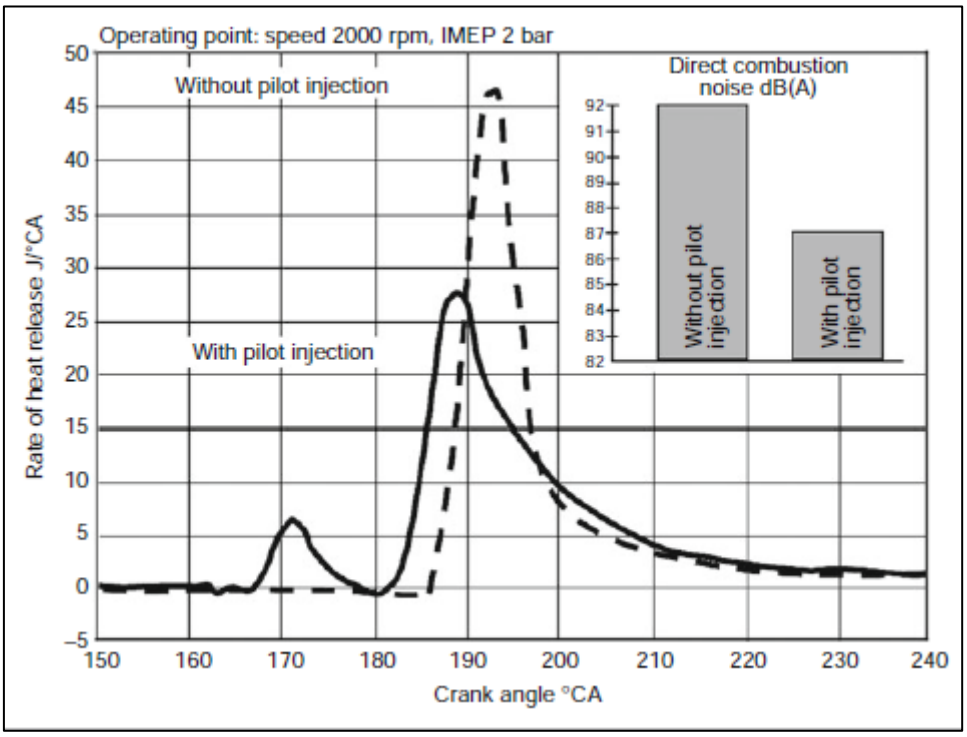

Figure 12. Effect of pilot-injection on heat release rate and combustion noise [20]

The late injection, also called post-injection, is a short injection that follows the main injection that is used during the expansion stroke, for aftertreatment purposes. The temperature generated by the post-injection combustion promotes the oxidation of the soot (produced from the combustion of the main injection). In addition, the turbulence created by post-pulse enhances mixture of air with the fuel from the main injection, thereby enhancing the soot oxidation, while burning the post injection fuel [21].

In addition, the timing of the post-injection has to be selected very carefully. If the dwell time[6] (DT) between the main injection and post-injection is too short, soot emission increase because of the cooling effect of the post-injection on the temperature of the main combustion. On the other hand, if the post-pulse is administered when the expansion stroke is too advanced, then the temperature will be too low to promote the oxidation of soot, and therefore, soot formation will increase [17].

The dependence of temperature and ϕ of NOx and soot formation is shown in Figure 13.

[6] Dwell time (DT) is the time between electric signals (see Figure 11).

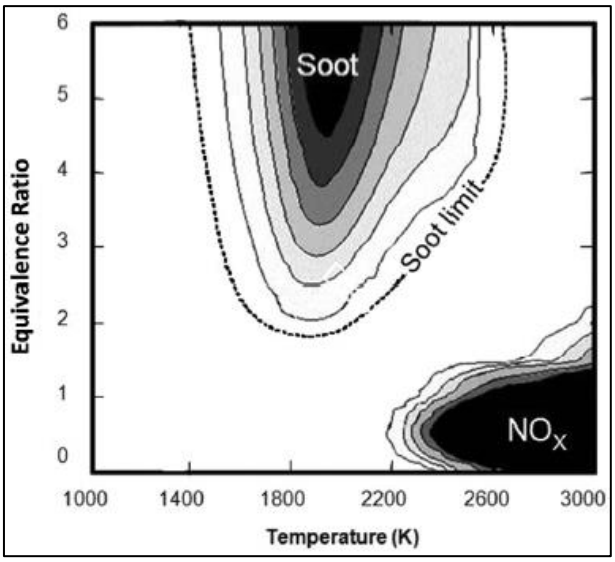

Figure 13. Equivalence ratio and temperature effects on soot and NOx formation [22]

When the dwell time between two pulses is very small, and the dwell time is shorter than the nozzle closing delay, there is a fusion of the fuel injected as shown in Figure 14. The injection fusion has to be avoided, unless the purpose is to create an injection rate shaping [16].

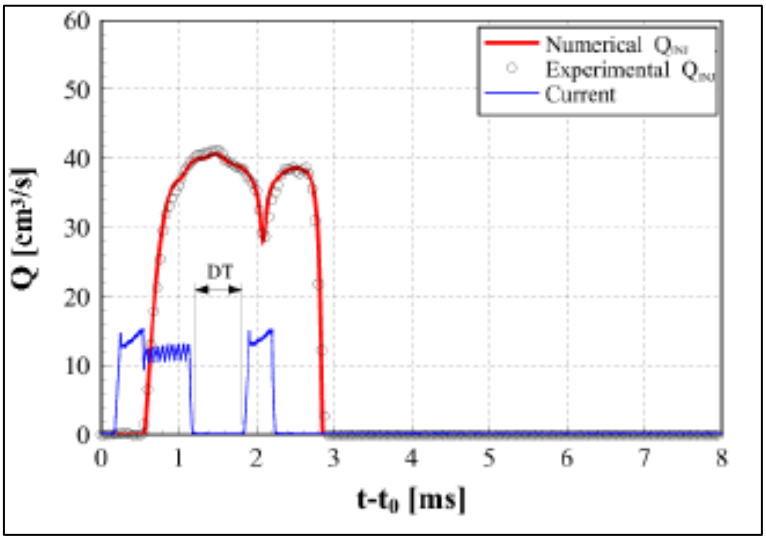

Figure 14. Injection fusion [16]

The injection rate shaping is another injection control strategy used in diesel engines. It consists of the modulation of the injection fuel rate with the aim of changing the heat release rate. This can be achieved through controlling the injection pressure or the injector needle lift. A single shot can be shaped as a rectangular, ramp or boot pattern. The boot injection consists of a low rate of injection at the beginning, followed by a higher injection rate. The difference between this strategy and the use of a pilot injection, is that boot injection is a continuous single shot rather than two or more interrupted pulses. Similar to the pilot injection, the purpose of the initial low rate injection is to limit the amount of fuel in the premix combustion, therefore reducing the heat release gradient of this phase. This brings about a reduction in combustion noise. Regarding pollutant emissions, limiting the initial heat release results in a restriction in NOx formation. During the controlled combustion, the flow is increased in order to enhance

mixing and reduce soot emissions [23] [24]. Figure 15 shows the injected flow rate pattern of a boot injection.

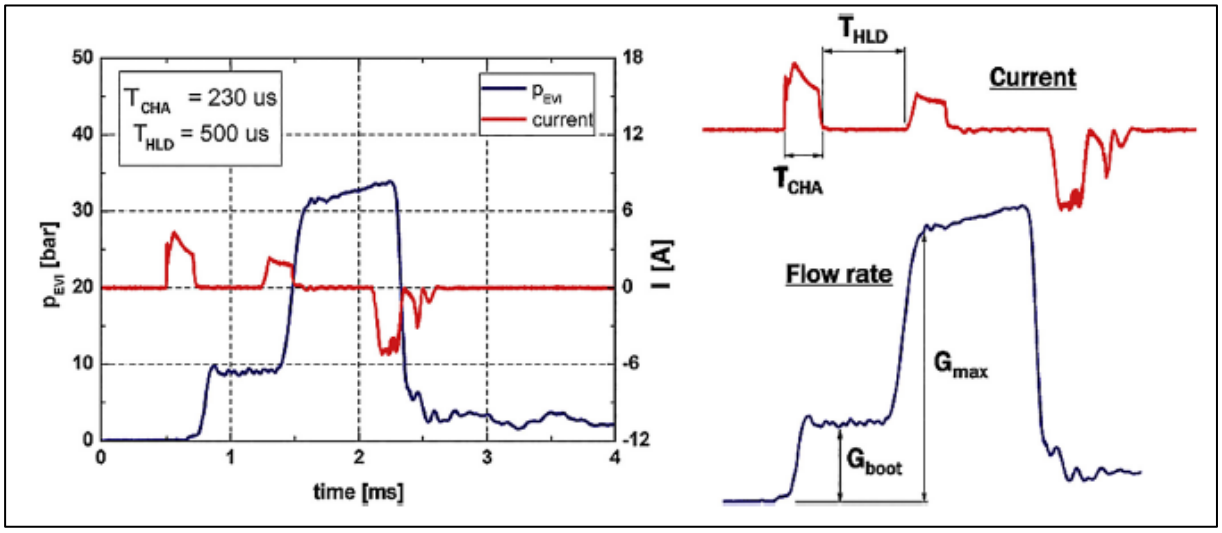

Figure 15. Boot injection [23]

2.3 Modelling in GT-Power

GT_SUITE is a 0D/1D/3D multi-physics CAE system simulation software developed by Gamma Technologies, used for full vehicle design and analysis. The library developed for engine simulation is GT-Power.

GT-POWER solver is based on one-dimensional solution of the fully unsteady, nonlinear Navier-Stokes equations. It employs thermodynamic and phenomenological model solvers to capture the effects of combustion, heat transfer, evaporation, in-cylinder motion and turbulence, and engine and tailpipe out emissions, among others [25].

The one dimensional fluid dynamics simulation, represents the flow and heat transferring within the components of the engine system. Each component of the system is discretized into one or more volumes. Each volume is connected to the others by boundaries. The fluid's scalar variables (e.g. pressure, temperature, enthalpy, etc.) of each volume are assumed to be constant, while for each boundary the vector variables (e.g. mass fluxes, velocity, etc.) are estimated [26]. Figure 16 illustrates the discretization performed by the software.

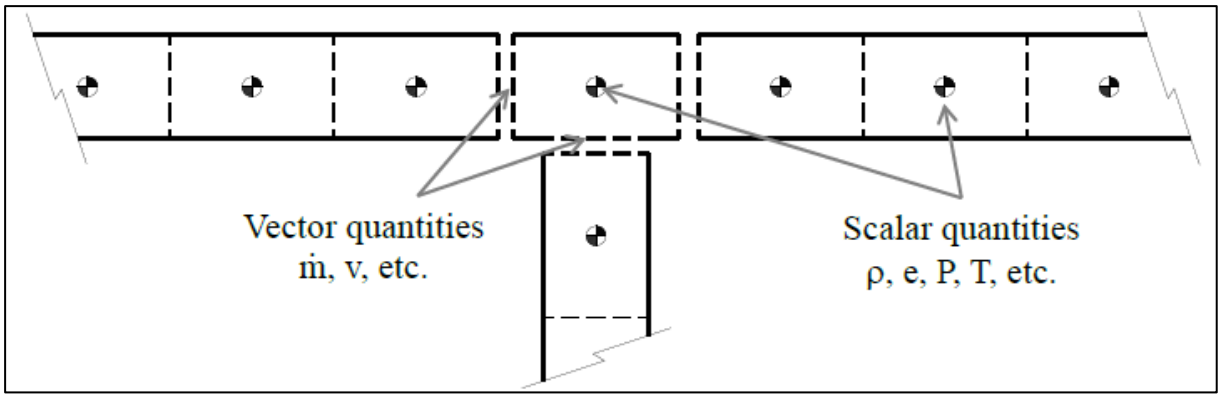

Figure 16. GT-SUITE discretization of components [26]

GT-Power counts with different combustion models, mainly depending on the intended use of the complete simulation model. Two kinds of these combustion models are:

- Non-Predictive Combustion Model: burn rate is imposed as an input of the simulation.
- Predictive Combustion Model: combustion rate is predicted from the inputs (such as pressure, temperature, air/fuel ratio, etc.), and then applied in the simulation.

2.3.1 Non-Predictive Combustion Model

In this simulation, the burn rate is imposed either as a function of crank angle or according to a prescribed Wiebe function. This burn rate is followed independently of the in-cylinder conditions, always ensuring that there is enough fuel to support the burn rate. In other words, the burn rate will not be affected by factors such as injection timing or residual fraction, among others. This model is appropriate when the intended use is to study a variable that has low impact on the burn rate, for instance exhaust configuration, acoustic performance of different muffler designs, to mention a few [27].

For this project, the burn rate is imposed as a function of the crank angle, because this method is more suitable to use as the in-cylinder pressure among other measurements were provided from Fiat Powertrain Technologies (FPT). GT-Power has the template 'EngCylCombProfile' which is very useful when the cylinder pressure is provided, as it calculates the burn rate from the measured cylinder pressure. There are two methods used by the software for this estimation:

- Three Pressure Analysis (TPA): requires the intake, exhaust and cylinder pressures.
- Cylinder Pressure Analysis Only (CPOA): only need the measured cylinder pressure.

2.3.1.1 Engine Burn Rate Analysis

In GT-Power the combustion rate is defined by the burn rate. The burn rate is the instantaneous rate of fuel consumption within the cylinder combustion process. This occurs when the molecules of the air/fuel mixture passes from the unburned zone to the burn zone and begin to participate in the combustion process.

The calculation of the burn rate from the measured cylinder power is referred to as *reverse run combustion calculation.* In the reverse run, the input of the simulation is the measured pressure

while the output is the apparent burn rate[7]. Instead, in a *forward run combustion calculation*, the input of the system is the burn rate while the in-cylinder pressure is the output. Both forward and reverse run calculations use the two-zone combustion equations [27].

The two-zone combustion model is composed by two different zones. The first one integrated by fresh air, residual gases and unburned fuel (in gaseous state for simplification), defines the unburned mixture. The second one, describes the burned mixture and consist of the burned fuel with fresh air and residual gases. The flame front is the separation between these two zones. During combustion, the elements from the unburned zone enter into the flame front where the primary oxidation takes place and then passes to the burn zone. The chemical reactions of the products of the incomplete oxidation of the primary oxidation take place in the burn zone [28].

2.3.1.1.1 Cylinder Pressure Only Analysis (CPOA)

CPOA calculates the burn rate for a specific operating point from the measured cylinder pressure along with the cylinder geometry and few engine performance parameters. To perform this analysis, a simple model can be used. This model has to include a cylinder block, an engine block and an injector block.

For the analysis of the measured pressure, the model run 2 cycles, therefore it is of major importance to be very careful setting the initial conditions. It is necessary to have particular aware of four parameters:

- Combustion chamber wall temperatures, composed by cylinder wall, piston wall and cylinder head.
- Volumetric efficiency.
- Air trapping ratio of the cylinder, which is the ratio of the air trapped in the cylinder to the air delivered to the cylinder. Typically, this value is 1.0, unless there is a significant valve overlap, in this case the value will be lower than 1.0.
- Residual gas fraction trapped at intake valve closing (IVC) which consists on the burned exhaust products trapped for the combustion process. It includes both trapped residual gases and inducted EGR gases.

Note that if instantaneous measurements of intake and exhaust port pressures are available from the engine test, a three-pressure analysis (TPA) simulation can predict the residual fraction. Please refer to the Engine Performance modeling application manual for more details on TPA.

As it is a reverse run calculation, GT-Power iterates the transfer of fuel from the unburned zone to the burn zone in each time step until de simulated pressure trace matches the measured cylinder pressure [27].

[7] Apparent burn rate is a specific term of GT-Power, it is the burn rate needed to be imposed in a non-predictive model to reproduce the measured cylinder pressure.

The main limitation of this method is that the latter two parameters are very difficult to measure in a test cell, therefore it may be necessary to estimate them. Meanwhile the advantage of this procedure is that it is fast and just requires the measured pressure trace of the cylinder.

2.3.1.1.2 Three Pressure Analysis (TPA)

TPA estimates the burn rate for a specific operating point, three different pressure measurements are required as input: the intake pressure, the cylinder pressure and the exhaust pressure. Besides the blocks mentioned in the CPOA, this model also has to include both intake and exhaust valves, as well as intake and exhaust ports.

The advantage of this method is that there is no need to set the trapping ratio nor the residual fraction as inputs, because they are going to be calculated. Additionally, it can analyze the system either in steady-state operating conditions over a single cycle or cyclic variations over multiple consecutive cycles. These types of analysis are referred as 'TPA steady' and 'TPA multicycle' respectively.

2.3.2 Predictive Combustion Model

When the intention of the simulation is to study variables that have a direct and big impact on the burn rate, the recommended combustion model to use is the predictive one, rather than the non-predictive one. In this case, because the burn rate is not imposed, a variation of the variable of interest will affect the outcome of the simulated burn rate. For example, a simulation in which the mass injection profile and quantity vary depending on the operating points of the engine, would need predictive capabilities to obtain reliable results, as the burn rate depends strongly on injection quantities. Predictive combustion models require higher computational time than non-predictive models, because they typically require calibration to measurement data in order to provide accurate results [27].

GT-Power has developed four different predictive combustion models:

- Spark-Ignition Turbulent Flame Model (SITurb)
- Direct-Injection Diesel Multi-Pulse Model (DIPulse)
- Direct-Injection Diesel Jet Model (DIJet)
- Homogeneous Charge Compression Ignition Model (HCCI)

The full engine model provided by FPT for this project is a direct injection diesel one, and the predictive models than can be used are the DIJet and DIPulse. Gamma Technologies recommends the use of the latter over the first one due to its benefits regarding the computational time without compromising its predictive accuracy.

2.3.2.1 Direct-Injection Diesel Multi-Pulse Model (DIPulse)

This model predicts the in-cylinder combustion and related emissions for direct injection diesel engines with single or multi-pulse injection. The DIPulse model uses a multi-zone combustion

model, as shown in Figure 17. This predictive diesel model divides the cylinder content into three thermodynamic zones, each with their own temperature and composition [27]:

- Main unburned zone (MUZ): includes all cylinder mass at IVC
- Spray unburned zone (SUZ): contains injected fuel and entrained gas
- Spray burned zone (SBZ): consists of combustion products

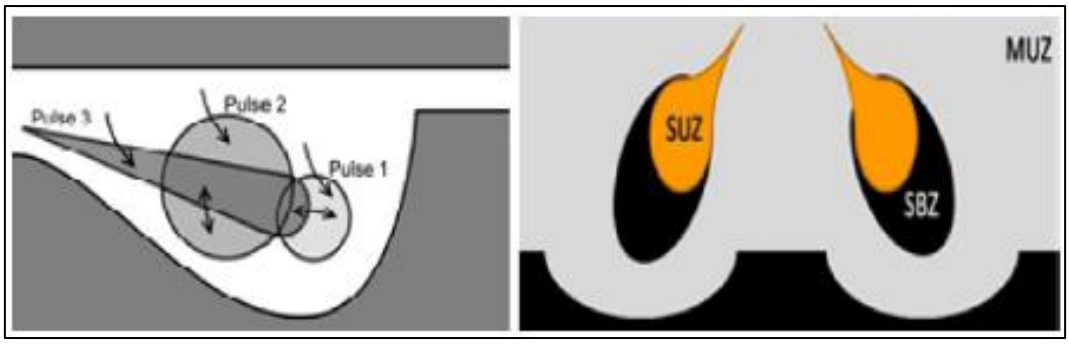

Figure 17. DIPulse multi-zone combustion [7]

The DIPulse model's basic approach is to track the evolution of each fuel injection event (or pulse) separately from all other pulses as it evaporates, mixes with surrounding gases, and burns. The injected fuel is added to the SUZ (see Figure 17). This predictive model uses different sub-models to simulate physical processes that occur during the combustion event, such as the atomization and evaporation of the fuel droplets and the mixing of the evaporated fuel and entrained gas. In the 'EngCylCombDIPulse' template, which contains the DIPulse model, there are four attributes or multipliers which are used for the calibration of the combustion model (see Figure 18) [27]. These multipliers control the main phases of the combustion event, from spray penetration to diffusion combustion.

Main | Emissions

Attribute	Unit	Object Value
Model Version		v2017
Entrainment Rate Multiplier		[entrain] ...
Ignition Delay Multiplier		[igndelay] ...
Premixed Combustion Rate Multiplier		[premix] ...
Diffusion Combustion Rate Multiplier		[diffusion] ...

Figure 18. DIPulse calibration multipliers

The DIPulse multipliers are described as follows:

- Entrainment Rate Multiplier: this parameter describes the spray penetration and the fuel mixing with the surrounding environment. When the injection event occurs, the injected fuel slows down due to the interaction between both the unburned and burned gases and the fuel jet. Also, for multi-pulses, the mixing between them occurs through

entrainment. By means of an empirical spray penetration law, it is possible to calculate the entrainment rate by applying conservation of momentum, as follows [27] [4]:

$$m_{inj}u_{inj} = \left(m_{inj} + m_a\right) \cdot u \tag{14}$$

Where m_{inj} is the injected fuel mass, u_{inj} is the injection velocity at the nozzle tip, m_a is the entrained mass of air, $u = \frac{dS}{dt}$ and S is the spray tip penetration. By rewriting equation (14), it can be seen that the entrained air is inversely proportional to the final velocity, as shown in equation (15):

$$m_a = \frac{m_{inj}u_{inj}}{u} - m_{inj} \tag{15}$$

Therefore, the entrainment rate can be estimated as follows:

$$\frac{dm}{dt} = -C_{ent}\frac{m_{inj}u_{inj}}{u^2}\frac{du}{dt} \tag{16}$$

The entrainment rate can be modified by the Entrainment Rate Multiplier (C_{ent}).

- Ignition delay multiplier: as mentioned in section 2.2.1, the ignition delay (τ_{ign}) is the time between the start of injection and the start of combustion. The ignition delay is estimated for each pulse with an Arrhenius expression that can be modified by the Ignition Delay Multiplier (C_{ing}) [27]:

$$\tau_{ing} = C_{ing}\rho^{-2}\exp\left(\frac{3000}{T}\right)[O_2]^{-0.5} \tag{17}$$

Where $[O_2]$ is the oxygen concentration, T is the pulse temperature and ρ is the gas density. Ignition occurs when:

$$\int_{\tau_0}^{\tau_{ing}} \frac{1}{\tau_{ign}}dt = 1 \tag{18}$$

- Premixed combustion rate multiplier: as mentioned in section 2.2.1, this is the first stage of the combustion event, in which the fuel accumulated during the ignition delay phase reaches ignitable conditions and burns abruptly. The Premixed Combustion Rate Multiplier (C_{pm}) can modify the rate of premixed combustion, which is assumed to be kinetically-limited [27]:

$$\frac{dm_{pm}}{dt} = C_{pm}m_{pm}k\left(t - t_{ign}\right)^2 f([O_2]) \tag{19}$$

Where t is time, t_{ign} is time at ignition, m_{pm} is the premixed mass and k is the turbulent kinetic energy.

- Diffusion combustion rate multiplier: as mentioned in section 2.2.1, after the cumulated fuel during the ignition delay burned in the premix combustion phase, the remaining fraction of unmixed fuel and entrained gas start to mix and burn in a primarily diffusion limited phase. The Diffusion Combustion Rate Multiplier (C_{df}) can adjust the rate of diffusion combustion. This combustion is affected by the load or injection duration, because of the spray-wall interactions and between the spray-spray interactions i.e. at high load, the diffusion combustion rate is reduced [27] :

$$\frac{dm}{dt} = C_{df} m \frac{\sqrt{k}}{\sqrt[3]{V_{cyl}}} f([O_2]) \tag{20}$$

Where m is the mass of air-fuel mixture and V_{cyl} is the cylinder volume.

3 Methodology

This section describes the methodology for calibrating the DIPulse model (see Figure 19). The first step was to analyze the data provided by Fiat Powertrain Technology and do a cross control with the full engine model provided. This data included mass injection rates, injection timing, total mass injected, power, torque, engine speed, among others. A total of 107 operating points were used for the study. As the intake pressure traces and the exhaust pressure traces were not measured, the Cylinder Only Pressure Analysis (CPOA) was selected as the best choice for conducting the analysis.

The next step was the modeling of a single cylinder model in GT-Power in order to perform the CPOA on the input data. Since the given measurements such as the wall temperature, air trapping ratio and residual gas fraction trapped at IVC were not included, an iterative process was conducted in order to obtain the proper values regarding these parameters. Moreover, the validation of the measured cylinder pressure was performed by an automated consistency check on the input data.

Once the validation was completed, both the non-predictive and predictive combustion models were carried out. The aim of the non-predictive model was to verify the behavior of the given model by FPT. Once this simulation was performed, the predictive model was implemented. For the predictive model, 31 well distributed operating points were selected on the engine map. The Optimization tool, given by Gamma Technology, was used for designating the final set of multipliers. Two types of multiplier selection analysis were adopted. For the first analysis, one set of multipliers was set for all cases. On the other hand, for the second one, a set of parameters was established for each case, and following this, a lookup map was built for each parameter, so they could be suitable for the validation process. Once the calibration process was completed, the validation was performed using all the available engine operating points in order to conceive the prediction ability of the model.

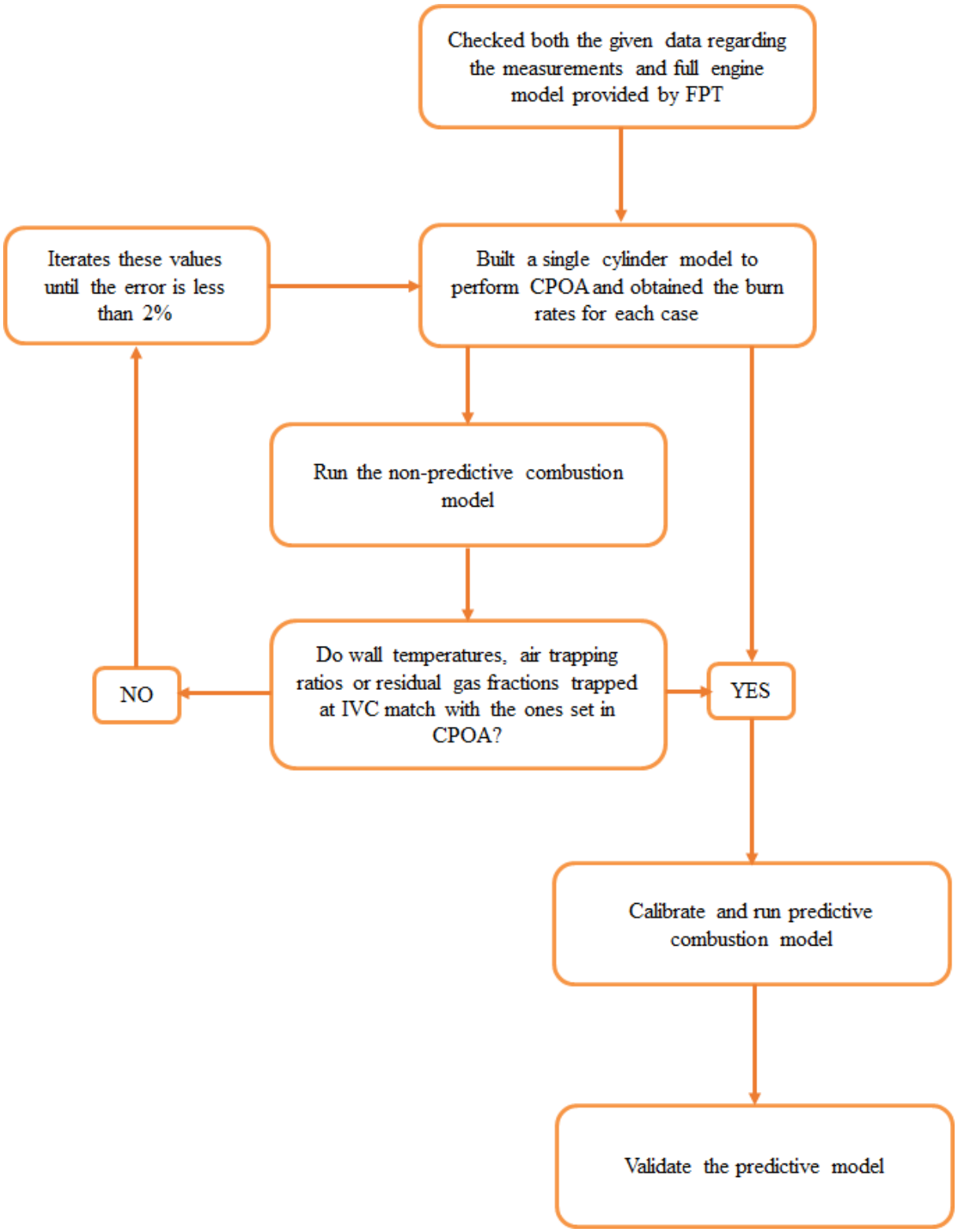

Figure 19. Methodology followed for simulating a Predictive Model

3.1 Checking the provided data

Before performing any simulation, the understanding and study of the given data and the provided full engine model is of primary importance. For the injection timings, GT-Power uses the hydraulic start of injection (SOI_h). Therefore, it is necessary to be aware of the electric start of injection (SOI_e) and the nozzle opening delay (NOD) provided by FPT. For calculating SOI_h, formula (21) was used:

$$SOI_h = SOI_e + \frac{NOD}{10^6} n \cdot \frac{360}{60} \tag{21}$$

Once defined, both the hydraulic start of injection and the mass fuel injected for each case and their respective maps were built in function of engine speed and brake mean effective pressure. Consequently, the model can work not only in steady state conditions, but also in transient ones. 2D lookup tables were also created for common rail pressure, boost and EGR for the same purpose. Figure 20 shows all the operating points measured by FPT (107 cases).

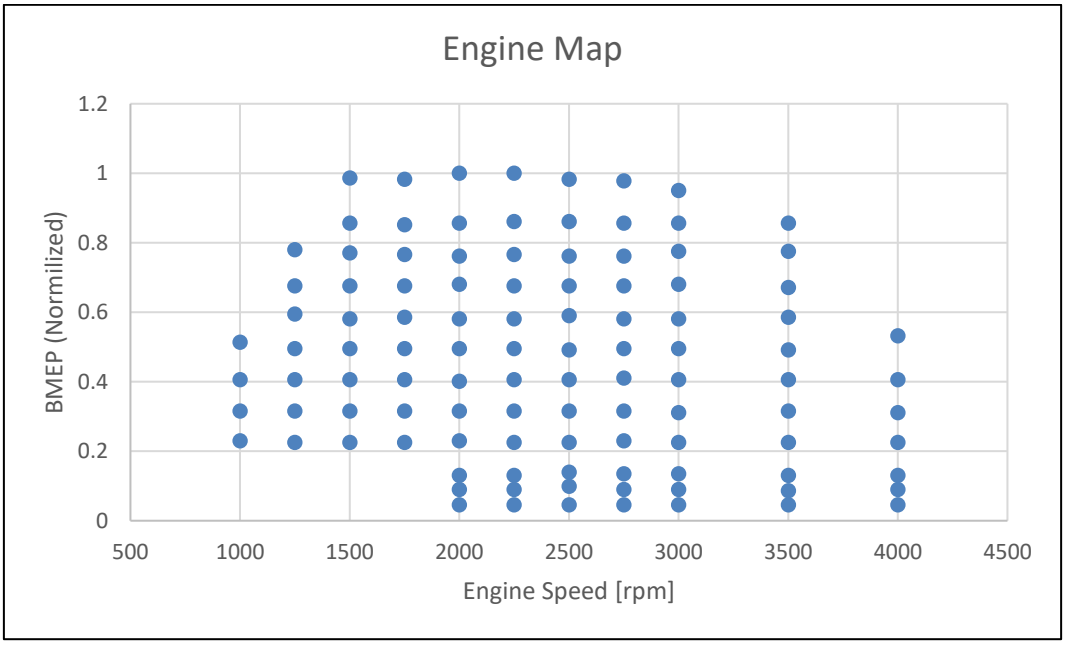

Figure 20. Operating points

3.2 Modelling of the Single Cylinder Engine

There should not be any significant cylinder to cylinder variations for the engine, and therefore, there was no need to start with the analysis with the full engine model. Thus, a single cylinder model was chosen, which not only simplifies the analysis, but also reduces simulation time. As mentioned in section 2.3.1.1.1, the single cylinder model for the Cylinder Pressure Only Analysis just requires the engine cranktrain block, the cylinder block and the injector bock. The later block is not mandatory for the construction of the single cylinder model, however, as the fuel supply into the cylinder of the studied diesel engine is through direct injection, an injector block has to be included. Figure 21 exemplifies the single cylinder model.

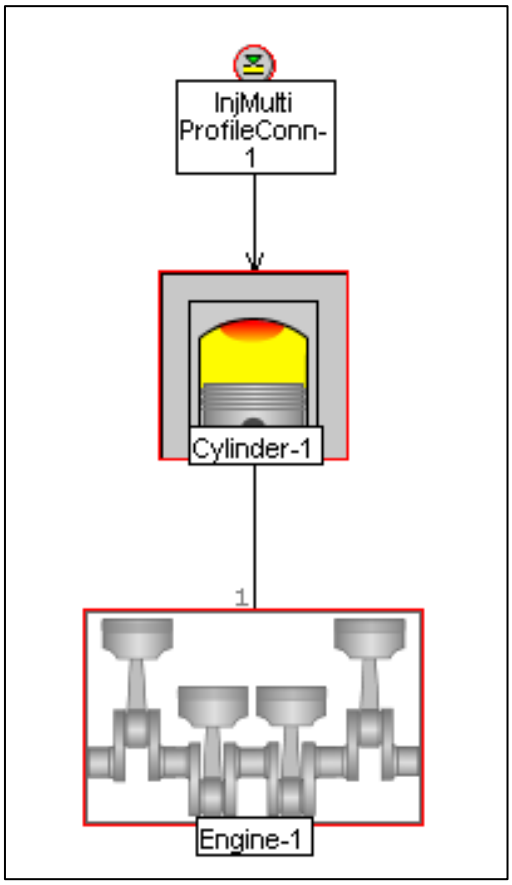

Figure 21. Single cylinder model

3.2.1 Cylinder Only Pressure Analysis (CPOA)

As referred to in section 2.3.1.1.1, if the crank angle resolved pressure measurements in both intake and exhaust ports are not available, the suggested procedure for continuing the burn rate estimation is the Cylinder Only Pressure Analysis. Therefore, the CPOA was performed in order to obtain the burn rate only using the instantaneous in-cylinder pressure measurement.

However, the main drawback of this method is that it requires the estimation of certain input parameters that are very difficult to measure or collect from the test ring. These attributes are the cylinder trapping ration, residual fraction and the wall temperatures.

Due to CPAO running just two cycles, reliable values for the combustion chamber wall temperatures and the residual gas fraction trapped at IVC are needed to initialize the analysis. Since the data of these inputs were not available, an iterative process had to be performed.

The process to determine the attributes mentioned above takes place in the following order:

1- Define the cylinder air trapping ratio

   This is the ratio between the air trapped in the cylinder and air delivered to the cylinder. If there is not a significant overlap, this value is typically 1.0. On the other hand, if the valve overlap is considerable, its value should be lower than unity.

2- Characterize combustion chamber wall temperatures

Gamma Technologies recommends as a first attempt, to start with the typical temperature values of the wall temperature of the head, piston and cylinder wall reach at full load. These quantities are reported in Table 1.

Table 1. Full load in-cylinder temperatures [27]

Head Temperature	550-600	[K]
Piston Temperature	550-600	[K]
Cylinder Temperature	400	[K]

Considering that the wall temperature solver is not active during CPOA, GT-Power uses these initial specified temperatures.

3- Determine the total residual fraction

Gamma Technologies suggests to set this parameter 4% higher than the EGR fraction for the first trial.

Another important input that had to be set for the running of the simulation was the volumetric efficiency. However, this parameter is easier to acquire either as given data or through its estimation using equation (10) where the intake pressure and temperature are easily obtained from the test bench.

Figure 22 illustrates the main templates needed for performing the CPOA analysis. The measured cylinder pressure is set in 'Measured Cylinder Pressure Analysis Object' attribute, while CPOA is selected in 'Cylinder Pressure Analysis Mode' (For more details about the templates and other attributes, please read the User Manual of Gamma Technologies).

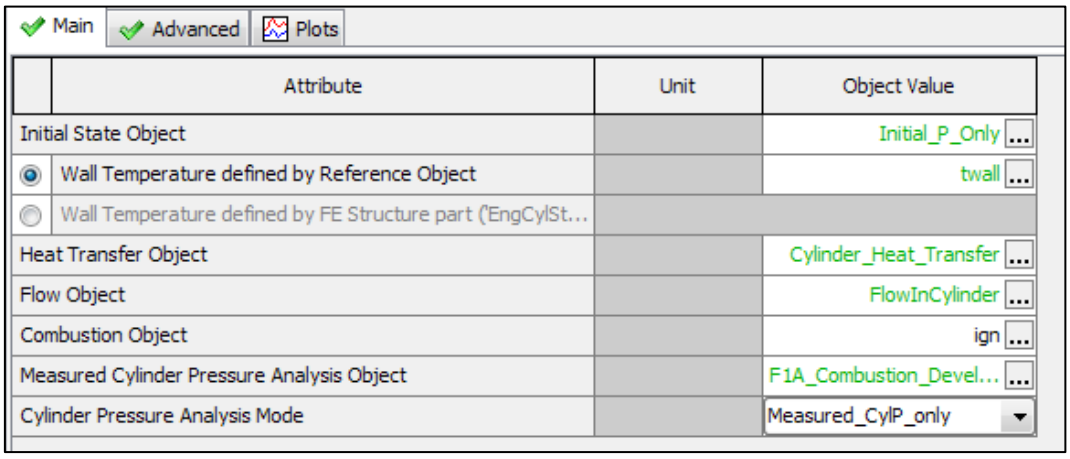

Figure 22. CPOA configuration

Once the initial conditions were set, the model was ready for its first simulation. As a result of the analysis, a burn rate profile as a function of crank angle was obtained for each case of study (Figure 23).

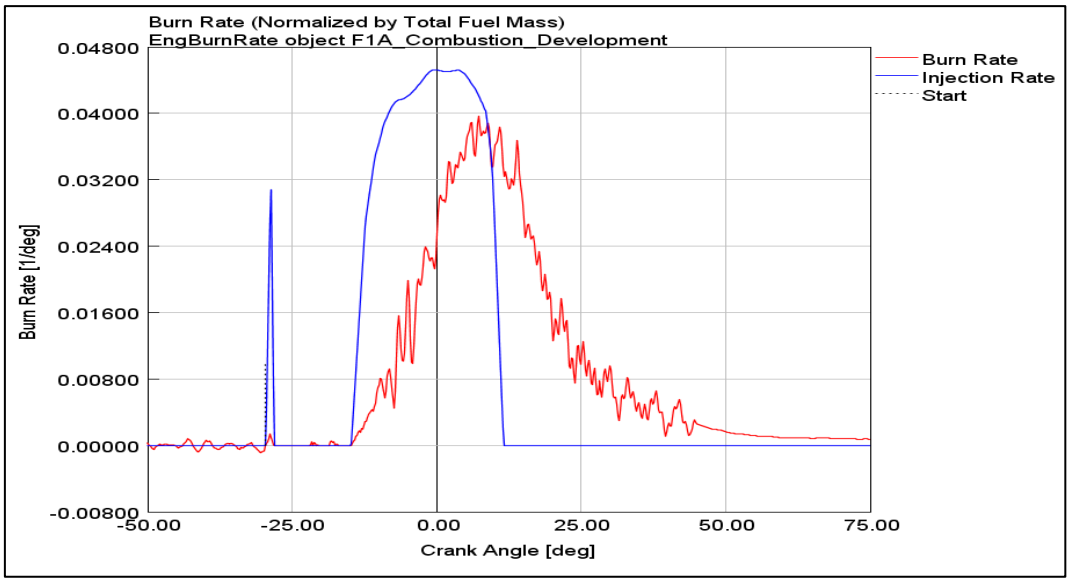

Figure 23. Burn rate profile

Subsequently, these profiles were implemented as part of the combustion object in the full engine model. As the combustion burn rate profile had been imposed, this model is known as a non-predictive combustion model.

In the non-predictive model, contrary to the CPOA simulation, the values of wall temperature and cylinder trapped quantities are estimated. Therefore, there is no need to define them.

In Figure 24, the combustion burn rate estimated in the cylinder pressure only analysis was used as 'Combustion Object', while the 'Measured Cylinder Pressure Analysis Object' attribute was empty and the 'Cylinder Pressure Analysis Mode' was set off.

Main | Advanced | Plots

Attribute	Unit	Object Value
Initial State Object		InitState_cylinder ...
(●) Wall Temperature defined by Reference Object		CylinderHeatSolver ...
( ) Wall Temperature defined by FE Structure part ('EngCylStrucCond')		
Heat Transfer Object		Cylinder_Heat_Transfer ...
Flow Object		FlowInCylinder ...
Combustion Object		Combustion_rate ...
Measured Cylinder Pressure Analysis Object		ign ...
Cylinder Pressure Analysis Mode		off

Figure 24. Non-predictive model configuration

Consequently, the variables mentioned above calculated in the non-predictive simulation were compared with the ones initially used in the CPOA. If the difference between them was higher than 1%, the CPOA analysis had to be run again, however, using the new values obtained from the non-predictive simulation. The characterization the combustion chamber wall temperatures and the total residual fraction had to be repeated until the temperatures and trapping fraction

values set in the CPOA analysis matched the estimated variables of the non-predictive model, or at least until the difference between them is less than 1%.

3.2.1.1 Consistency Check

After running the cylinder pressure only analysis, GT-Power perform a consistency check on the input data to verify the overall quality, because there is always some amount of error in a calculation of burn rate from cylinder pressure, due to simplifications, inaccuracies and/or assumptions in the model. Also, there are uncertainties in the acquisition of measured quantities used as inputs [27]. The following are the consistency checks performed:

- Reasonable *imep*: the *imep* calculated by integrating the cylinder pressure profile should be compared to the *bmep* obtained from measurements. *imep* should be greater than *bmep* equation (5) describes. If this equation is not satisfied, it may indicate an error in the measured pressure data [27].
- Pressure smoothing: the measured cylinder pressure profile should be reasonably smooth. In order to avoid performing an analysis on a signal with unwanted disturbances, GT-Power uses a low pass filter on the raw pressure. After smoothing the input signal, the root mean square error (RMSE) is performed between the raw and the smoothed pressure curves. If the value of the RMS pressure is greater than 0.02, an error is flagged, which means either there is a loss of data while smoothing the curve or it requires more smoothing [27].
- Cumulative burn during compression: during the compression stroke, the apparent burn rate is calculated up until the start of combustion. Along this period there should be no fuel burning. If during these periods the integrated energy release is not zero (or close to zero), it indicates an inconsistency in the input data. If the cumulative burn during compression is greater than 2% of the total fuel, an error is marked [27].
- Fraction of fuel injected late: in direct injection models, if there is insufficient fuel present in the cylinder, before or during the injection event, to support the predicted burn rate, the amount of fuel "missing" is tracked and integrated over the cycle. The amount of missing fuel should always be zero, but if this value is higher than 0.02, an error is flagged. This error could be related to late injection timing or a mismatch between the injection profile and the cylinder pressure trace [27].
- LHV multiplier change: the lower heat value (LHV) multiplier indicates the cumulative error in the burn rate calculation. In the best case, the LHV multiplier value should be 1 and if it requires an adjustment greater than 5%, it could indicate a problem with the inputs [27].
- Combustion efficiency comparison to target: the combustion efficiency indicates the fraction of fuel burned to the total amount of fuel injected in the cylinder. The LHV is adjusted to match the burned fuel fraction at the end of the analysis with the target value. If this adjustment requires more than 5%, it indicates there is an error [27].
- Apparent indicated efficiency: if the calculated indicated efficiency is higher than 45%, it highlights an error [27].

The previously mentioned criteria are very useful as a warning for potential errors in the input model. The consistency check gives specific error codes which may help to track the input data that is creating an inaccurate burn rate calculation.

After the wall temperatures and trapped gasses at IVC were rectified, the CPOA was performed for all operation points. Therefore, the consistency check was executed too. Some cases presented errors during the consistency check related with the LHV multiplier and fraction of fuel injection late. Some operating points were able to be corrected, while others were neglected for the rest of the analysis. Figure 25 shows the comparison between the simulated pressure and the measured one for one operating point.

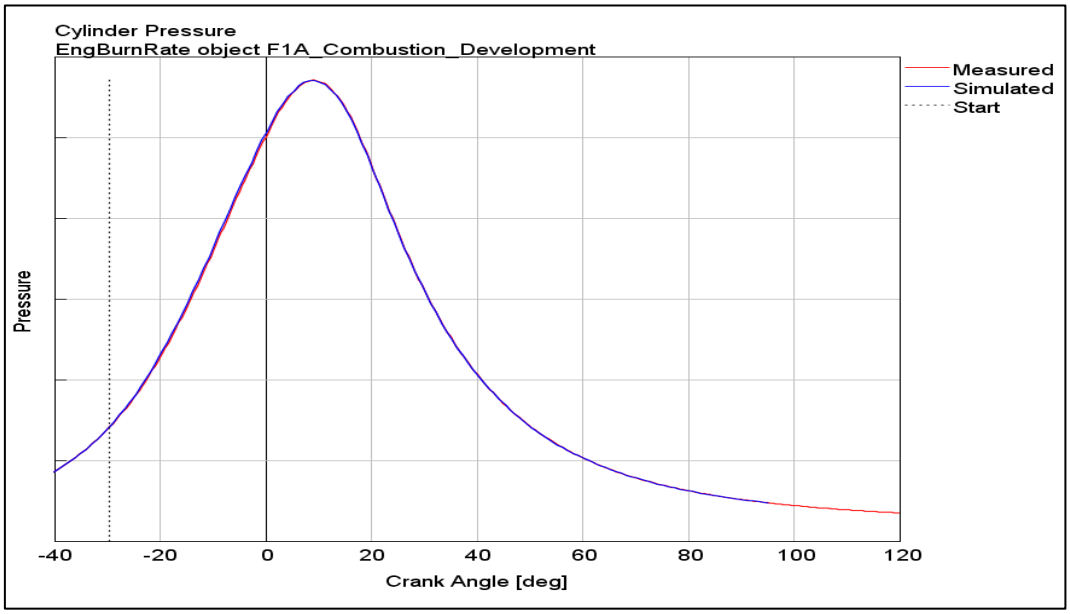

Figure 25. Measured Pressure vs Simulated Pressure

3.2.2 DIPulse Calibration

After the CPOA, the following step was to create and calibrate a predictive combustion model. For this stage, not only does the measured pressure trace have to be used, but the Direct-Injection Diesel Multi-Pulse Model (DIPulse) also has to be selected.

Similar to CPOA, the calibration model was implemented in a single cylinder model (which included only the cylinder, cranktrain and injector) and a closed volume pressure analysis was performed, i.e. no gas-exchange was included. In this case, instead of 2 cycles, the software runs 5 cycles. The first two cycles are based on the analysis of the measured pressure (the same analysis performed by CPOA model). In the third cycle, the predictive combustion model is run (forward run only). In the fourth and fifth cycles, the analysis of the predictive pressure is run (this analysis is done to the results of the third cycle). In other words, the model will provide a comparison of cylinder pressure and burn rate between the measurement and the predictive combustion model.

Gamma Technologies suggested to use a minimum of 25 operating points to perform the calibration. Due to runtime and computational capacity, 31cases were selected for calibrating the model, while the rest of points were used for validation.

In order to calibrate the system, four multipliers – found in the DIPulse template – had to be defined:

- Entrainment rate multiplier
- Ignition delay multiplier
- Premix combustion rate multiplier
- Diffusion combustion rate multiplier

The typical ranges for these multipliers are:

Table 2. DIPulse multipliers range [27]

Attribute	Minimum	Maximum
Entrainment rate multiplier	0.95	2.8
Ignition delay multiplier	0.3	1.7
Premix combustion rate multiplier	0.05	2.5
Diffusion combustion rate multiplier	0.4	1.4

Each case has their own set of multipliers, and through a calibration tool it was possible to find the optimal match between the predictive combustion events and the calculated burn rates from cylinder pressure analysis. Each of these attributes had to be set as parameters, so the software could be able to analyze each case individually. GT-Power has its own optimizer tool called 'Direct Optimizer'.

The optimization tool has two types for case handling (Figure 26):

1- Single-set or sweep optimization: the optimization finds a single set of optimized multipliers with respect to all cases.
2- Independent optimization: the optimization finds a separate set of optimized multipliers for each case.

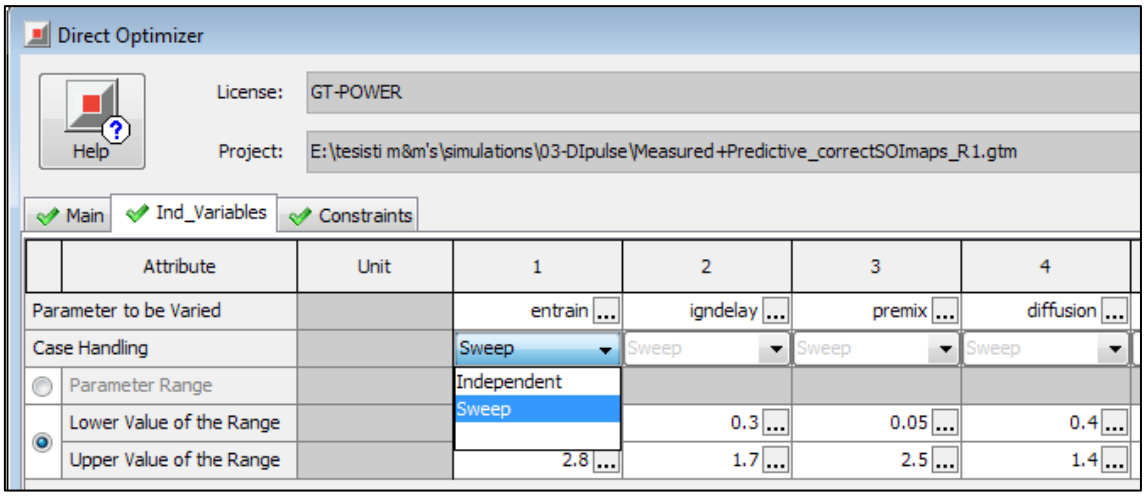

Figure 26. Optimization case handling types

For this project, three different optimization approaches were selected:

1- Single-set optimization of 31 operating points: the optimization was performed to obtain a single set of optimized multipliers with respect to all the calibration points.
2- Independent optimization of 31 operating points: the calibration procedure was carried out for every single case independently, therefore optimized values were found for each case. Following this, a lookup table for each multiplier was built, in which the inputs were engine speed and brake mean effective pressure.
3- Independent optimization of all operating points: idem, however in these cases all operating points were used, instead of the 31 calibration points.

Once the optimization type was defined, it was necessary to specify the optimizer objective as well as the variable to be optimized. The minimization of the improved burn rate root meant the square error[8] between both measured and predictive combustion burn rate was selected.

Apart from comparing both the burn rate and pressure profiles between measured and predicted simulations, Gamma Technologies also recommended observing the average result error (also known as 'mean absolute error') of:

- *imep [%[*
- *maximum pressure [bar]*
- *crank angle for 50% of mass fuel burn (MFB50) [deg]*

The suggested limits for these errors are shown in Table 3.

[8] The Improved Burn Rate Root Mean Square Error (RMS Error) is the error between both the predictive and measured combustion burn rate over time, during the 0.1% and 90% burn angle and is also weighted by the LHV multiplier of the predictive analysis. This value describes the quality of fit between the predicted and the measured burn rate curve, thus simplifying the automated optimization of the predictive combustion model. A big value represents a high deviation between the two curves [27].

Table 3. Recommended error threshold for DIPulse [27]

Metric	Error limit	Average error
imep [%]	± 5	2
MFB50 [deg]	± 2	1
Max. Pressure [bar]	± 5	3

3.2.2.1 NOx Calibration

Once the calibration of the combustion burn rate multipliers were defined, it was possible to continue with the calibration of NOx emissions.

Gamma Technologies suggested to calibrate the two more influent parameters (out of six) defined in the NOx emission template for DIPulse model.

Table 4. NOx multipliers range [27]

Attribute	Minimum	Maximum
NOx calibration multiplier	0.1	2
N2 oxidation activation energy multiplier	0.3	1.1

The objective for this optimization is to minimize the error between the predicted NO_xconcentration and measured NO_x concentration.

$$\%\ error_{NOx} = \frac{\left|\left(NOx_{pred} - NOx_{meas}\right)\right|}{NOx_{meas}} \cdot 100 \qquad (22)$$

For this calibration just the single-set optimization was performed. Then a minimal manual tuning was performed in order to improve the results. Table 5 shows the recommended limits for this analysis.

Table 5. Recommended NOx limits [27]

Metric	Range	Average error
NOx Concentration ppm [%]	20	13

3.3 Validation of the Predictive Model

Once the calibration procedure was over, the following step was to validate the predictive model.

For the validation, the full engine model was used (Figure 27) and the predictive DIPulse combustion model was set as combustion object (Figure 28).

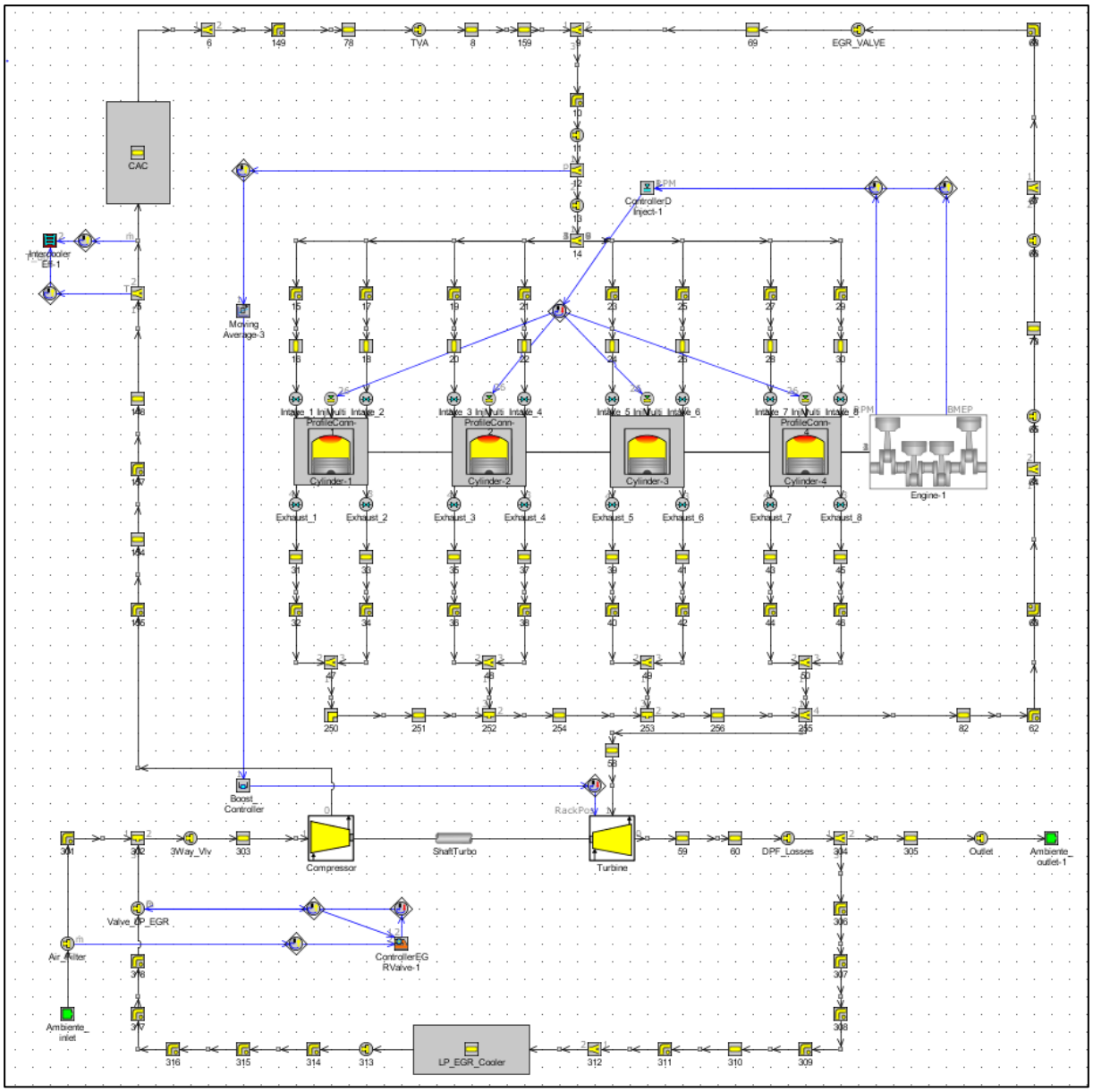

Figure 27. Full engine model

Main | Advanced

Attribute	Unit	Object Value
Initial State Object		InitState_cylinder ...
Wall Temperature defined by Reference Object		CylinderHeatSolver ...
Wall Temperature defined by FE Structure part ('EngCylSt...		
Heat Transfer Object		Cylinder_Heat_Transfer ...
Flow Object		FlowInCylinder ...
Combustion Object		DIPulse ...
Measured Cylinder Pressure Analysis Object		ign ...
Cylinder Pressure Analysis Mode		off

Figure 28. Validation of DIPulse

This time, the DIPulse model was set as the ‘Combustion Object’.

Two validations were performed:

1- The DIPulse parameters obtained from the single-set optimization were set for all engine operating points.
2- The lookup tables created from the optimized values obtained through the independent optimization of the 31 calibration points were set as the DIPulse multipliers.

The generated maps from the calibration of all the cases were also used in the full engine model. However, this simulation was performed in order to compare its accuracy with the other two validation procedures.

4 Results and Discussion

In this section, the results of the non-predictive combustion model and the results of both predictive combustion model procedures are discussed.

4.1 Checking the provided data

According to the given data, the nozzle opening delay (NOD) is 350μs, also, FPT provided the electric start of injection (SOI_e) measurements for all the pulses. Therefore SOI_h was estimated through equation (21).

After calculating these values for all the operating points a simulation was performed on the full engine model. A predictive model was used (without calibrating its multipliers) in order to just compare the burn rate trace calculated through the measured in-cylinder pressure and the combustion rate simulated though the predictive combustion model. Four cases were simulated:

- High speed: 4000 [rpm] x 12 [bar]
- Low speed: 1000 [rpm] x 9 [bar]
- High load: 2250 [rpm] x 22 [bar]
- Low load: 2750 [rpm] x 2 [bar]

Figure 29 shows the results of the simulations mentioned above.

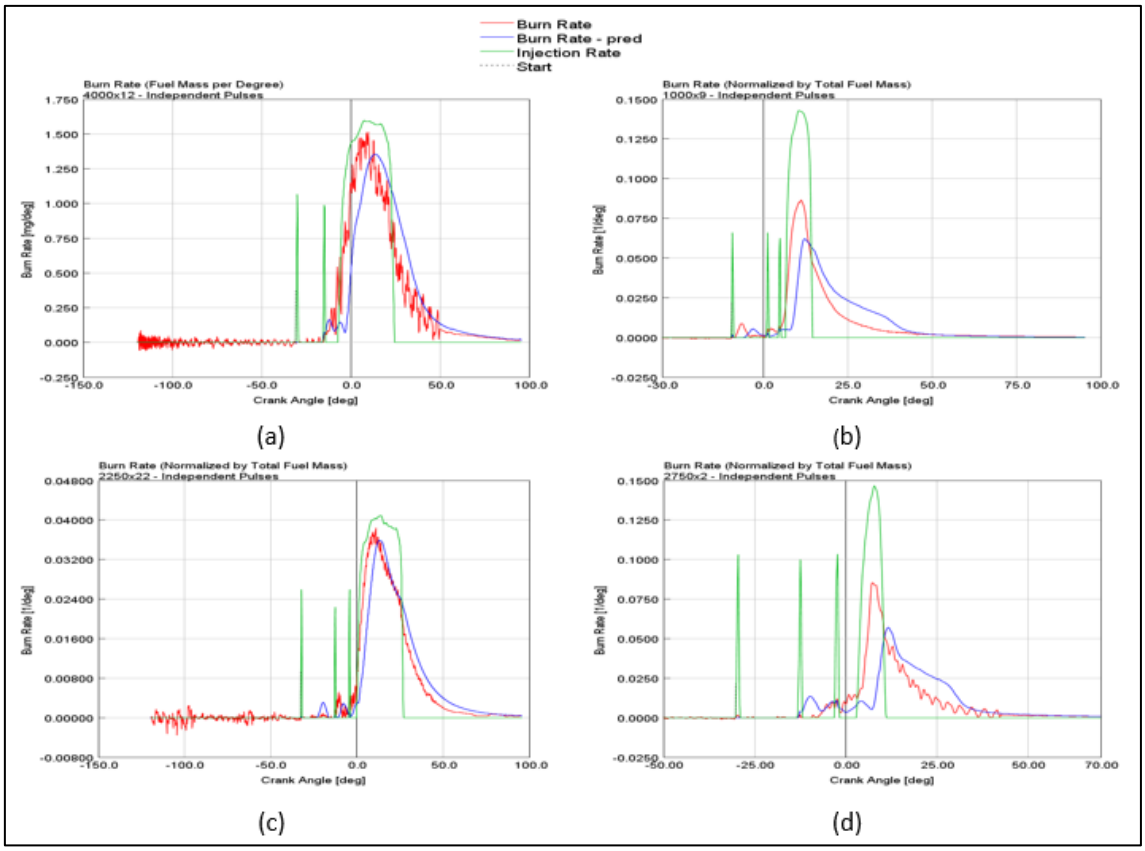

Figure 29. Comparison between both the measured burn rate and the predictive burn rate

From the previous analysis, the following observations were noticed:

- The predicted burn rate seems to be delayed with respect to the burn rate simulated from the measured cylinder pressure.
- Both SOI_e of the main pulse and SOI_e of the pre-main pulse were very close to each other.
- The SOI_e of the main injection always occurred before SOI_h of the pre-main pulse (bearing in mind that the nozzle closing delay is higher than the nozzle opening delay).
- Considering the combustion burn rate calculated from the measured pressure (in Figure 29), the identification of both the start of combustion of the pre-main injection and the SOC of the main injection was not clear.

Based on these observations, an injection fusion event between the main injection and the pre-main pulse was considered.

Since GT-Power is not capable of reproducing this event and the injection profile rate of the fusion injection was not provided by FPT, there was a need to define some key assumptions:

- Merge the mass fuel injected of both the main and pre-main pulses into a single shot.
- Define the SOI_h for this new merged injection.

Since the mass fuel rate and injection timing are variables that affect the burn rate calculation significantly, a predictive model (without calibrating its multipliers) was run in order to analyze the heat release rate of the new injection configuration. Two cases were tested:

1- Merged injection in which the SOI_h of the pre-main was used.
2- Merged injection in which the SOI_h of the main was used.

Figure 30 and Figure 31 show the traces of the burn rate of both the reverse run combustion calculation and the predicted burn rate for both high/low speed and high/low load operating points respectively. From these it can be observed that when the SOI_h of the main was selected, the predicted heat release was always delayed with respect to the measured energy release. On the other hand, when the SOI_h of the pre-main was tested, the predicted combustion burn rate seemed to have a better match with the measured burn rate. However, depending on the engine conditions, the predictive energy release was delayed or in advanced of the measured one.

The hydraulic start of injection of the pre-main pulse was selected as the SOI_h of the new merged injection, due to the fact that the difference between the predictive burn rate using the SOI_h of the pre-main and the measured burn rate was shorter than the lag obtained using the SOI_h of the main.

Since there was no boot injection profile, the new injection rate profile was defined as a single injection profile. Therefore, some inaccuracies were expected due to the sensitivity of the predictive combustion model with respect to the burn rate calculation.

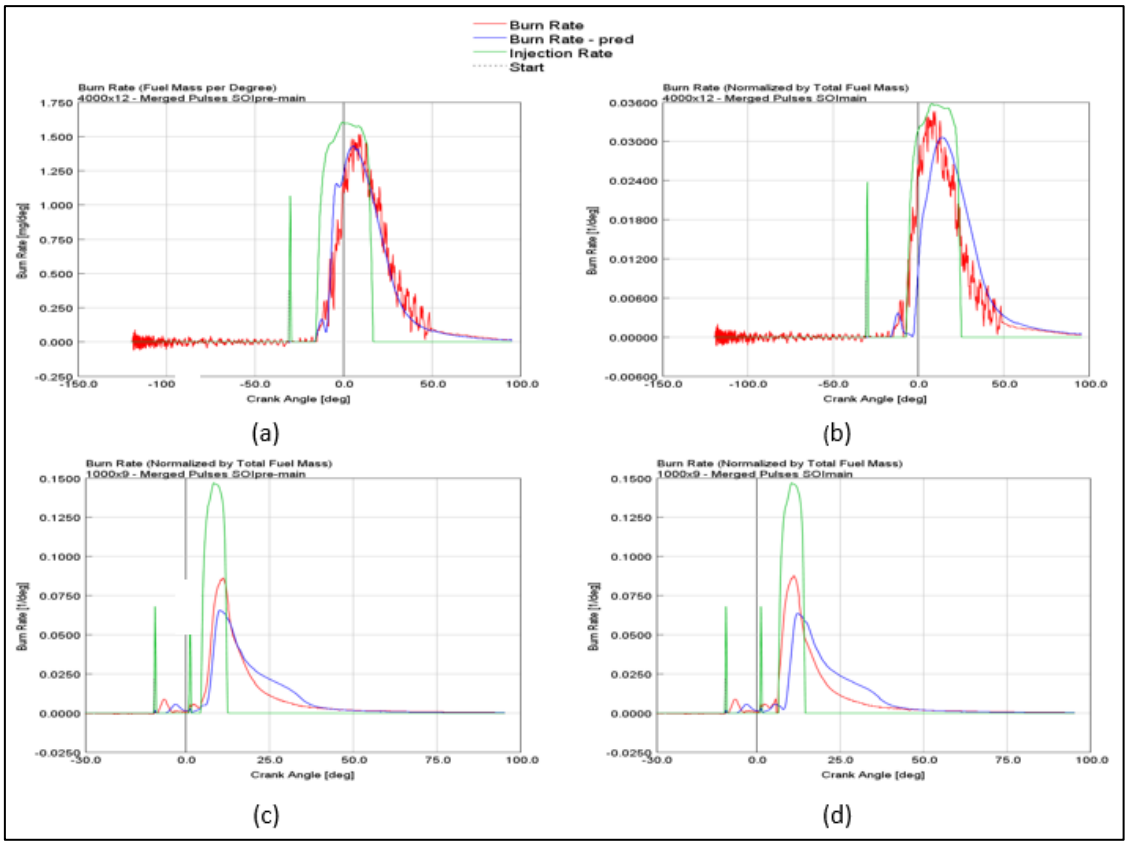

Figure 30. Burn rate of high/low speed operating points. (a) 4000x12 SOIpre-main (b) 4000x12 SOImain (c) 1000x9 SOIpre-main (d) 1000x9 SOImain

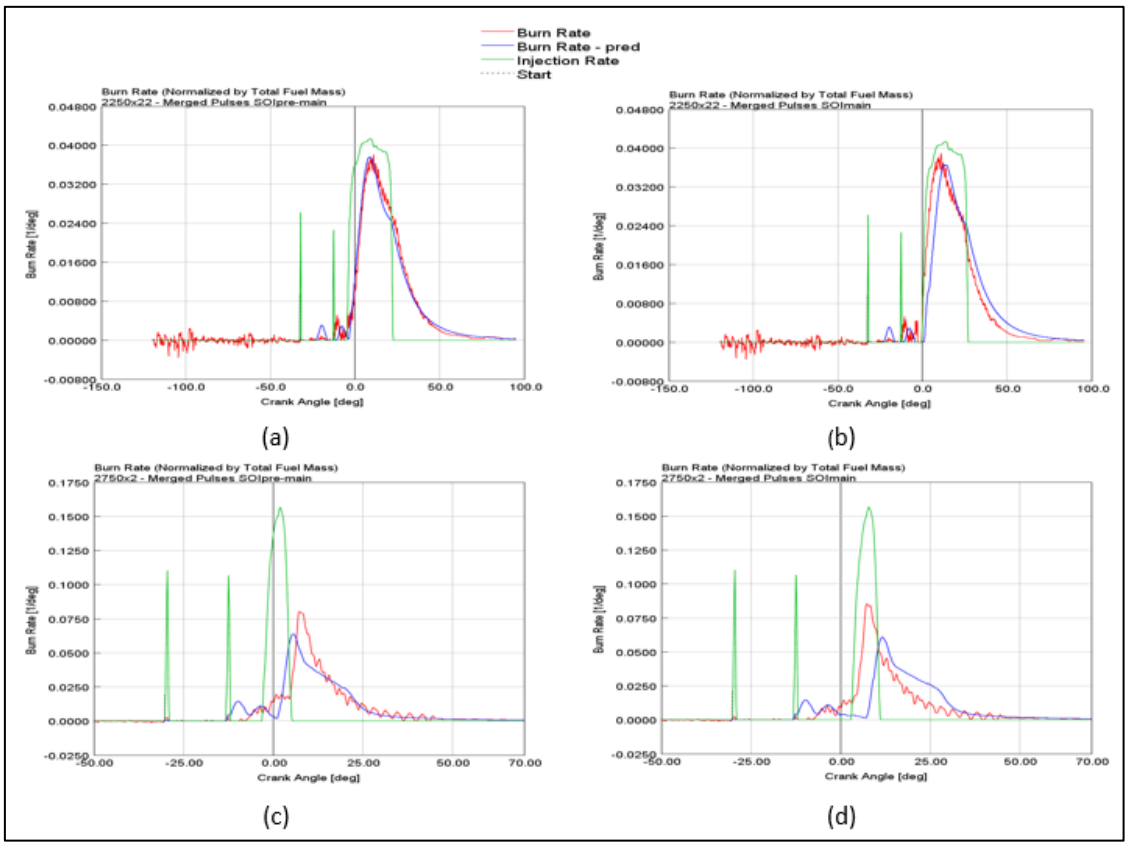

Figure 31. Burn rate of high/low load operating points. (a) 2250x22 SOIpre-main (b) 2250x22 SOImain (c) 2750x2 SOIpre-main (d) 2750x2 SOImain

4.2 Cylinder Only Pressure Analysis (CPOA)

Once the SOI_h of the new merged injection was selected, the following step was the analysis of the single cylinder model.

As mentioned in section 3.2.1, the downside of the cylinder pressure only analysis is that the definition of certain variables from the engine are very difficult to measure. However, they can be found through the full engine model. These variables were defined as follows:

1- Cylinder trapping ratio

Figure 32 highlights both the intake and exhaust valve lift simulated by GT-Power for a certain operating point. Similar behavior was observed in the other operating points.

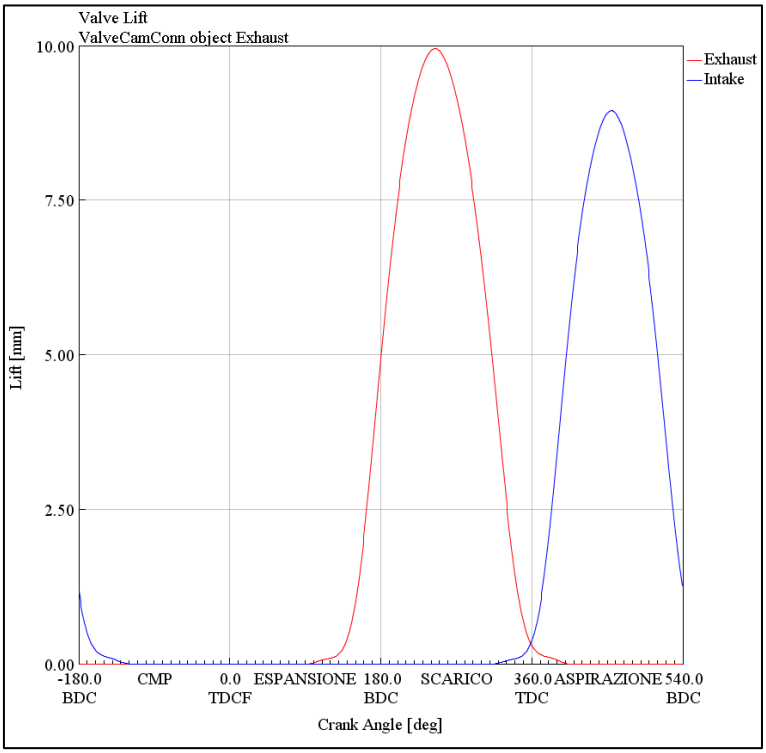

Figure 32. Intake and Exhaust valves lift

Figure 32 shows how there was not a significant valve overlap, hence a value of 1.0 can be assumed for this variable.

2- Combustion chamber wall temperatures

As a first attempt, the typical wall temperature at full load values suggested by Gamma Technologies were used and reported in Table 6.

Table 6. Full load in-cylinder temperatures

Head Temperature	550	[K]
Piston Temperature	550	[K]
Cylinder Temperature	400	[K]

3- Total residual fraction

For the first trial, the total residual gas fraction was set 4% higher than the measured exhaust gas recirculation fraction.

After setting these values in the CPOA analysis and running the simulation, a new burn rate profile for each operating point was generated. These burn rate profiles were inserted in the non-predictive combustion model in order to revise the head temperature, cylinder temperature, piston temperature and burned mass fraction at the start of combustion. Once these estimated values from the non-predictive model matched the input data set in the CPOA, the automated consistency check was performed in order to verify the quality of the input data. The results are shown in Figure 33.

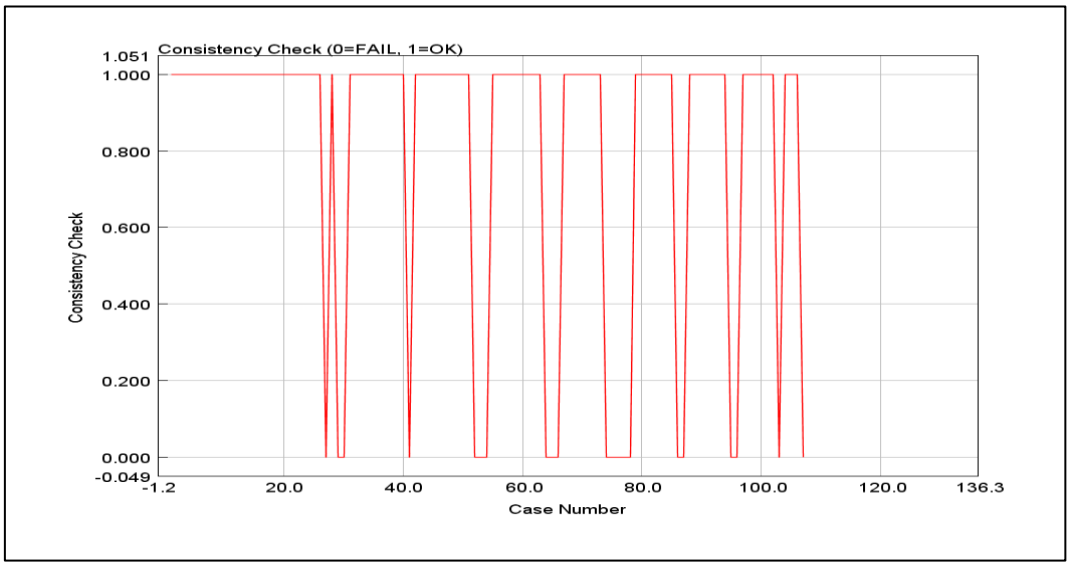

Figure 33. Consistency check summary

From 107 measurements, 28 cases did not pass the burn rate input data consistency checks. The flagged errors are reported in Table 7.

Table 7. Consistency check errors

Error Type	Number of Cases
Fraction of Fuel Injected Late	1
Large change of LHV Multiplier	27

The majority of the errors were due to a large change of LHV multiplier. This means GT-Power had to make big adjustments to the fuel energy content (LHV) to match the predicted fuel burned with the measured one. These errors were located at low load operating points, and they could be related with the mismatch between the selected injection profiles used for the simulations and the real boot injection profiles. This dissimilarity affects the heat transfer inside the combustion chamber, therefore, in order to counterweight this, the 'Overall Convection Multiplier' was modified. After rectifying this attribute, the consistency check was run again and the results are shown in Table 8.

Table 8. Consistency check error after correction

Error Type	Number of Cases
Large change of LHV Multiplier	21

This time, the amount of errors regarding the quality of the input data decreased to 21. These operating points were not considered any more for the rest of the analysis. In other words, the final amount of cases in consideration for the present project were 86 - these points are represented in Figure 34.

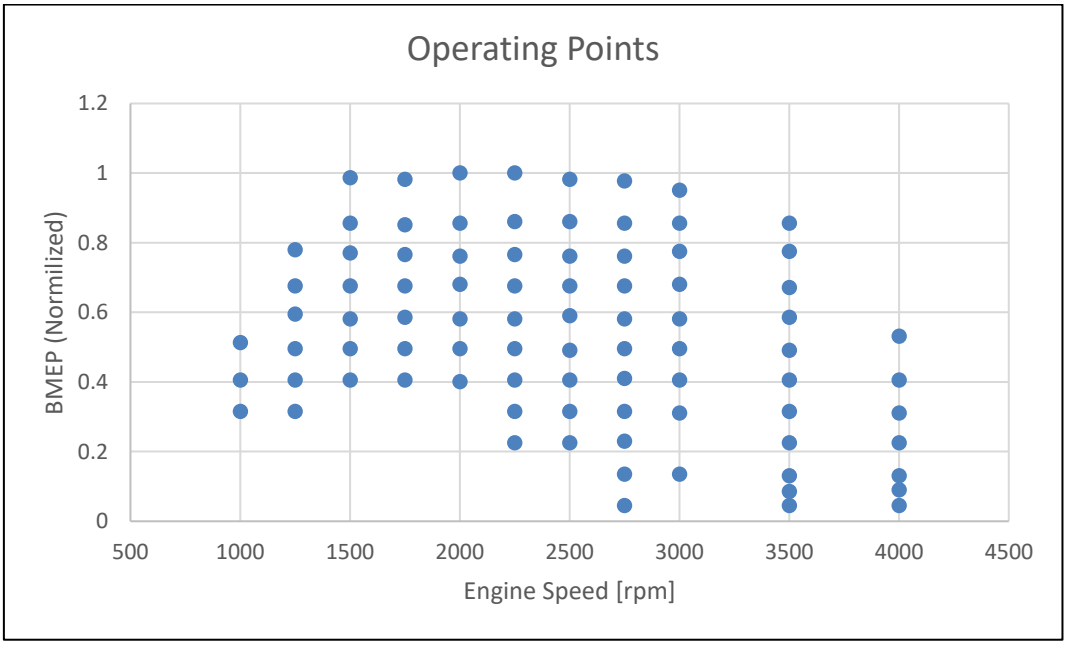

Figure 34. New operating points

In addition, the non-predictive combustion model was run in order to compare its results with the measured data. The *imep* error and maximum pressure error are shown in Figure 35 and Figure 36:

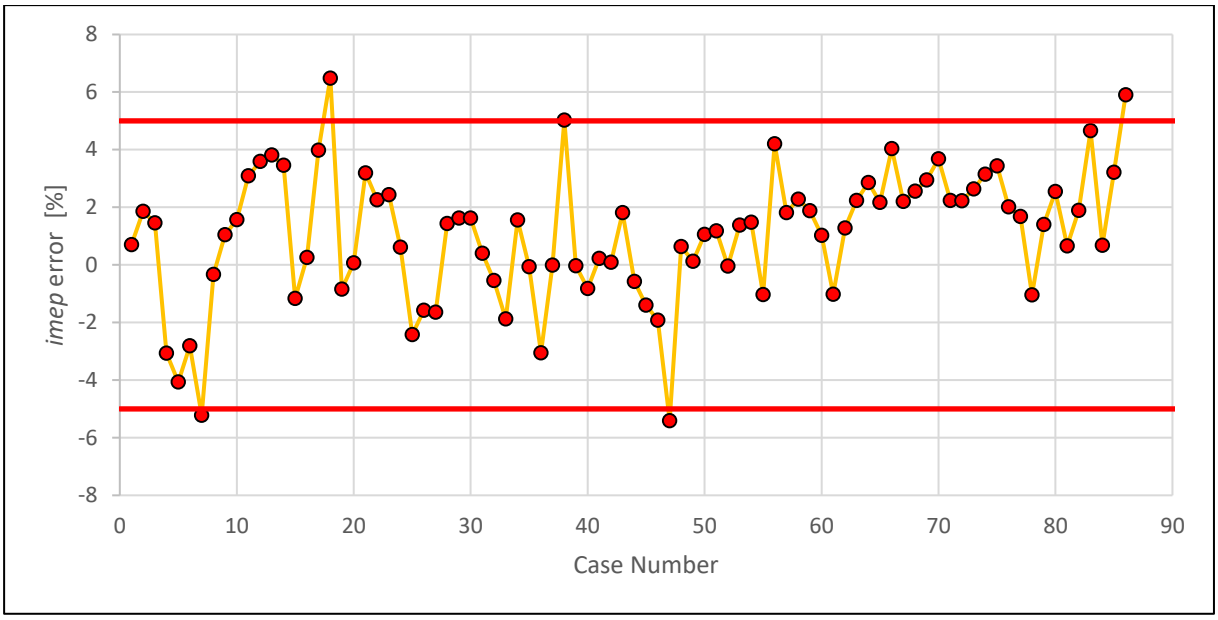

Figure 35. imep error. Non-predictive model

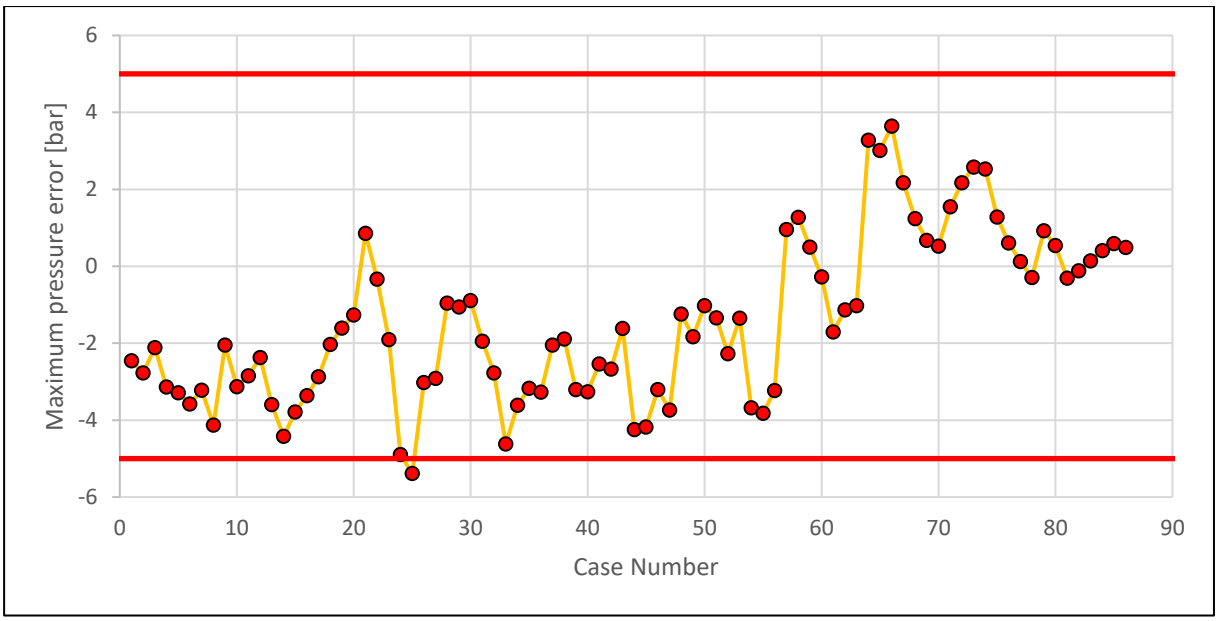

Figure 36. Maximum pressure error. Non-predictive model

Figure 35 and Figure 36 show how there was a low margin of error between the simulated results and the acquired data given by FPT. In addition, the mean absolute error of the imep, MFB50 and maximum pressure were calculated:

Table 9. Average error of non-predictive model

Metric	Average error
imep [%]	2.1
MFB50 [deg]	0
Max. Pressure [bar]	2.2

The average errors were also low, therefore the model can be considered acceptable for the validations. It is important to note, that the average error of the MFB50 is zero. The reason is that the calculation methods of the MFB50 used by the measurement equipment differs from how GT-Power simulates MFB50. Therefore, for all the following comparisons of MFB50, the MFB50 simulated from the CPOA is going to be considered as the measured MFB50. Figure 37 shows the difference between the measured MFB50 (using CPOA) and the non-predicted MFB50 using the full engine model.

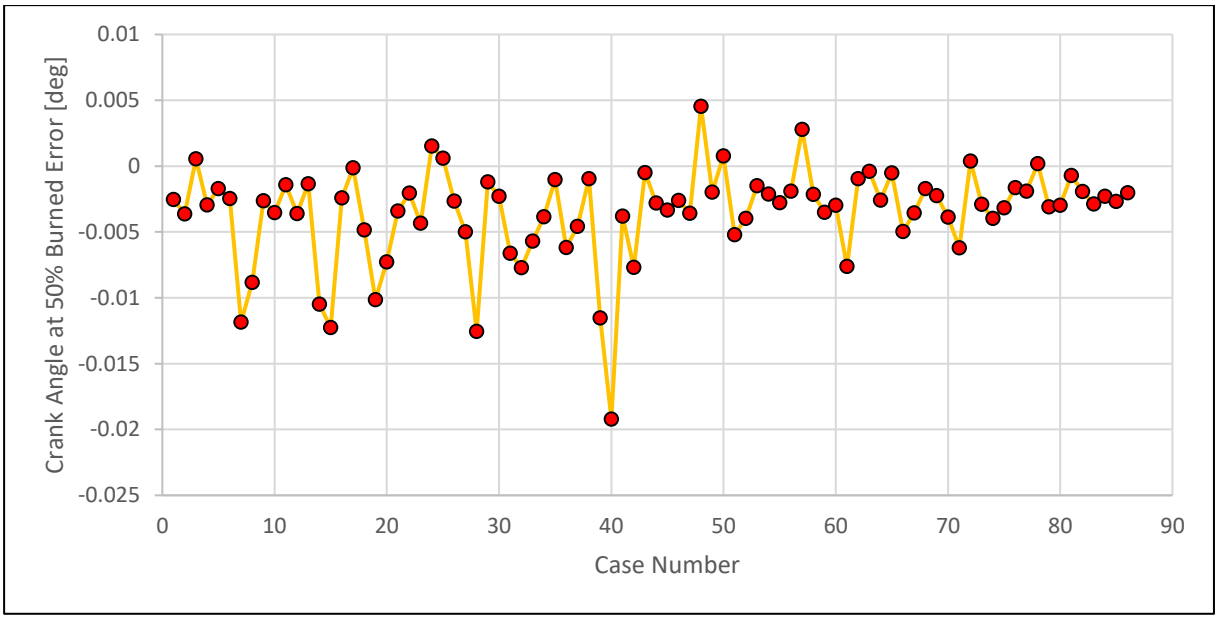

Figure 37. MFB50 simulated vs MGB50 measured

4.3 DIPulse Calibration

After verifying the quality of the input data, the calibration procedure was the next step to follow. As mentioned in section 3.2.2, the calibration was performed in three different ways.

4.3.1 Single-set optimization

In this case, 31 points out of 86 cases were chosen for the optimization (see Figure 38). A single set of optimized multipliers were found for all the calibrating cases, as shown in Table 10.

Table 10. DIPulse multipliers. Single-set Optimization

Attribute	Constant
Entrainment Rate Multiplier	1.11
Ignition Delay Multiplier	0.528
Premix Combustion Rate Multiplier	0.05
Diffusion Combustion Rate Multiplier	0.998

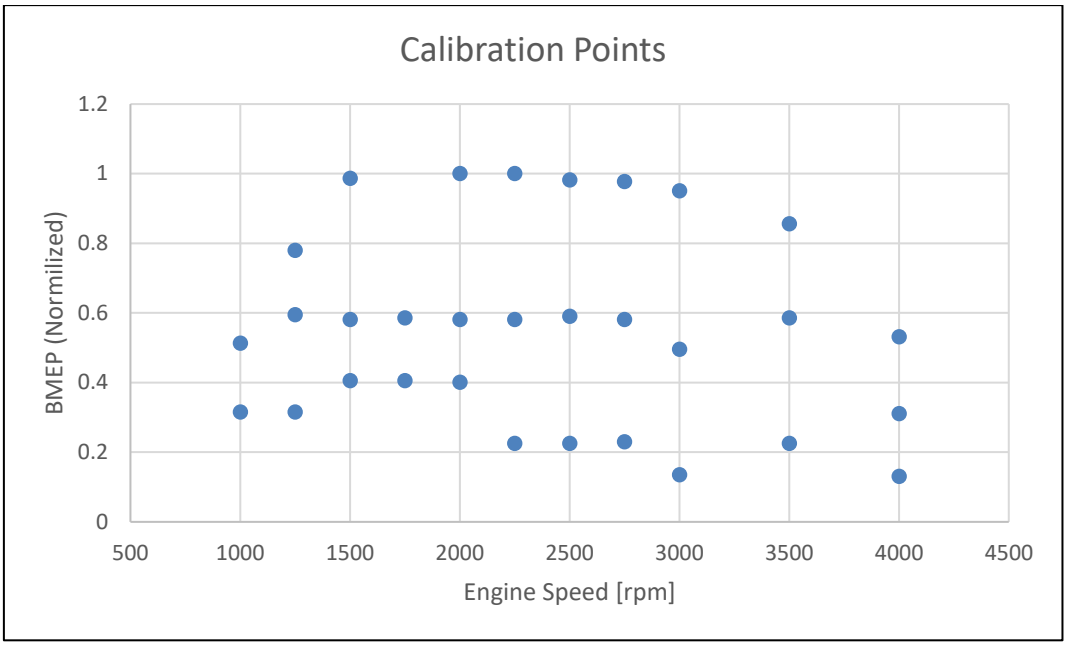

Figure 38. Calibration points

The optimization objective selected was to minimize the RMSE between the measured burn rate and the predicted one (the measured burn rate is referring to the burn rate obtained through the reverse combustion simulation). The results are shown in Figure 39, in which the best case (in green) and the worst case (in red) were identified. A visual check of these cases are represented in Figure 40 and Figure 41.

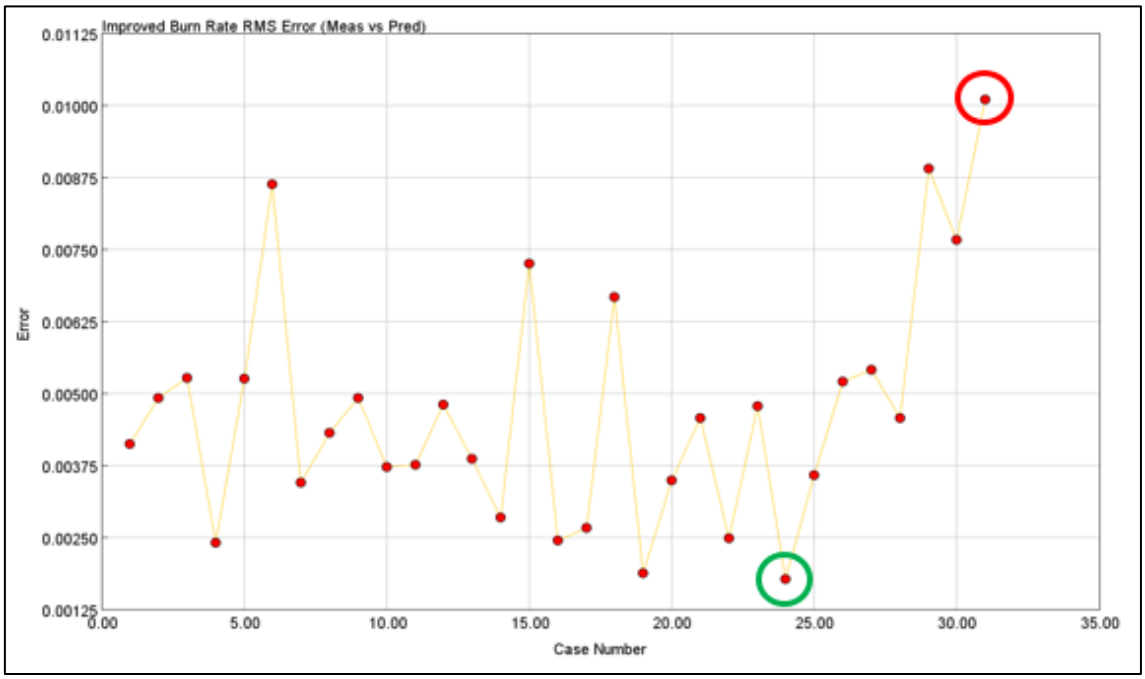

Figure 39. Burn rate RMSE (measured vs predicted). Single-set optimization

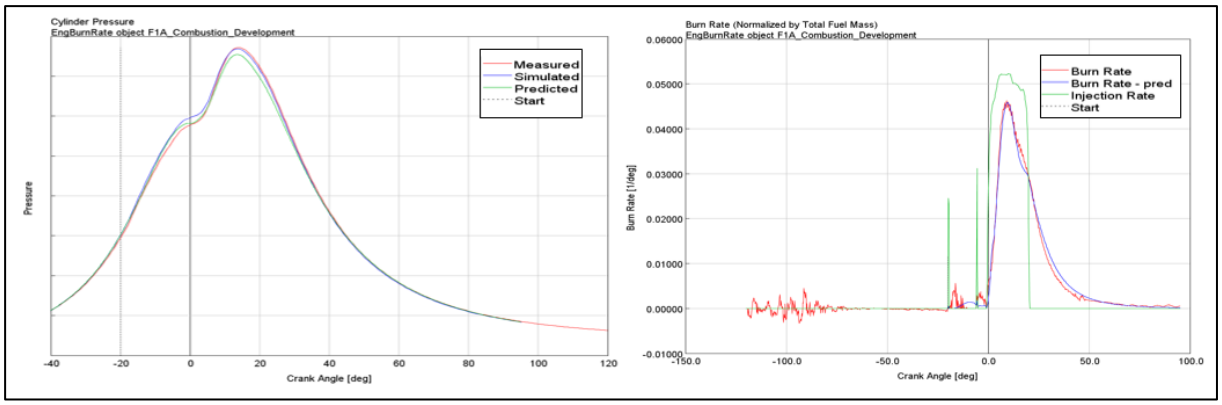

Figure 40. Pressure trace and burn rate. Best case. Single-set optimization

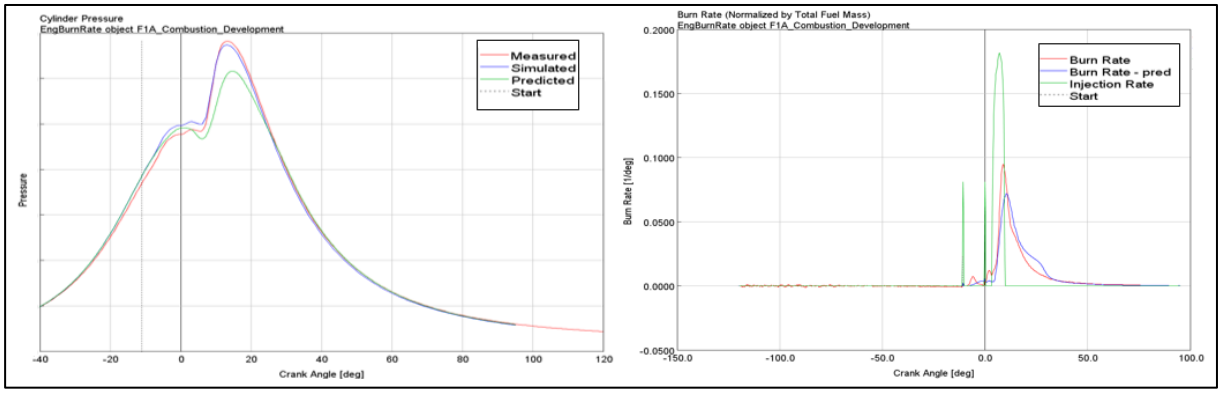

Figure 41. Pressure trace and burn rate. Worst case. Single-set optimization

Figure 42, Figure 43 and Figure 44 show the effect of different engine speeds on both the predicted pressure profile and the predicted burn rate.

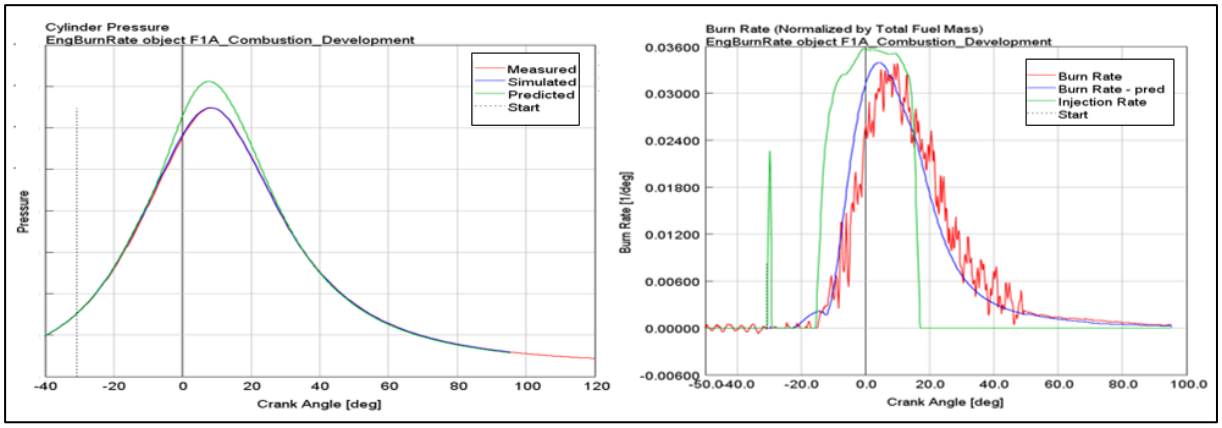

Figure 42. Pressure trace and burn rate for single-set optimization. 4000 rpm x middle load

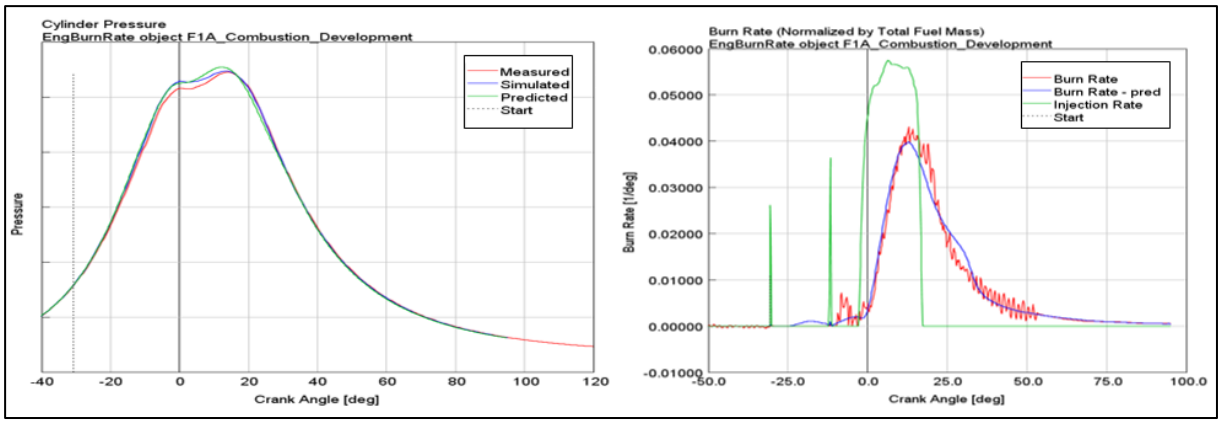

Figure 43. Pressure trace and burn rate for single-set optimization. 2500 rpm x middle load

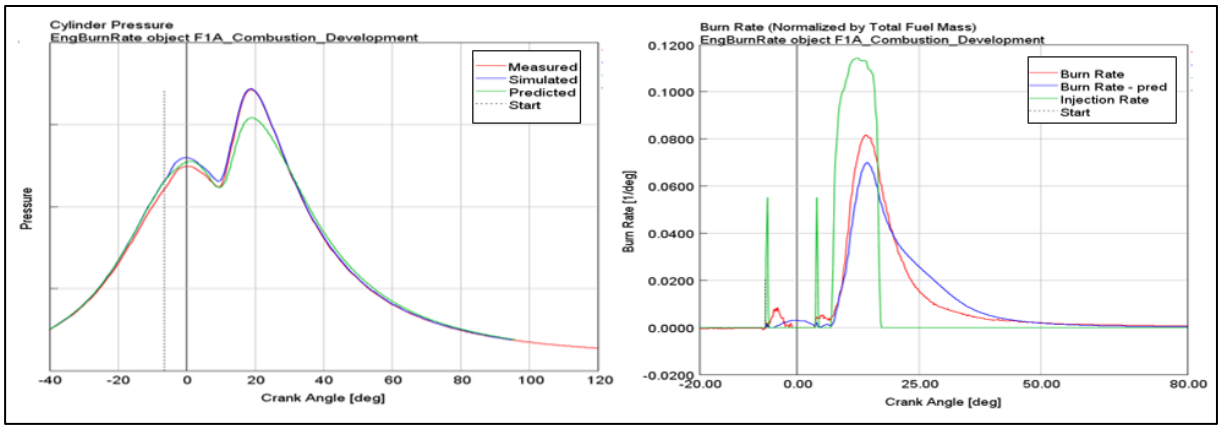

Figure 44. Pressure trace and burn rate for single-set optimization. 1000 rpm x middle load

At high speeds, the predictive pressures reached higher values than the measured one. This was also reflected in the burn rate graphs, in which the fuel started burning faster than the rate it was supposed to burn. On the other hand, at low speeds the predictive pressure traces got shorter compared to the measured pressure. The reason for this was that the predicted combustions started a few crank angle degrees delayed in comparison with the measured burn rate. At middle speeds, both pressure and burn traces matched well.

Figure 45, Figure 46 and Figure 47 illustrate the effect of the engine load on the prediction of the pressure traces and burn rates.

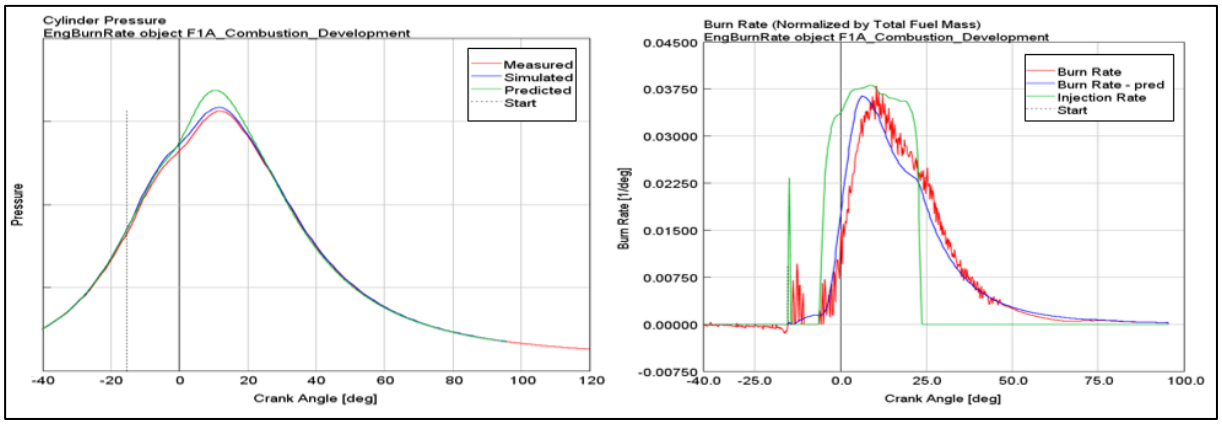

Figure 45. Pressure trace and burn rate for single-set optimization. 2500 rpm x high load

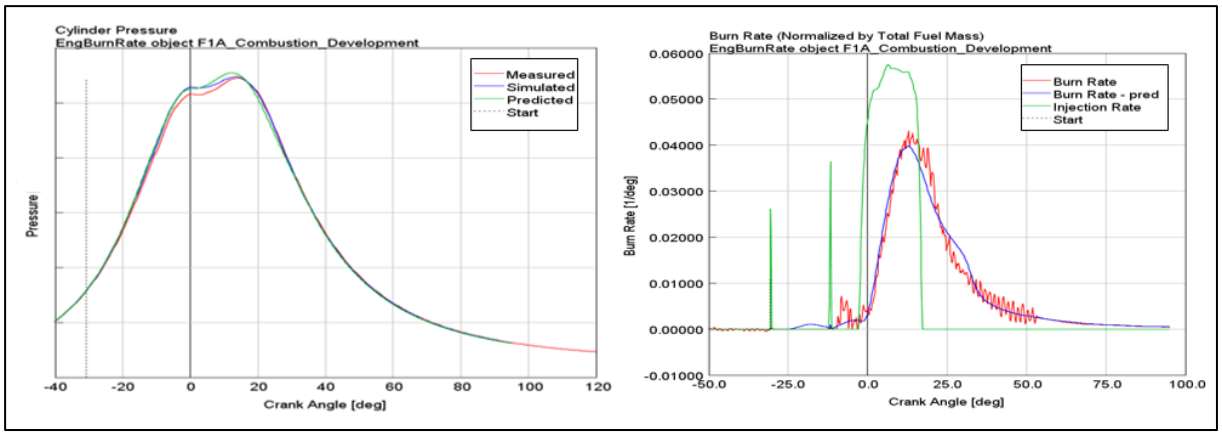

Figure 46. Pressure trace and burn rate for single-set optimization. 2500 rpm x middle load

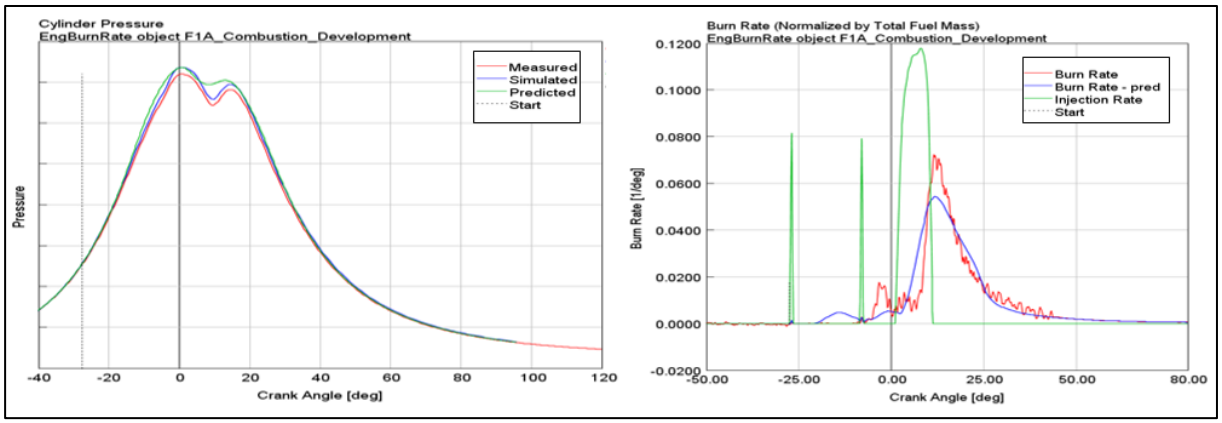

Figure 47. Pressure trace and burn rate for single-set optimization. 2500 rpm x low load

The effect of varying the engine load did not have a significant impact on the predicted outputs.

The error between the simulated and predicted *imep* was estimated and plotted in Figure 48.

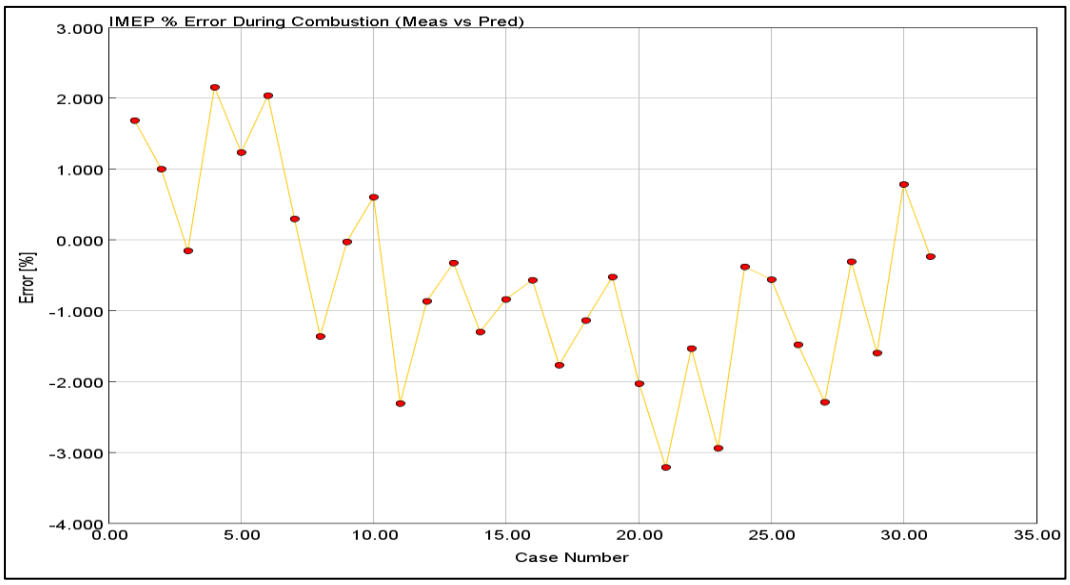

Figure 48. imep error. Single-set optimization

As the Figure 48 shows, the *imep* variation is within the recommended limits of ±5 (referred to in Table 3).

Figure 49 illustrates the error between the measured maximum pressures and predicted pressures, while the errors between the simulated MFB50 and predicted MFB50 are shown in Figure 50.

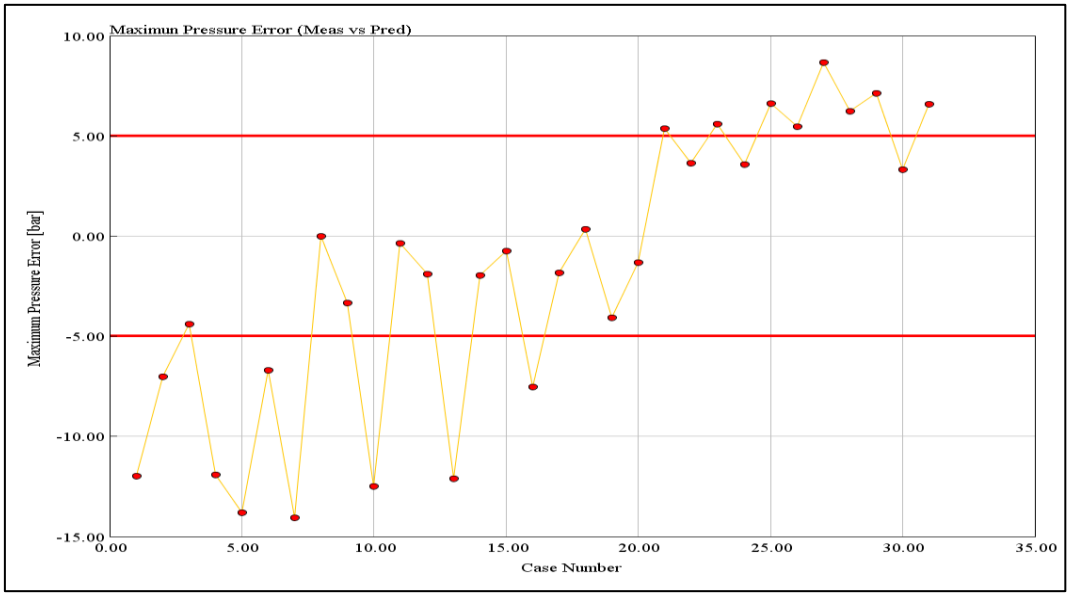

Figure 49. Maximum pressure error. Single-set optimization

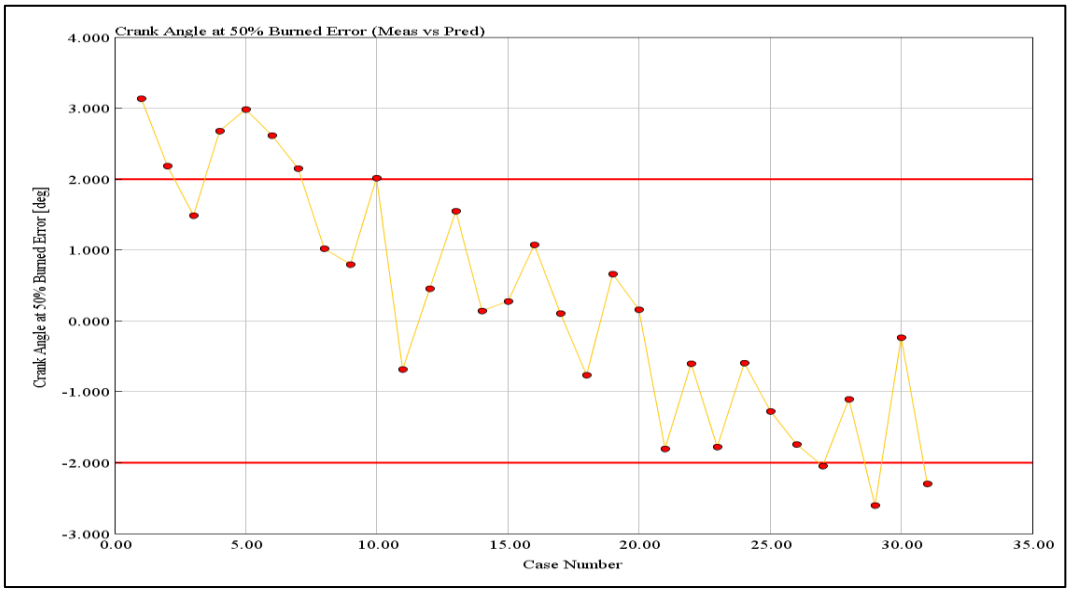

Figure 50. MFB50 error. Single-set optimization

The 'case number' in the 'x' axis of all the figures were arranged from high speed to low speed, i.e. in Figure 50, case number 1 represented an engine point at 4000 rpm, while case number 31 characterized an operating point at 1000 rpm. These errors highlighted the effect of the engine speed on the model's predictions. For the maximum pressure error, the recommended limit is ±5, while for the MFB50 error it is ±2. In both cases, just at middle speeds, the operating points were within the recommended error range.

Figure 50 confirmed that the fuel was burning faster than it should at high speeds (as the predicted SOC were occurring closer to TDC, higher pressures were expected). On the other

hand, at low speeds the MFB50 were occurring farther from the TDC during the expansion stoke, therefore lower pressures developed.

4.3.2 Independent optimization

31 points out of 86 operating points were chosen for this type of optimization. The difference, with respect to the previous calibration analysis is that the DIPulse multipliers were optimized independently for each calibration case instead of finding a common set of values for all cases. The independent optimization was a countermeasure for the lack of accuracy of the injection rates.

The optimization objective selected was to minimize the RMSE between the measured burn rate and the predicted one. The results are shown in Figure 51, in which the best case (in green) and the worst case (in red) were identified. These cases are represented in Figure 52 and Figure 53 respectively.

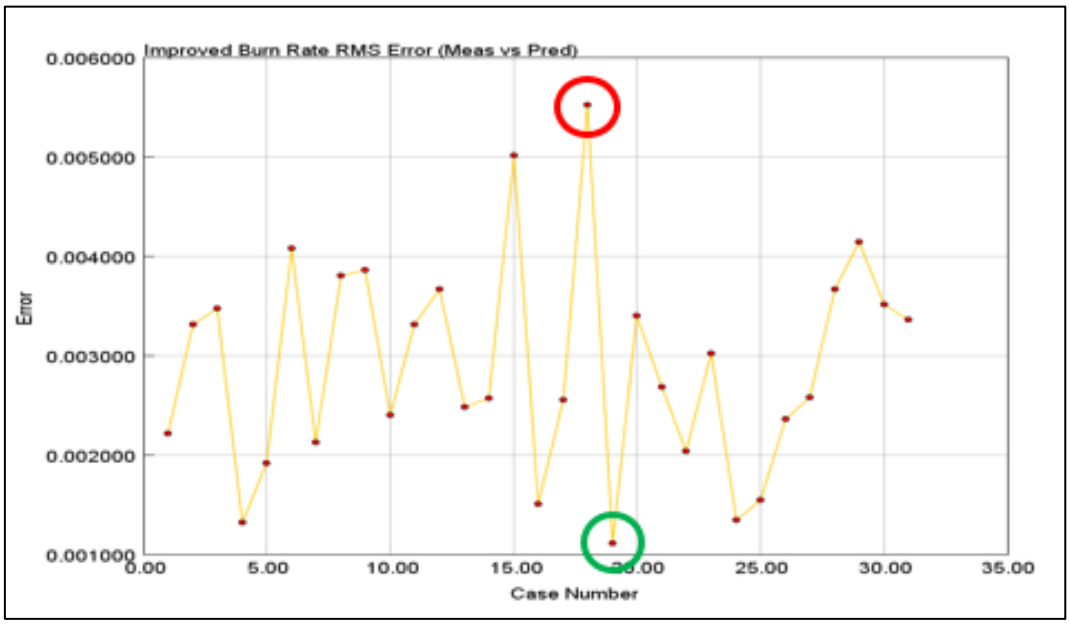

Figure 51. Burn rate RMSE (measured vs predicted). Independent optimization

Figure 51 demonstrates how the magnitude of the maximum RMS error decreases almost to half of the maximum error obtained in the single-set optimization (see Figure 39). This is also reflected in Figure 53, where the predictive pressure trace and burn rate matched well with the corresponding measured traces.

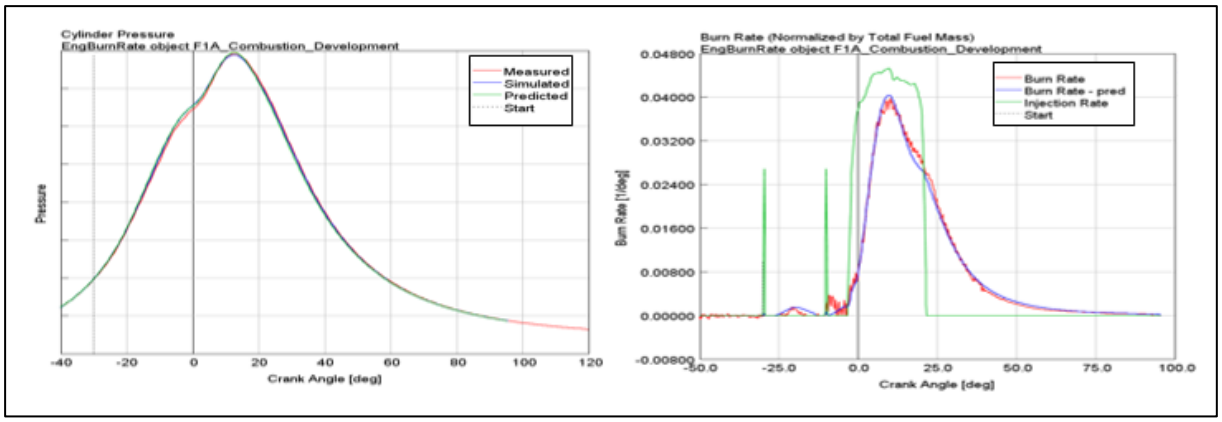

Figure 52. Pressure trace and burn rate. Best case. Independent optimization

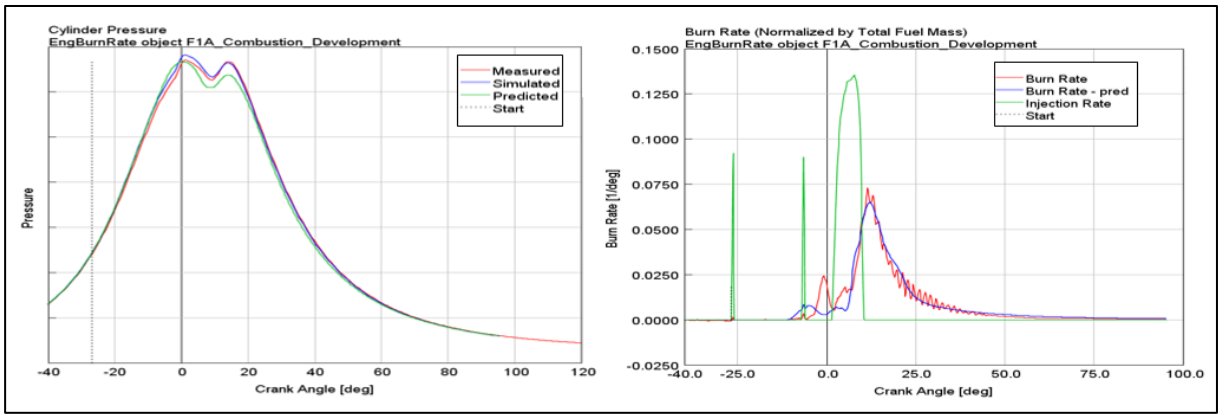

Figure 53. Pressure trace and burn rate. Worst case. Independent optimization

Figure 54, Figure 55 and Figure 56 illustrates the errors of *imep*, maximum pressure and MFB50 respectively.

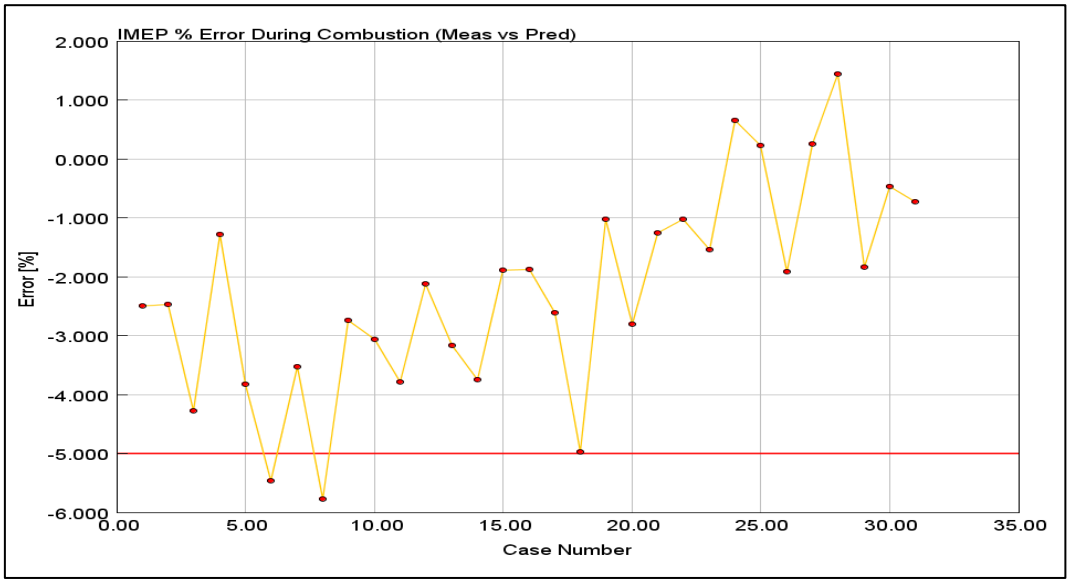

Figure 54. imep error. Independent optimization

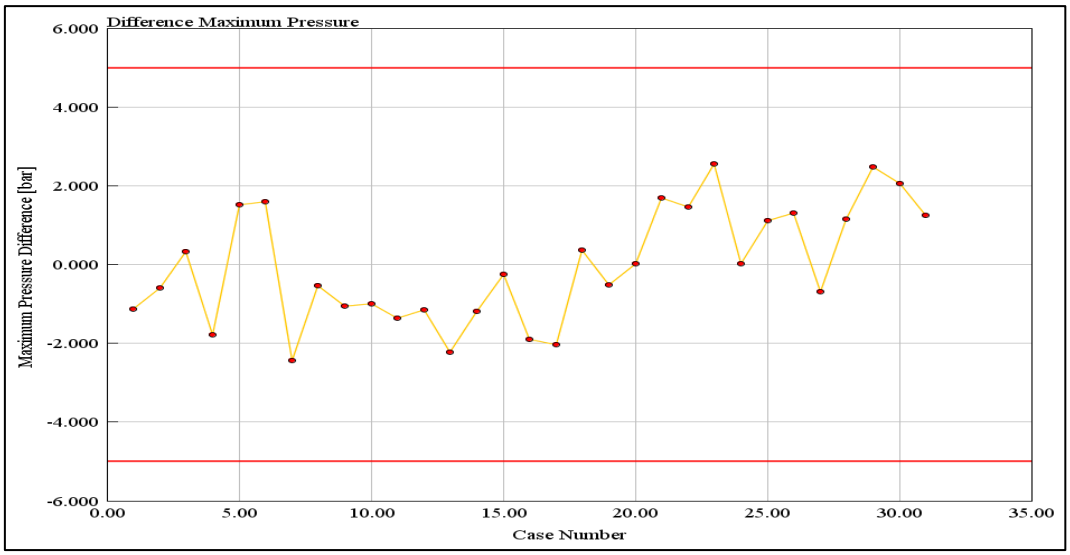

Figure 55. Maximum pressure error. Independent optimization

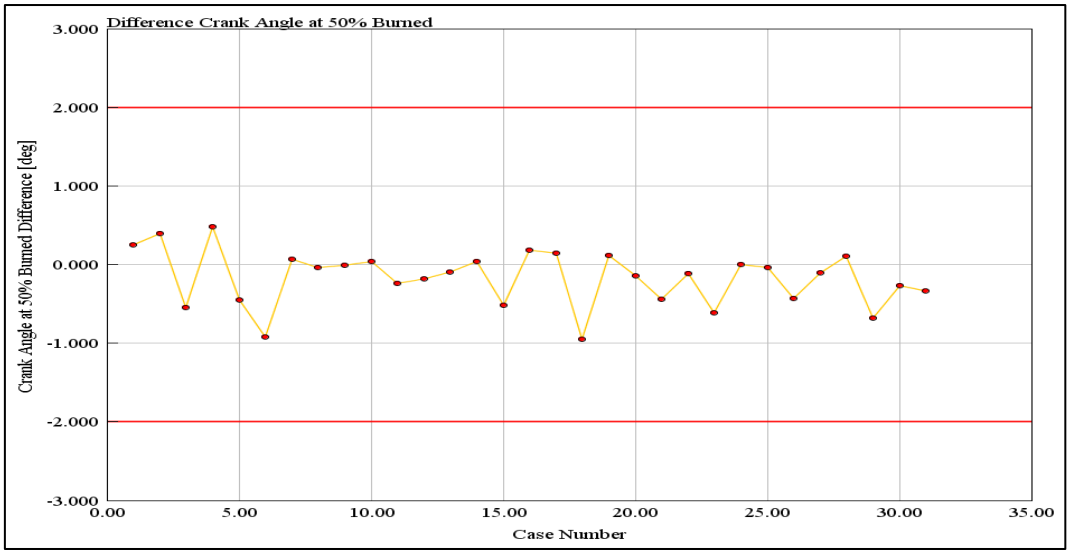

Figure 56. MFB50 error. Independent optimization

With the independent optimization, the simulated results from the DIPulse calibration seemed to match better with the measured values, more than the results from the single-set optimization. It should be noted, that all the errors for maximum pressure and MFB50 were within the recommended limits, and for imep errors, just a few cases were out of the permissible range.

4.3.3 Independent optimization of all 86 operating points

The analysis is similar to the previous case. However, the difference is that all the operating points are used for the calibration.

Figure 57, Figure 58 and Figure 59 illustrates the errors of *imep*, maximum pressure and MFB50 respectively.

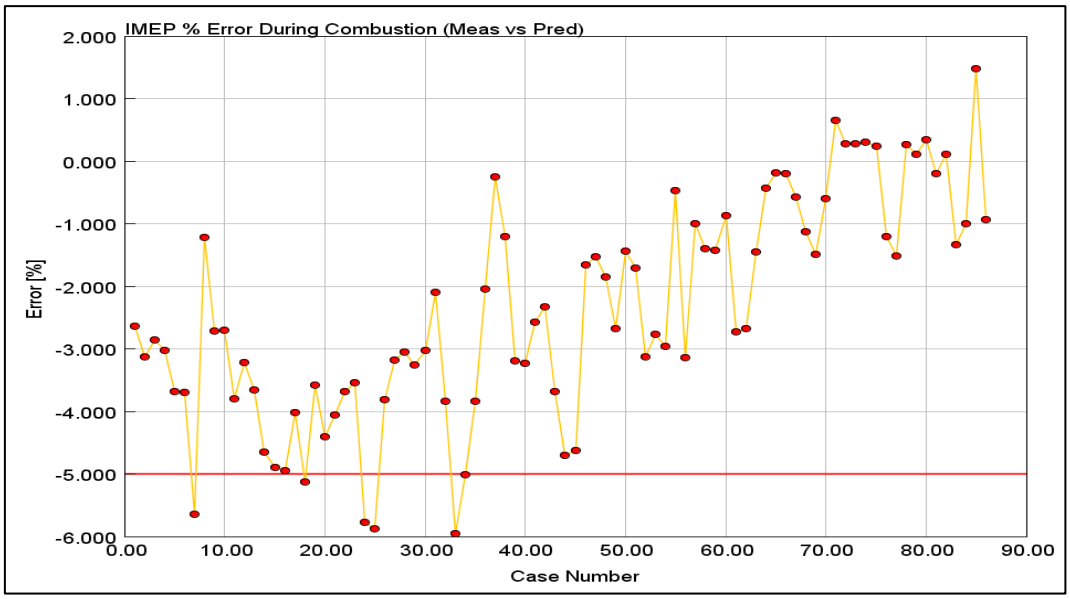

Figure 57. imep error. Independent optimization for all cases

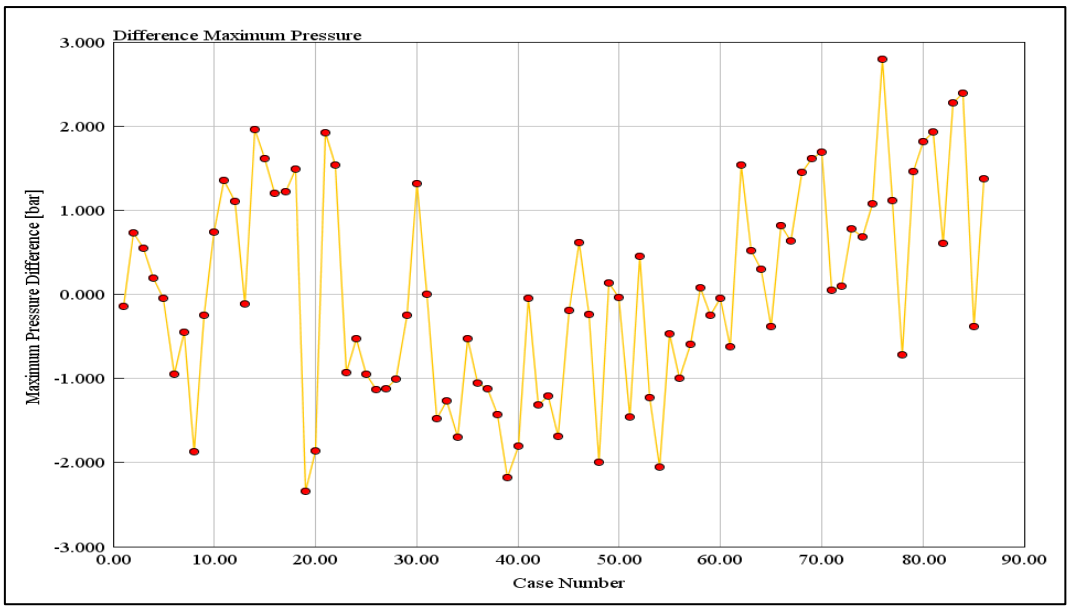

Figure 58. Maximum pressure error. Independent optimization for all cases

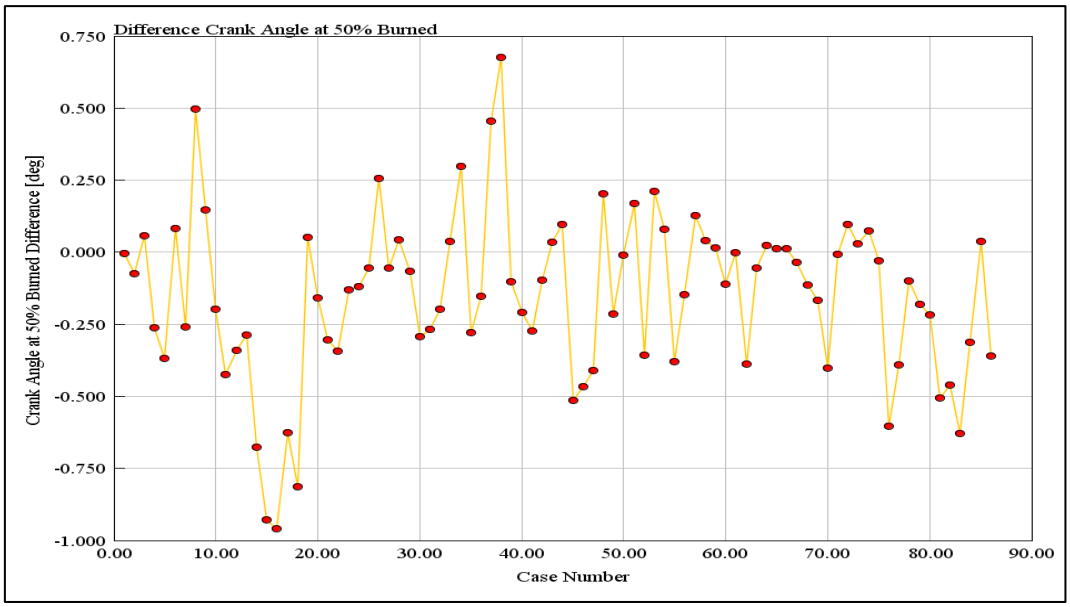

Figure 59. MFB50 error. Independent optimization for all cases

Even though in few cases the *imep* error were out of the recommended ranges, both the maximum pressure error and MFB50 error were between the thresholds. The goal of this last simulation was to check the trade-off between computational time and the accuracy of the results.

The main drawback of calibrating so many operating points, was that more computational time was needed for the simulation, without taking into account the consumed time for performing the measurements on the test rig.

4.3.4 NOx Calibration

Once the calibration of the combustion burn rate multipliers were defined, it was possible to continue with the calibration of NOx emissions. As mentioned later in section 4.5, the independent optimization for 31 operating points is the best one of all the options. Therefore, the results reported from the NOx calibration are related just with this optimization.

The optimization type chosen for the NOx was the single-set optimization. The results obtained for this simulation are reported in Table 11:

Table 11. NOx multipliers

Attribute	Constant
NOx calibration multiplier	0.594
N2 oxidation activation energy multiplier	1.01

As the N2 oxidation multiplier did not change so much with respect to the default value (default value=1), the NOx calibration multiplier was adjusted manually in order to obtain a better match. The final value used was

- NOx calibration multiplier = 0.75

4.4 Validation of the Predictive Model

Once the calibration procedure is over, the following step is the validation of the predictive model.

For the validation the full engine model was used, in which the predictive DIPulse combustion object was set in the cylinder block (see Figure 28).

Before changing the multipliers of the DIPulse, a simulation was run with the predetermined value of its variables. In other words, the constants used for each multiplier were set to 1.

4.4.1 DIPulse multipliers = 1

The error of *imep*, maximum pressure between the prediction and the measurements, and error between predicted MFB50 and measured MFB50 are shown as follows:

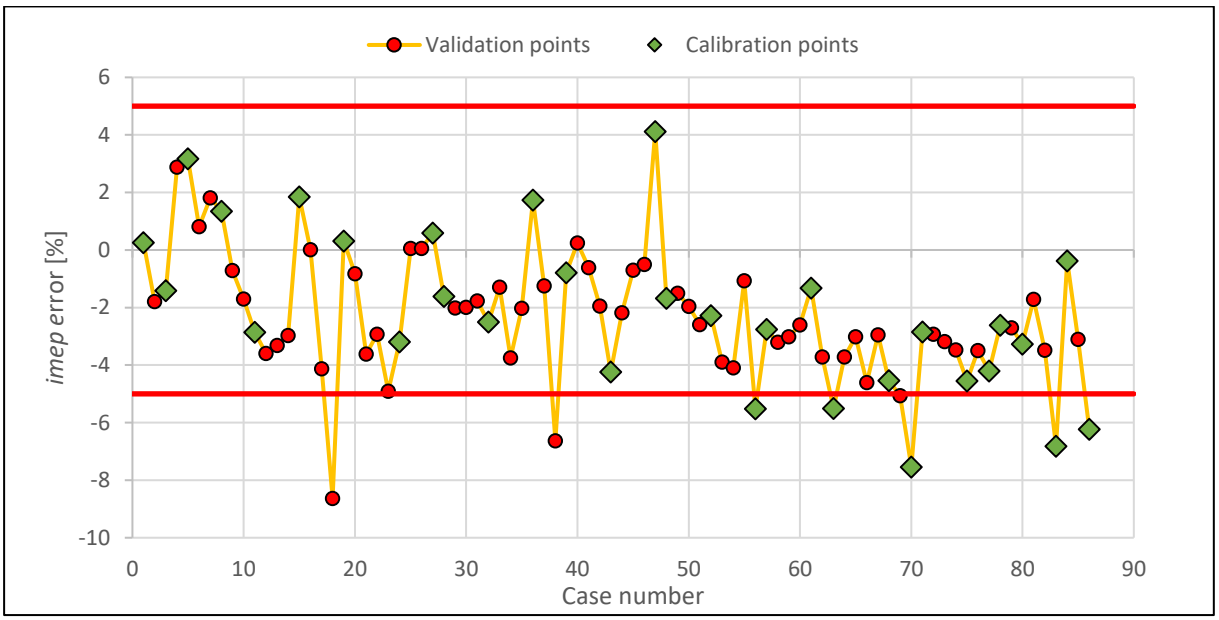

Figure 60. imep error validation. DIPulse multipliers = 1

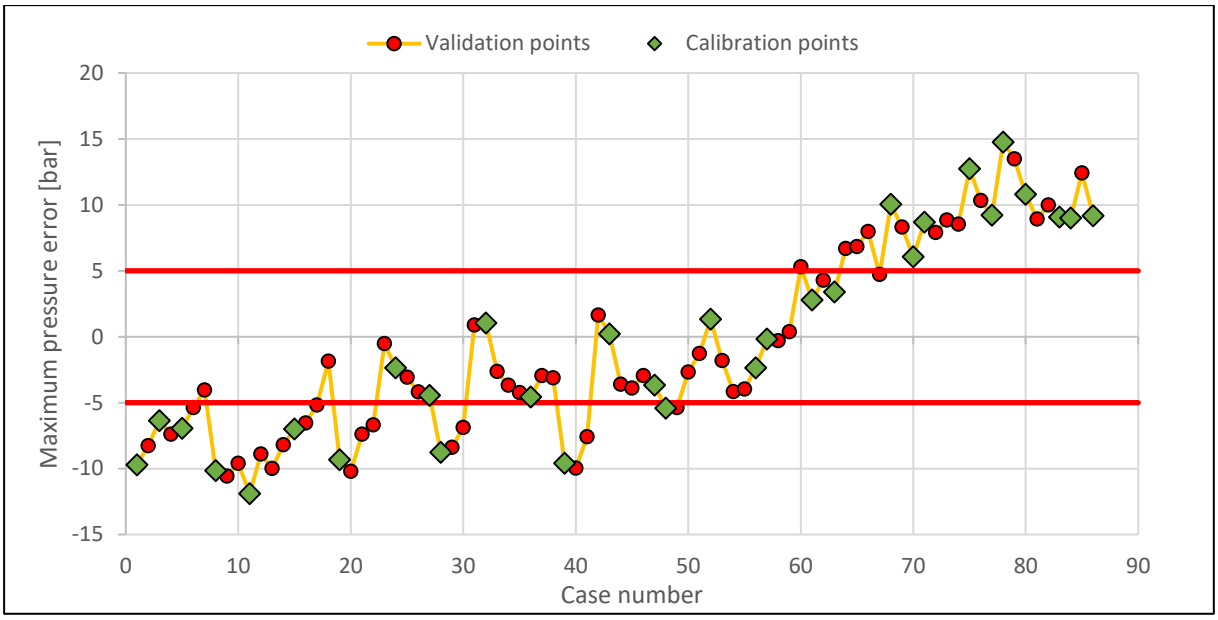

Figure 61. Maximum pressure error validation. DIPulse multipliers = 1

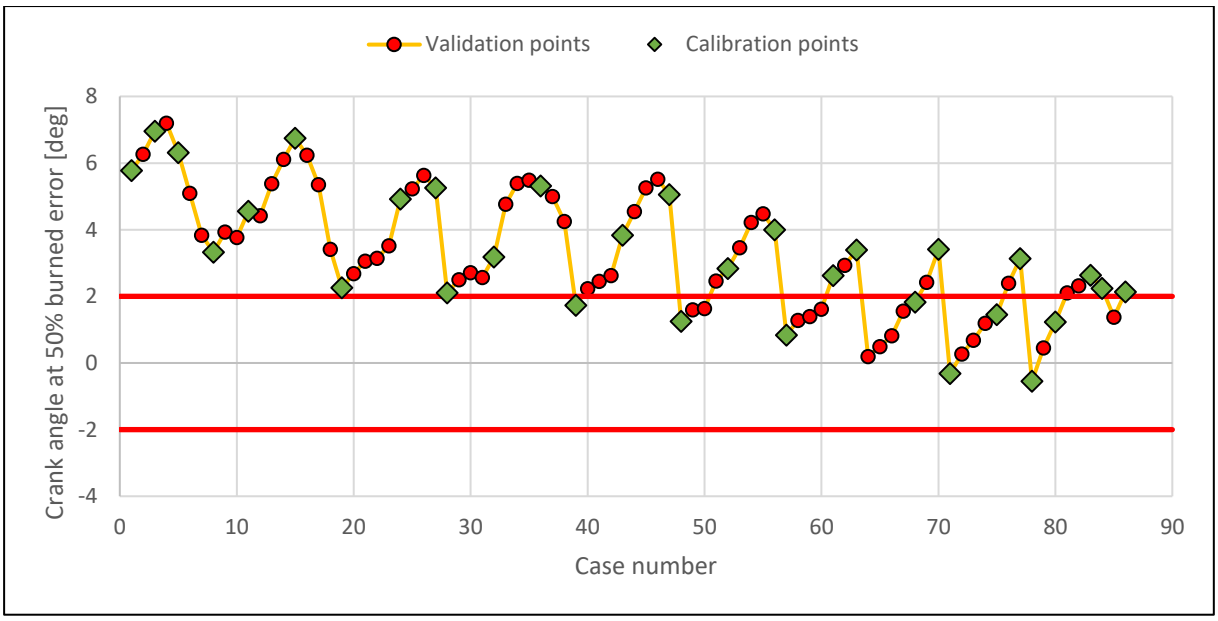

Figure 62. MFB50 error validation. DIPulse multipliers = 1

Without calibrating the system, almost all cases were inside the recommended range of the *imep* error, as shown in Figure 60. However, both the predicted maximum pressures and the predicted MFB50 were not very accurate, especially at high speeds and low speeds. These results are reflected on Figure 61 and Figure 62 respectively.

After obtaining these results, the following validations were performed:

4.4.2 Validation of single-set optimization

The DIPulse parameters obtained from the single-set optimization (see Table 10) were set for all engine operating points. The RLT (results) variables[9] were compared with their respective measurement data. The margin of error for each variable given by Gamma Technology was used to check the accuracy of the predictive model.

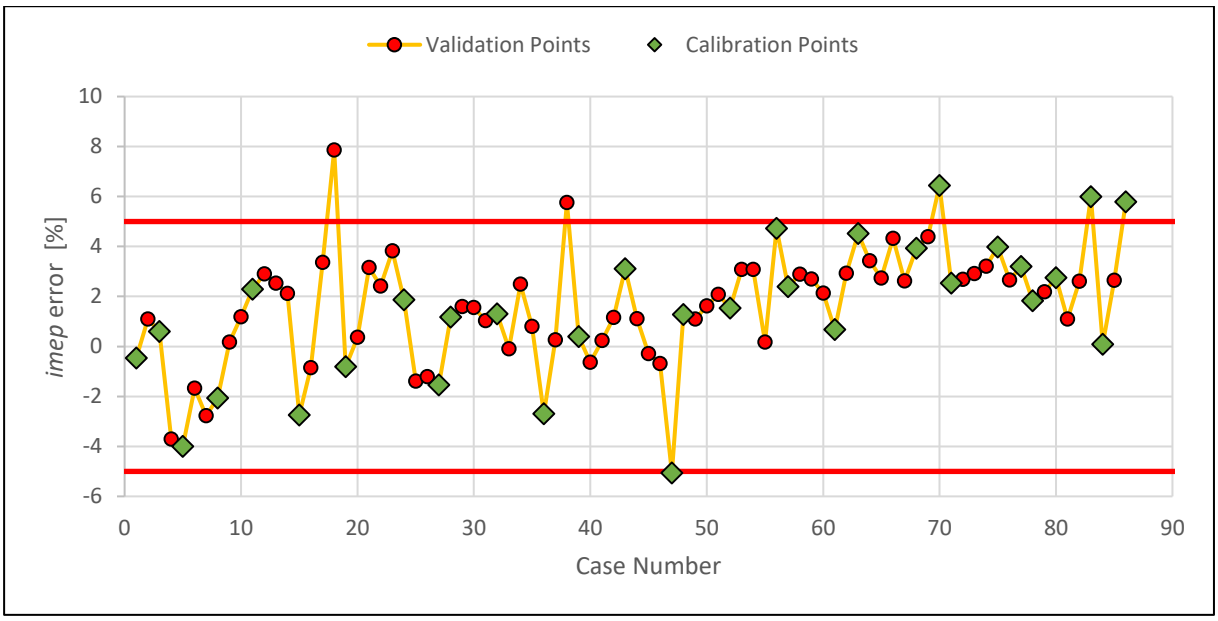

Figure 63. imep error validation. Single-set optimization

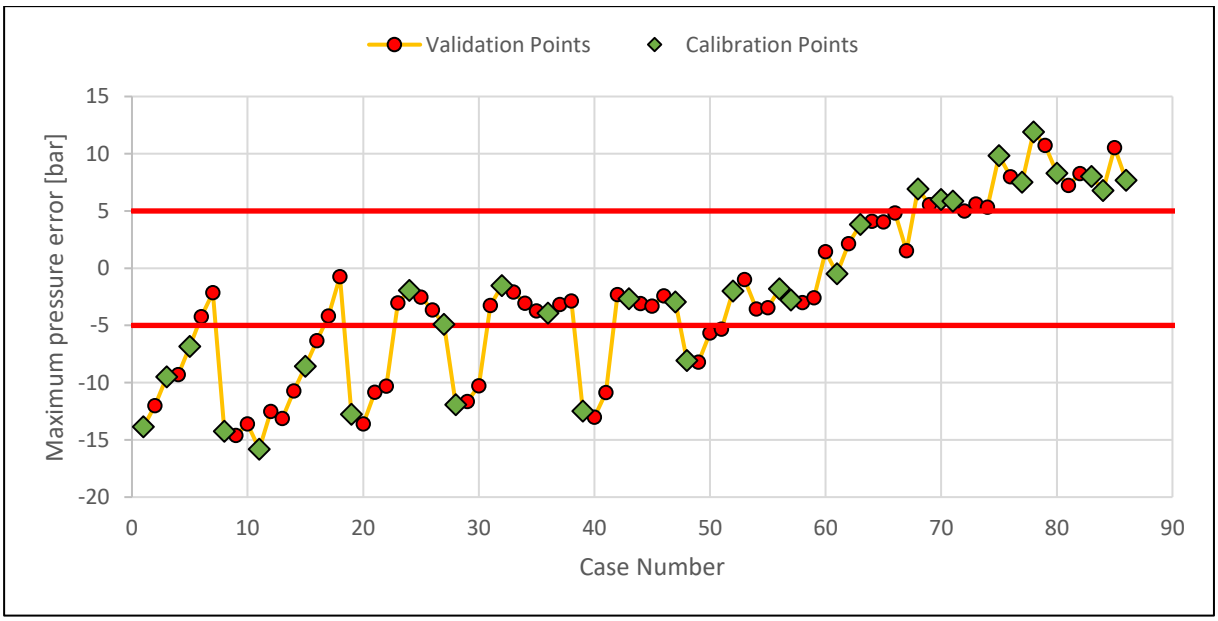

Figure 64. Maximum pressure error validation. Single-set optimization

[9] CaseRLT (result) variable is any simulation result which is calculated by GT-Suite for the last cycle of each case [27].

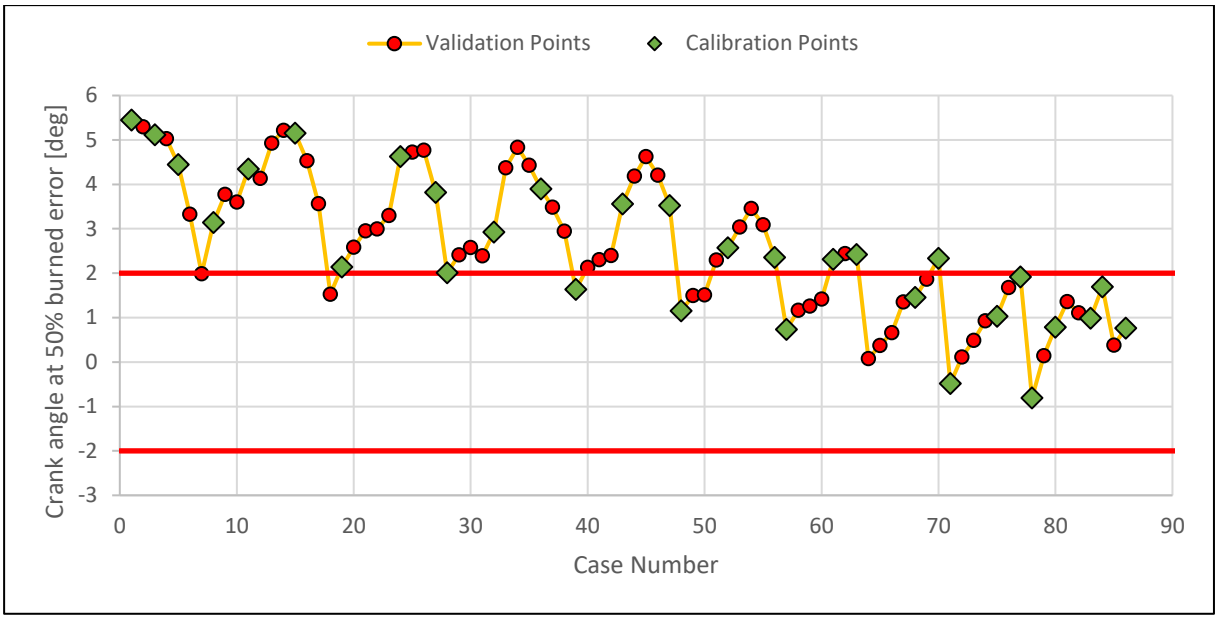

Figure 65. MFB50 error validation. Single-set optimization

By comparing the validation results using multipliers obtained from the single-set optimization and using the default value for the multipliers, it can be observed that the tendency of the errors were the same. At higher speeds, the predicted MFB50 were advanced and the predictive maximum pressures were higher with respect to the measurements. While at lower speeds, the predicted MFB50 were delayed and maximum pressures were lower than the measured ones. However, in the single-set optimization there was a noticeable improvement in the MFB50 error (see Figure 65). Meanwhile, for both *imep* and maximum pressure, the amount of errors outside of the accepted range slightly decreased, as shown Figure 63 and Figure 64 respectively.

4.4.3 Validation of independent optimization

From the optimized values obtained through the independent optimization of the 31 calibration points, a map for each multiplier was built and set as ´Object Value' in the DIPulse object. The maps for entrainment rate multiplier, ignition delay multiplier, premix combustion rate multiplier and diffusion combustion rate multiplier are shown in Figure 66.

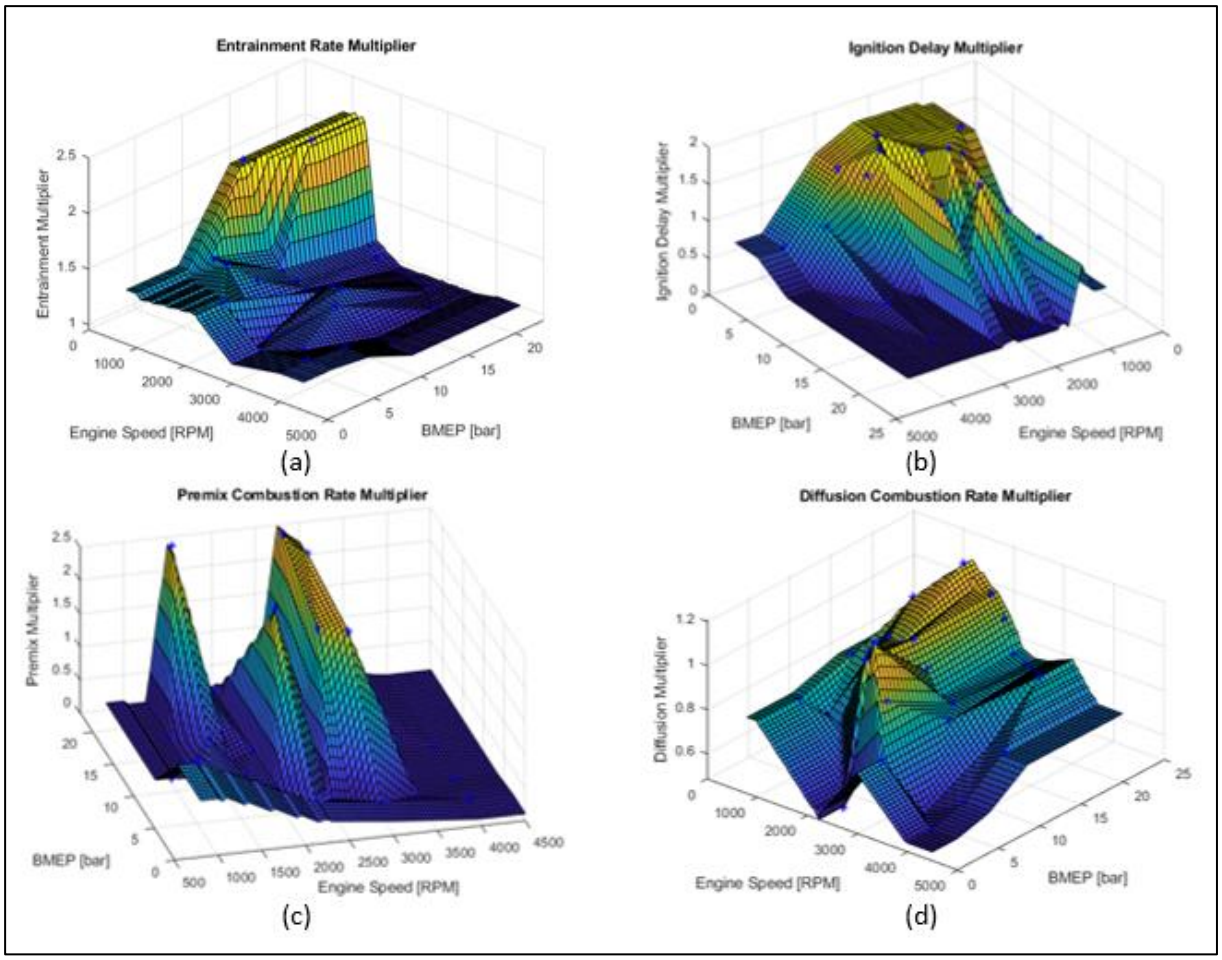

Figure 66. DIPulse multiplier maps: (a) Entrainment rate (b) Ignition delay (c) Premix combustion rate (d) Diffusion combustion rate

The premix combustion rate multiplier had several maximum and minimum points randomly along the lookup table. In addition to this, its effect on the simulations did not seem to have a big impact on the results. Therefore, this multiplier was defined as 1 for all the cases instead of using its map.

The errors of the resulting variables are shown in Figure 67, Figure 68 and Figure 69.

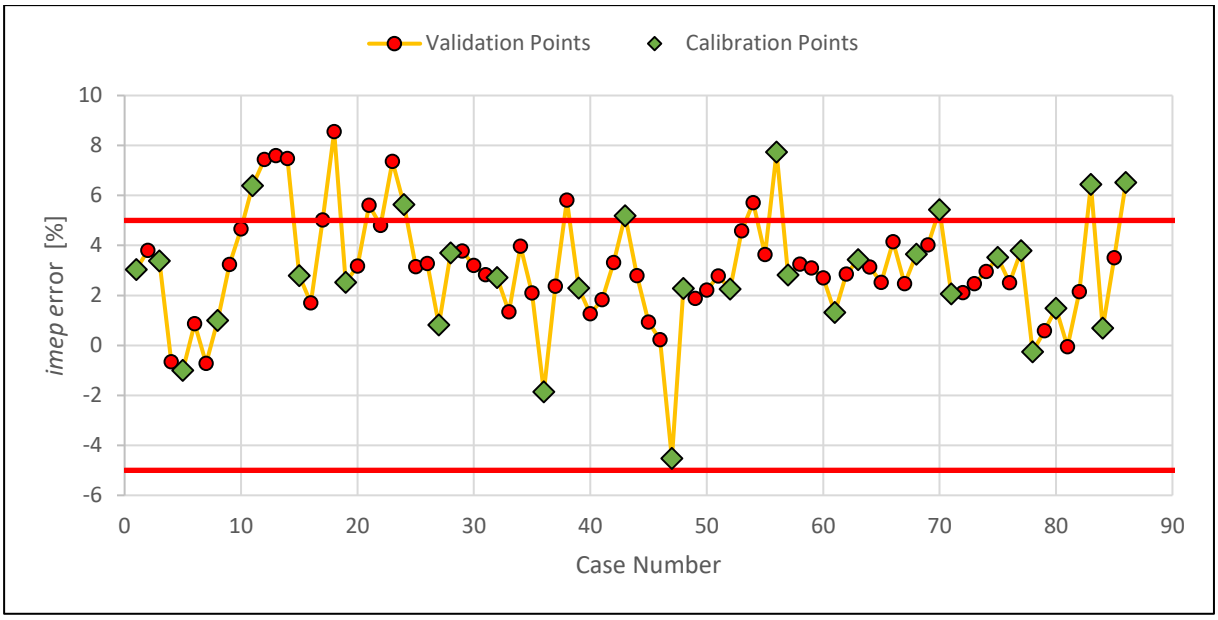

Figure 67.imep error validation. Independent optimization

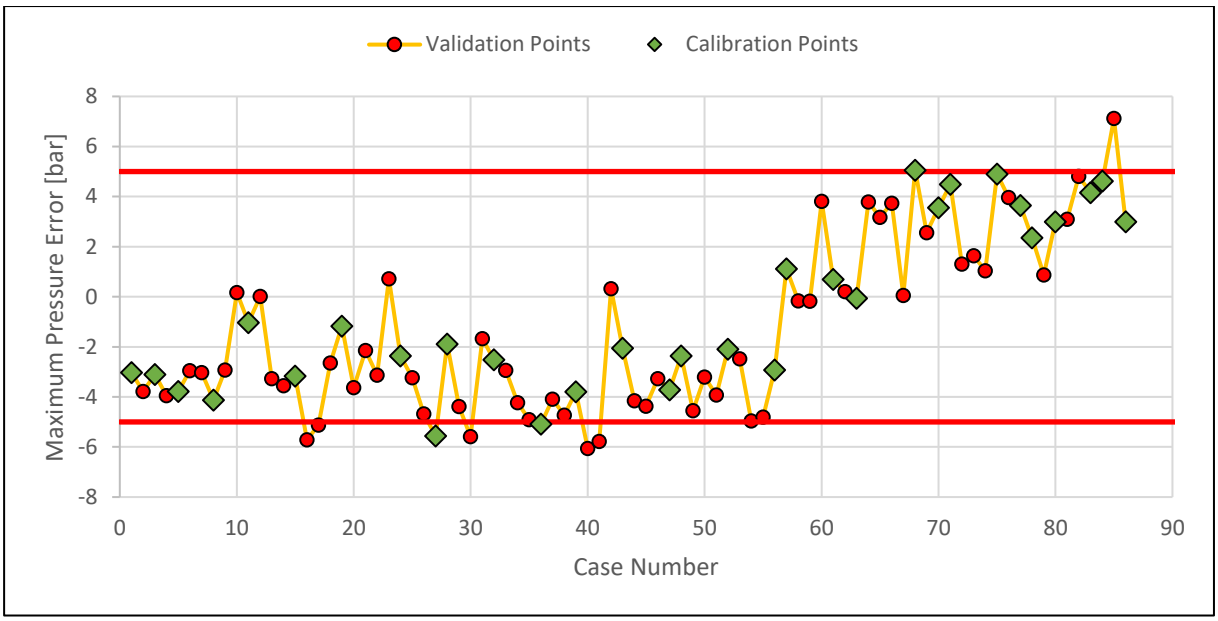

Figure 68. Maximum pressure error validation. Independent optimization

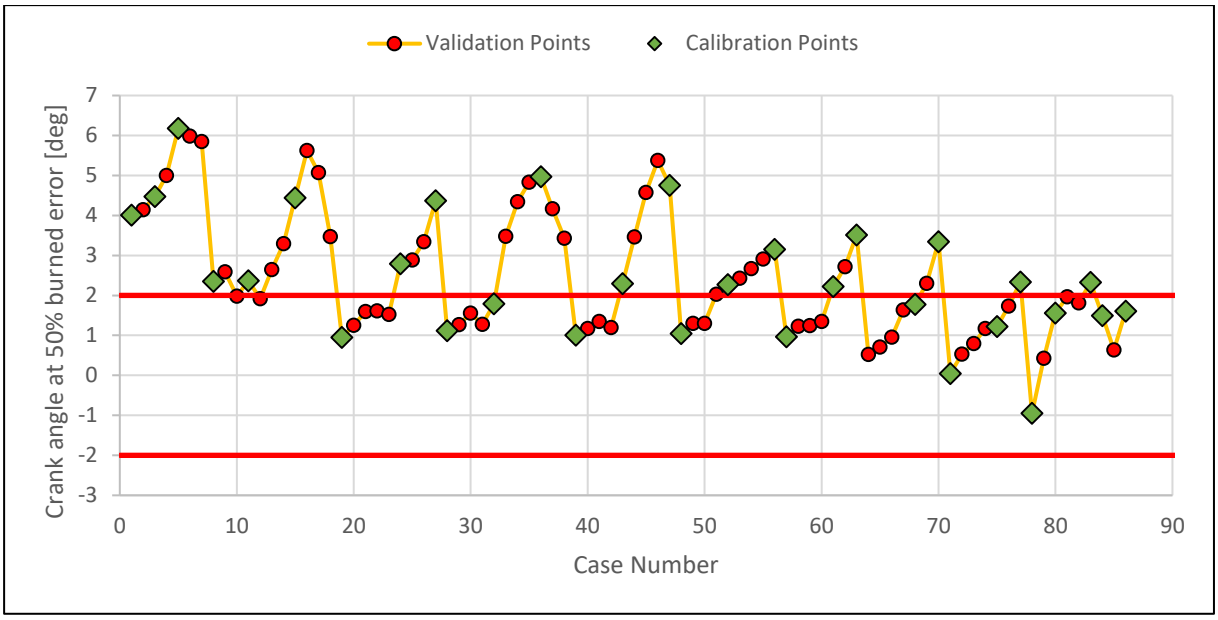

Figure 69. MFB50 error validation. Independent optimization

An important improvement in the accuracy of maximum pressure can be noticed by comparing the results of this validation with the one that used a single set of multipliers for all cases. Also, the MFB50 errors decreased, however, the amount of imep errors increased slightly in comparison to the single-set optimization.

4.5 Comparison of results

After analyzing the obtained results in section 4.3.3, section 4.4.2 and section 4.4.3 (independent optimization for all 86 operating points, validation of single-set optimization and validation of independent optimization respectively), it can be concluded that the independent calibration using all the operating points had the best match with the experimental measurements. However, its results were not so different to those obtained from the independent optimization using 31 calibration points. Thus, a sample of 31 operating points was enough to not compromise the accuracy of the predictive model, while achieving a faster runtime. But the main drawback of the implementation of lookup maps is that the extrapolation behavior is outside the range of the calibration data. Nevertheless, this risk seemed to be the best solution to compensate for the inaccuracy of the injection rate maps used in the simulations.

Also, the average error for each performed validation was compared with the suggested values. They can be observed in Table 12.

Table 12. Average error of validations

Metric	Suggested Average Error	Non-Predictive	Single-set Optimization	Independent Optimization (31 calibrating points)	Independent Optimization (86 calibrating points)
imep [%]	**2**	2.0	**2.3**	3.3	3.3
Maximum Pressure [bar]	**3**	2.2	6.5	3.2	**2.9**
MFB50 [deg]	**1**	0	2.6	**2.5**	**2.5**

In order to revise the accuracy of the models, the RMSE is also estimated and shown in Table 13.

Table 13. RMSE imep, maximum pressure and MFB50

Metric	Non-Predictive	Single-set Optimization	Independent Optimization (31 calibrating points)	Independent Optimization (86 calibrating points)
imep [bar]	0.30	**0.36**	0.52	0.53
Maximum Pressure [bar]	2.54	7.69	3.54	**3.28**
MFB50 [deg]	0.00	3.03	**2.90**	2.96

From Table 12, it can be observed that the validation in which the single-set calibration was performed had the best match predicting *imep*. However, the maximum pressure errors are higher than the recommended errors. On the other hand, in both independent optimizations, the prediction of the maximum pressure improved considerably, compromising the accuracy of the *imep* only slightly. The average error value of MFB50 remained almost the same in all validations.

Table 13 verifies the results obtained in Table 12. For the prediction of the *imep*, the independent optimizations had bigger errors than the single-set optimization. On the other hand, the maximum pressure RMSE showed that the accuracy between both independent combustion models was similar (RMSE values were 3.54 [bar] and 3.28 [bar]) and slightly below the accuracy obtained from the non-predictive model (RMSE value was 2.54 [bar]). However, the maximum pressure error magnitudes obtained from the single-set model were more significant, obtaining a higher RMSE value (7.69 [bar]). For the MFB50 RMSEs, the accuracy was almost the same for the three predictive simulations.

It is important to note the similarity between not only the average errors, but also the amount of errors between the recommended limits of the two independent optimization procedures, and the magnitudes of their RMSE. In other words, the extended runtime used for the calibration of all 86 operating points did not justify the results obtained. Thus, an optimization process of the 31 sample points would be enough for obtaining reliable predictive results. Even though there could be problems with the extrapolation of the multipliers during the validation, the lookup maps worked well enough to compensate for the impact of using simplified injection rate profiles in the predictive combustion model.

In order to deeply analyze the impact of the simplifications and assumptions made in this project, the average error of the abovementioned metrics and the RMSE were calculated for different ranges of speed and load. The results regarding the *imep* are shown in Table 14 and Table 15.

Table 14. imep average error [%] for different speed ranges and load ranges

Combustion Model	***imep* average error [%] Speed Range**			***imep* average error [%] Load Range**		
	High speed	*Middle speed*	*Low speed*	*High load*	*Middle load*	*Low load*
Non-Predictive	2.3	1.4	2.6	1.5	1.6	2.8
Single-set Optimization	2.2	**1.9**	3.2	**1.9**	2.1	2.9
Independent Optimization (31 calibrating points)	3.9	3.0	**2.9**	**2.7**	3.3	3.7
Independent Optimization (86 calibrating points)	4.0	3.0	**3.0**	**3.0**	3.4	3.5

Table 15. imep RMSE [bar] for different speed ranges and load ranges

Combustion Model	***imep* RMSE [bar] Speed Range**			***imep* RMSE [bar] Load Range**		
	High speed	*Middle speed*	*Low speed*	*High load*	*Middle load*	*Low load*
Non-Predictive	0.27	0.22	0.42	0.39	0.29	0.23
Single-set Optimization	**0.27**	0.30	0.51	0.46	0.36	**0.27**
Independent Optimization (31 calibrating points)	0.61	0.48	**0.47**	0.62	0.57	**0.37**
Independent Optimization (86 calibrating points)	0.61	0.49	**0.47**	0.69	0.55	**0.34**

From Table 14 and Table 15, it can be observed that regarding the load range, the best *imep* average error and *imep* RMSE were obtained in the validation of the single-set of multipliers, in which the lower error was found at high load (1.9 [%]) and the lower RMSE was found at low load (27[bar]). It is important to mention that the *imep* mean absolute error was estimated from the calculated percentage errors between the predicted *imep* and the measured *imep*, while the RMSE was estimated from the difference between them. For this reason, even if the average errors in all the simulations are smaller at high loads, the RMSE showed better accuracy at low loads for all the models. In addition, the fluctuation of the RMSE was higher for the independent models (0.34 [bar] for the optimization of 86 operating points and 0.26 [bar] for the simulation where 31 operating points were used), than the RMSE of single-set model (0.19 [bar]).

Regarding the impact of the speed, the single-set simulation also had the best results at middle speed for average error and at high speed for RMSE. Regarding both independent models, the best average errors and RMSE values were obtained at low speed. Also, the variation of the RMSE was lower for the independent models (0.14 [bar] for both models), than the RMSE of the single-set model (0.24 [bar]).

Table 16 and Table 17 show the maximum pressure average error and the maximum pressure RMSE respectively.

Table 16. Maximum pressure average error [bar] for different speed ranges and load ranges

Combustion Model	Maximum pressure average error [bar] Speed Range			Maximum pressure average error [bar] Load Range		
	High speed	*Middle speed*	*Low speed*	*High load*	*Middle load*	*Low load*
Non-Predictive	2.9	2.3	1.3	1.9	1.9	2.7
Single-set Optimization	8.7	**4.6**	6.9	8.7	**5.8**	6.0
Independent Optimization (31 calibrating points)	**3.0**	3.1	3.3	3.1	**2.3**	4.0
Independent Optimization (86 calibrating points)	2.7	**2.3**	4.1	**2.4**	2.7	3.6

Table 17. Maximum pressure RMSE [bar] for different speed ranges and load ranges

Combustion Model	Maximum Pressure RMSE [bar] Speed Range			Maximum Pressure RMSE [bar] Load Range		
	High speed	*Middle speed*	*Low speed*	*High load*	*Middle load*	*Low load*
Non-Predictive	3.08	2.56	1.67	2.16	2.25	3.00
Single-set Optimization	9.88	**5.82**	7.33	9.54	7.27	**6.44**
Independent Optimization (31 calibrating points)	**3.36**	3.59	3.66	3.47	**2.75**	4.15
Independent Optimization (86 calibrating points)	2.98	**2.82**	4.16	**2.92**	3.09	3.67

In the simulation that used a single-set of multipliers for all cases, it can be noticed that there was an improvement at middle speed in both RMSE and average error (even though this last value was still higher than the recommended one by Gamma Technologies). While observing the behavior of the data in function of the load, the average error was similar at both low load and middle load. However, when observing the RMSE, the predicted maximum pressure fit better with the measured one at low load rather than at middle and high loads.

In the validation of the independent calibration using 31 operating points, the average error did not have significant variations along the whole speed range, however, it obtained better results at middle load. On the other hand, the results of the RMSE were also similar along the speed range, achieving better accuracy at high speed, while in the load range it obtained the best predictions at middle load.

In the simulation where all 86 operating points were calibrated independently, the mean absolute errors were similar at high speed and middle speed, while obtaining the worst average error at low speed. A similar tendency can be observed along the load range. The tendencies of the RMSE in both speed range and load range were similar to those obtained from the average error behaviors.

In addition, the fluctuation of the RMSE was lower in the validation of the independent optimization of 31 operating points than in the simulation of the independent optimization of the 86 operating points and in the validation of the single-set of multipliers. The variations of the RMSE were: 0.30[bar], 1.34[bar] and 4.06[bar] respectively, while the variations of the RMSE along the load range were: 1.39[bar], 0.75 [bar] and 3.10[bar] respectively. These values show that the single-set optimization had a bigger dependence on the speed and load than the other two models.

Table 18 and Table 19 Table 17show the average error and RMSE of the MFB50 respectively.

Table 18. MFB50 average error [deg] for different speed ranges and load ranges

Combustion Model	MFB50 average error [deg] Speed Range			MFB50 average error [deg] Load Range		
	High speed	*Middle speed*	*Low speed*	*High load*	*Middle load*	*Low load*
Non-Predictive	0.0	0.0	0.0	0.0	0.0	0.0
Single-set Optimization	3.9	2.7	**1.0**	**1.6**	2.6	3.6
Independent Optimization (31 calibrating points)	3.4	2.5	**1.4**	**1.2**	2.0	3.8
Independent Optimization (86 calibrating points)	3.5	2.5	**1.4**	**1.2**	2.0	3.9

Table 19. MFB50 RMSE [deg] for different speed ranges and load ranges

Combustion Model	MFB50 RMSE [deg] Speed Range			MFB50 RMSE [deg] Load Range		
	High speed	*Middle speed*	*Low speed*	*High load*	*Middle load*	*Low load*
Non-Predictive	0.01	0.01	0.00	0.01	0.00	0.00
Single-set Optimization	4.09	2.91	**1.17**	**1.87**	2.88	3.75
Independent Optimization (31 calibrating points)	3.73	2.83	**1.58**	**1.27**	2.14	4.08
Independent Optimization (86 calibrating points)	3.84	2.87	**1.58**	**1.25**	2.16	4.19

Regarding the prediction of MFB50, for all cases, the best results were obtained at low speed and high load. In the speed range, the single-set simulation obtained both the best average error value and lower RMSE, however, it also had the worst results of all models at high speed. It is important to notice that both independent models obtained very similar results along the whole speed range.

Regarding the load range, for both independent models, the predicted values fit better with the measured ones than the values predicted by the single-set model. However, at low load the accuracy was worse in these two cases than the single-set simulation. Once again, the results obtained for the mean average value and the RMSE were very similar between the independent models along the whole load range.

In addition, the fluctuation of the RMSE was slightly lower for the validation of the independent optimization of 31 operating points, than the simulation of the independent optimization of the 86 operating points and the validation of the single-set of multipliers. The variation of the RMSE were: 2.15[deg], 2.26[deg] and 2.92[deg] respectively, while the variations of the RMSE along the load range were: 2.82[deg], 2.94[deg] and 1.87[deg] respectively. These values show a bigger dependency of the sweep optimization on the speed than in the other two models.

From the previous results, the effect of the speed and load on the prediction of the models can be verified. The predicted *imep* was more accurate using the single-set model, however, there was a loss in accuracy at high speed. While, on the other hand, the predicted *imep* of both independent models were similar. Regarding the maximum pressure, the DIPulse model that used the independent calibration of 86 operating points predicted better results than the other two models. However, the results obtained by the DIPulse model that used the lookup maps created from the 31 calibration points had similar results. Finally, the predicted MFB50 from both models that used the independent optimization obtained the best fit with the measured MFB50.

4.5.1.1 NOx Validation

The validation of the NOx calibration was conducted by using the full engine model and the maps obtained from the independent optimization of 31 operating points.

Figure 70 reflects the error of the predicted NOx concentration and the measured NOx concentration for all cases, and their respective EGR mass flow rate.

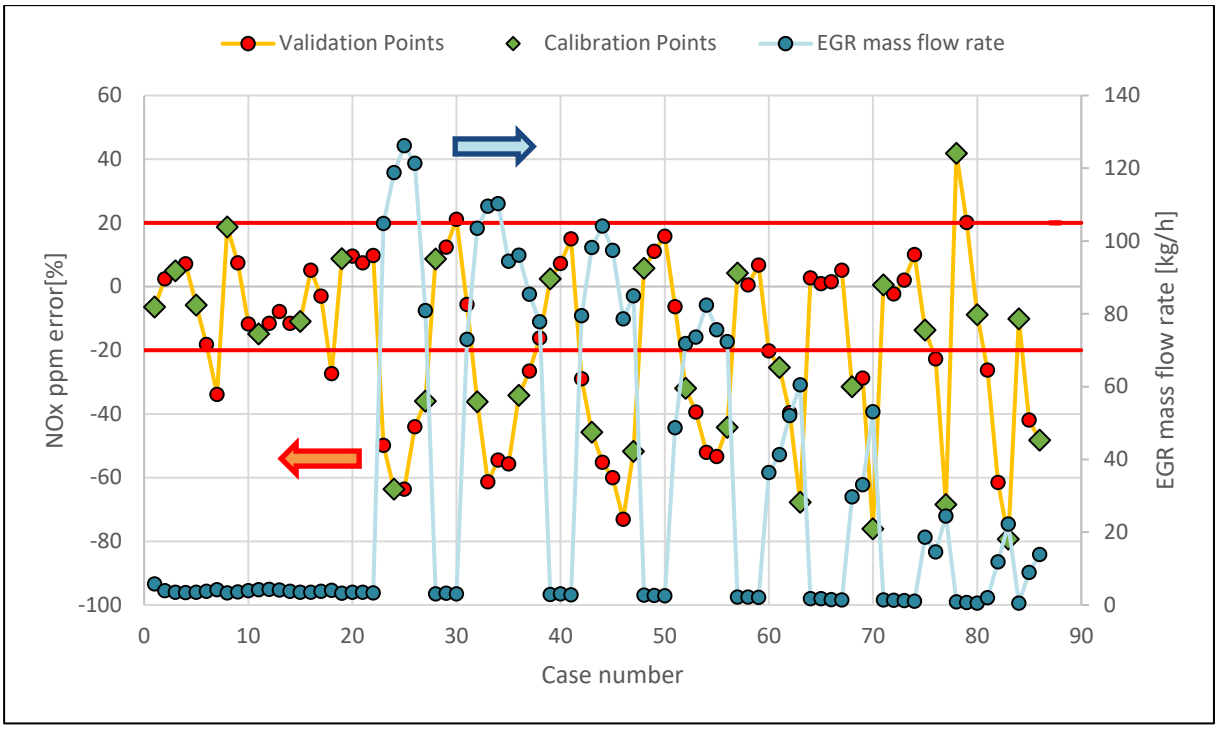

Figure 70. NOx ppm error validation

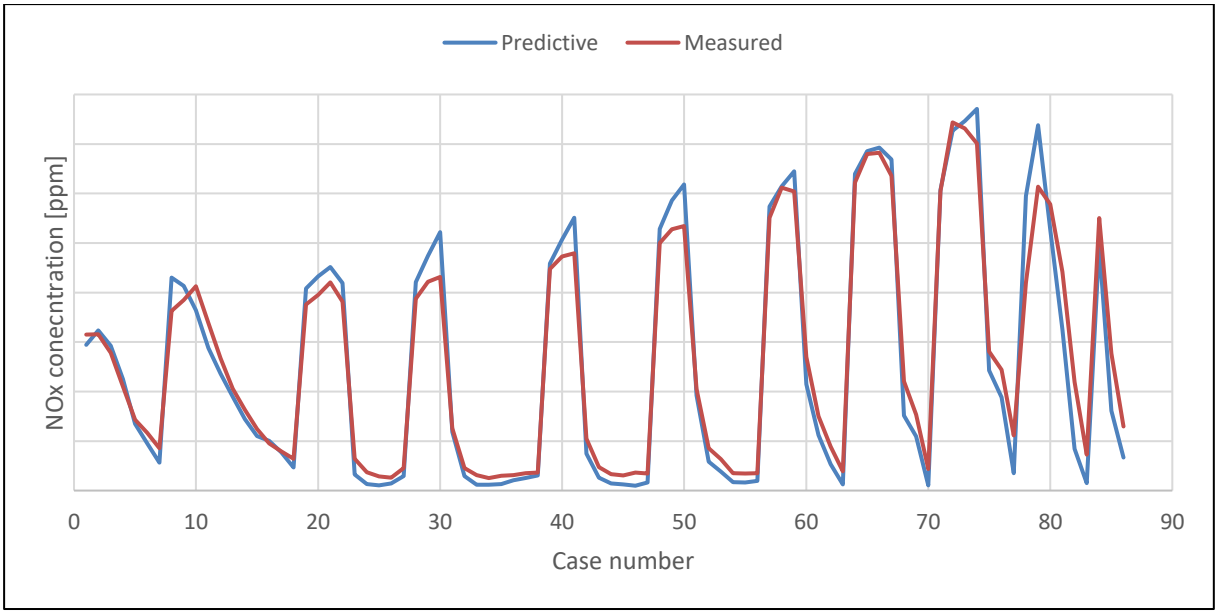

Figure 71. NOx concentration

From Figure 70 it can be observed that the majority of the errors outside the suggested limits of ± 20 matched when there were high EGR mass flow rates. These points coincided at low loads and high speed ranges, and at middle and low loads at middle and low speeds. On the other hand, during high speed ranges and middle and low loads, and at middle and low speed ranges but high loads, the EGR rates were low, and this is where the NOx predictions were acceptable. Even though the average NOx concentration error is 25%, which is higher than the recommended average error (13%), and the RMSE was 119.54 [ppm], Figure 71 shows that the prediction of NOx concentration matches well with the tendency of the measured NOx concentration.

5 Conclusion

The aim of this project was to calibrate and evaluate a predictive combustion model in GT-power to characterize the behavior of a 2.3L diesel engine for light-duty applications. As the supply system of the engine was direct injection, the Direct-Injection Diesel Multi-Pulse Model (DIPulse) was chosen.

The provided data were analyzed, and it was verified that a fusion injection event was occurring between the main pulse and the pre-main pulse for all cases. As GT-Power was not able to simulate these injection rate profiles, some assumptions were implemented in order to reproduce real injection patterns. These formulated assumptions were of significant importance, because they are the main reason for error in the final results of the project.

The cylinder pressure only analysis (CPOA) was performed to obtain the burn rate profiles from the given measured pressure traces. After finishing the iterative process to estimate the combustion chamber temperatures and trapping ratio, a consistency check was performed on the input data to verify their quality. Then, the overall convection multiplier was corrected in order to compensate for both the effect of the injection profile on the heat transfer calculation and the simplifications made by GT-Power regarding the selected heat transfer model. A new consistency check was performed, and as a result, 21 operating points were dismissed. A total amount of 86 operating points were used for the rest of the analysis. Then, the full engine model was tested with the non predictive combustion model. The results between the simulated variables and the measured variables matched well.

For the calibration of the DIPulse model, 31 operating points distributed on the engine map were selected. Two types of calibrations were performed. In the first one, a single set of the DIPulse multipliers were estimated. This set should be the best possible match to a wide range of operating points of the engine. The validation's results highlighted the effect of the engine speed on the assumed injection profile. The faster the engine speed, the earlier the predicted MFB50 took place with respect to the simulated one - occurring closer to TDC – therefore, higher peak pressures were predicted. While, at lower engine speeds, the predicted 50% of mass fuel burned inside the cylinder developed later than the simulated one during the expansion stroke, generating lower peak pressures.

The second type of performed calibration was the independent calibration, in which the best combination of DIPulse multipliers were found separately for each engine operating point. It was observed from the validation's results that the dependency of the prediction on the engine speed decreases, generating an improvement in the predicted variables in comparison with variables obtained through the single-set calibration. This was verified with the variation of the RMSEs on the speed range analysis, in which the fluctuations of the independent validation RMSEs were: for *imep* 0.14[bar], for maximum pressure 0.30[bar] and for MFB50 2.1[deg], while the variation of RMSEs of the single-set validation were: for *imep* 0.24[bar], for maximum pressure 4.1[bar] and for MFB50 2.9[deg].

Then, later results were compared with the outputs obtained from the independent calibration of the 86 points. The difference between the simulated variables was not significant, but not the computational time. The time consumed for the calibration of the 86 points was three times more than the time needed for the calibration of 31 points. Therefore, the independent optimization of 31 points was selected as the best calibration procedure.

Even though the tendency of the predicted NOx concentration was similar to the measured NOx concentration, the model was not able to obtain trustful predictions when a high amount of EGR was inducted in the cylinder.

Computational simulations are powerful tools which lead to reliable results and reduce testing time. The results obtained can be improved by using either the proper injection profiles or a detailed 1-D model of the injector to predict the injection rates. In that case, it is recommended to use the single-set optimization then the independent optimization. The usage of lookup maps could generate some inaccuracies when extrapolating outside the range of the calibration data.

6 Bibliography

[1] S. Pischinger, J. Schnitzler, M. Rottmann, H. Busch and F. Fricke, "Future of Combustion Engines," *SAE Technical Paper 2006-21-0024,* 2006.

[2] R. Folkson, Alternative Fuels and Advanced Vehicle Technologies for Improved Environmental Performance: Towards Zero Carbon Transportation, Woodhead Publishing Limited, 2014.

[3] W. A. Majewski and H. Jääskeläinen, "Exhaust Particulate Matter," 2018. [Online]. Available: https://www.dieselnet.com/tech/dpm.php.

[4] D. Jung and D. N. Assanis, "Multi-Zone DI Diesel Spray Combustion Model for Cycle Simulation Studies of Engine Performance and Emissions," *SAE Technical Paper 2001-01-1246,* 2001.

[5] F. Payri, J. M. Desantes and J. Benajes, "Compression Ignition Engines: State-of-the-Art and Current Technologies, Future Trends and Developments," in *Handbook of Clean Energy Systems*, Online, John Wiley & Sons, Ltd, 2015.

[6] D. K. Manley, A. McIlroy and C. A. Taatjes, "Research Needs for Future Internal Combustion Engines," *Physics Today,* vol. 61, no. 11, 2008.

[7] A. Piano, F. Millo, G. Boccardo and M. Rafigh, "Assesment of the Predictive Capabilities of a Combustion Model for a Modern Common Rail Automotive Diesel Engine," *SAE Technical Paper 2016-01-0547,* 2016.

[8] J. B. Heywood, Internal Combustion Engine Fundamentals, New York: McGraw-Hill, 1988.

[9] C. N. Grimaldi and F. Millo, "Internal Combustion Engine (ICE) Fundamentals," in *Handbook of Clean Energy Sysyem*, Online, John Wiley & Sons, Ltd., 2015, pp. 1-32.

[10] Energy, Office of Energy Efficiency & Renewable, "Internal Combustion Engine Basics," 22 11 2013. [Online]. Available: https://www.energy.gov/eere/vehicles/articles/internal-combustion-engine-basics.

[11] C. F. Taylor, The Internal-Combustion Engine in Theory and Practice Volume 1 - Thermodynamics, Fluid Flow, Performance, Second ed., The M.I.T. PRESS, 1985.

[12] G. Ferrari, Motori a Combustione Interna, Bologna: Societá Editorice Esculapio, 2016.

[13] C. F. Taylor, The Internal-Combustion Engine in Theory and Practice Volume 2 - Combustion, Fuels, Materials, Design, Second ed., vol. 2, The M.I.T. Press, 1985.

[14] F. Millo, *Engine Emission Control couse's material.*

[15] J. E. Dec, "A Conceptual Model of DI Diesel Combustion Based on Laser-Sheet Imaging," *SAE Technical Paper 970873,* 1997.

[16] E. Spessa, " Design of Engine and Control System couse's material".

[17] M. Badami, F. Mallamo, F. Millo and E. E. Rossi, "Influence of Multiple Injection Strategies on Emissions, Combustion Noise and BSFC of a DI Common Rail Diesel Engine," *SAE Technical Paper 2002-01-0503,* 2002.

[18] S. Biswas, M. Bakshi, G. Shankar and A. Mukhopadhyay, "Experimental Investigation on the Effect of Two Different Multiple Injection Strategies on Emissions, Combustion Noise and Performances of an Automotive CRDI Engine," *SAE Technical Paper 2016-01-0871,* 2016.

[19] M. Badami, F. Millo and D. D. D'Amato, "Experimental Investigation on Soot and NOx Formation in a DI Common Rail Diesel Engine with Pilot Injection," *SAE Technical Paper 2001-01-0657,* 2001.

[20] K. Mollenhauer and H. Tschöke, Handbook of Diesel Engines, Berlin: Springer-Verlag, 2010.

[21] J. O'Connor and M. Musculus, "Post Injections for Soot Reduction in Diesel Engines: A Review of Current Understanding," *SAE Int. J. Engines,* vol. 6, no. 1, pp. 400-421, 2013.

[22] G. T. Kalghatgi, "The outlook for fuels for internal combustion engines," *International Journal of Engine Research,* vol. 14, no. 4, pp. 383-398, 2014.

[23] S. d'Ambrosio and A. Ferrari, "Boot injection dynamics and parametrical analysis of boot shaped injections in low-temperature combustion diesel engines for the optimization of pollutant emissions and combustion noise," *Energy,* vol. 134, no. 1, pp. 420-437, 2017.

[24] "The modification of the fuel injection rate in heavy-duty diesel engines. Part 1: Effects on engine performance and emissions," *Applied Thermal Engineering,* vol. 24, no. 17-18, p. 2701–2714, 2004.

[25] Gamma Technologies, "GT-POWER Engine Simulation Software," 2019. [Online]. Available: https://www.gtisoft.com/wp-content/uploads/2015/01/Power1.pdf.

[26] Gamma Technologies, *GT-SUITE: Flow Theory Manual,* 2017.

[27] Gamma Technologies, *Engine Performance Application Manual,* 2017.

[28] G. P. Merker, B. Hohlbaum and M. Rauscher, "Two-Zone Model for Calculation of Nitrogren-Oxide Formation inDirect-Injection Diesel Engines," *SAE Technical Paper 932454,* 1993.

[29] B. Kegl, M. Kegl and S. Pehan, Green Diesel Engines, London: Springer, 2013.